UNIVERSITY OF CALIFORNIA
RIVERSIDE

Studies on the Interactions of the Ribosome and RNA Polymerase and its Effects on Transcription in *E. Coli*

A Dissertation submitted in partial satisfaction
of the requirements for the degree of

Doctor of Philosophy

in

Biochemistry and Molecular Biology

by

Stephen J. Diggs

December 2021

Dissertation Committee:
Dr. Gregor Blaha, Chairperson
Dr. Russ Hille
Dr. Rong Hai

The Dissertation of Stephen J. Diggs is approved:

_____

_____

_____

Committee Chairperson

University of California, Riverside

Acknowledgments:

I would like the thank my PI, Dr. Gregor Blaha. He took me in as an undergrad and showed me the ropes in lab. Still to this day he answers all of my questions, usually without rolling his eyes. I would also like to thank my committee members, Dr. Hille, Dr. Hai, Dr. O'Leary, and Dr. Song. I would also like to Dr. Hai for allowing me to learn about other polymerases and viruses during the Covid-19 pandemic. I would like to give a special thanks to my lab mates, especially, Tim, Adam, Tynan, Sheron, Haitian, and Carlos. My time would not have been possible without support and guidance from Dr. Song's lab members, specifically, Box, Jian, and Jiuwei. My time at UCR has allowed me to participate in many meaningful collaborations. I would like the thank the Wang group, specifically Preston Williams for mass spec analysis, the Higgs group for work with MrpC, and the Artsimovitch group for materials used in this dissertation. For financial support, I would like to thank the Wedding foundation. I would also like to thank the students I have TA'd over the years for voting for me to win two TA of the year awards in the biochemistry department. I would like to acknowledge *Nucleic Acids Research, Int. J. Mol. Sci.,* and the scientific community for giving me permission to use material in this dissertation

On a more personal note, I would like to thank my grandparents for always pushing me to pursue my education. I would also like to thank my parents for always believing in me and pushing me to work hard and to follow my passions. To my wife Andie, I love you more, regardless of what your dissertation says…

ABSTRACT OF THE DISSERTATION

Studies on the Interactions of the Ribosome and RNA Polymerase and its Effect on Transcription in *E coli*

by

Stephen J. Diggs

Doctor of Philosophy, Graduate Program in Biochemistry and Molecular Biology
University of California, Riverside, December 2021
Dr. Gregor Blaha, Chairperson

RNA polymerase and the ribosome are two of the most well-studied macromolecules in all of molecular biology. Most research done on RNA polymerase and the ribosome has been done in isolation from each other. However, the cellular processes the RNA polymerase and ribosome carry out, transcription and translation, respectively, occur in the same cellular compartment in bacteria. In fact, the process of transcription and translation are coupled. Despite a detailed understanding of various aspects of transcription and translation, the coupling of both processes has remained enigmatic. This includes the interaction interface between the RNA polymerase and the ribosome, and between the RNA polymerase and the ribosomal subunits. Furthermore, we know how only a few ribosomal proteins influence transcription, a need for additional detailed studies are required to elucidate their potential effects on transcription during coupling.

In my thesis, I first aimed to determine the interaction interface between RNA polymerase and the ribosome and between the RNA polymerase and the small and large

ribosomal subunit. To do this, RNA polymerase was cross-linked with either the ribosome or one of the ribosomal subunits. The mixture was run on an SDS polyacrylamide gel, the crosslinked protein bands were excised from the gel, and the crosslinked proteins were identified in collaboration with Dr. Wang groups in the Chemistry department at UC Riverside. Based on this analysis we could identify several proteins on the ribosome that may participated in different interactions between the RNA polymerase and ribosome during transcription-translation coupling. For three of these ribosomal proteins, I determined their effects on transcription. Each ribosomal protein exerted a unique and unexpected effect on transcription. They all slowed the RNA polymerase at the *his* pause sequence. Two of them even hampered factor-mediated transcription termination, while one bound directly to core RNA polymerase. To enable a smooth follow-up of my initial studies of the ribosomal proteins' effect on transcription, I have included an extended appendix that details all aspects critical to performing these transcription assays successfully.

Table of Contents

List of Figures

Chapter 1: Introduction

Chapter 2: *E. coli* Ribosome and Ribosomal Subunits Direct Coupling to RNAP

Chapter 3: The Intrinsic Effects of Universally Conserved Ribosomal Proteins uS2, uS3, and uS4 on Transcription

Chapter 4: Review of Transcription-Translation coupling

Appendix

List of Tables

Chapter 2: *E. coli* Ribosome Direct Coupling to RNAP

Chapter 3: The Intrinsic Effects of Universally Conserved Ribosomal Proteins uS2, uS3, and uS4 on Transcription

Chapter 1:

Introduction

Introduction:

The work I have accomplished during my graduate studies has revolved around: the interactions between RNA polymerase and the ribosome and its' subunits (chapter II), and the effects of the universally conserved ribosomal proteins S2, S3, and S4 on transcription (chapter III). As my work was more focused on the aspects of transcription, I will provide a more detailed overview on the structure of the RNA polymerase and on transcription. To provide more context for my work on transcription-translation coupling, I will also give a succinct overview on the structure of the ribosome and on translation. As my thesis includes an extensive review on transcription-translation coupling (chapter IV), I will forgo a discussion of the said coupling of both here.

Transcription and its key player, the RNA polymerase

Assembly of the core enzyme

In bacteria, transcription of the genetic information into RNA is performed by only one enzyme, the RNA polymerase (RNAP). RNAP core enzyme consists of two α, one β, one β', and one ω subunit. These subunits are assembled in cells starting with the dimerization of the N-terminal domains of the α subunit (Decker and Hinton 2013), which then binds the β subunit. Finally, the complex of the ω and β' subunit joins the two α and one β subunit complex to form the full core enzyme. The weight of the fully assembled core enzyme is ~390 kDa (Sutherland and Murakami 2018). The overall structure of the core enzyme is commonly referred to as having a crab claw shape. The

core RNAP enzyme is highly conserved from prokaryotes to eukaryotes (Darst, Opalka et al. 2002).

Promoter and RNAP interactions

To initiate transcription the RNAP needs to recruit an additional protein factor known as sigma factor (σ) such as σ^{70}. Although there are at least four other sigma factors in *E. coli*, σ^{70} regulates the expression of all housekeeping genes in *E. coli*. Its binding to the core RNAP results in the formation of the holoenzyme. The σ^{70} has four domains σ_1, σ_2, σ_3, and σ_4. These domains are further subdivided into smaller domains, such as the two subdomains of σ_1, $\sigma_{1.1}$ and $\sigma_{1.2}$. The different subdomains of the sigma factor make extensive contacts with the promoter region of housekeeping genes. In *E. coli*, the promoter region consists of (starting from the 5' end) the UP element, the -35 sequence, the EXT sequence, the spacer, the -10 sequence, the discriminator, and lastly the transcription start site, commonly referred to as +1 site (Figure 1.1A, bottom).

While the RNAP-bound σ^{70} makes these extensive contacts with the promoter region, the RNAP contacts UP element with the C-terminal domain of both α subunits (Figure 1.1A). It is important to note that only the holoenzyme binds to the promoter and not the σ^{70} alone, as the $\sigma_{1.1}$ domain autoinhibits free σ association to the promoter DNA (Dombroski, Walter et al. 1992; Camarero, Shekhtman et al. 2002). Only the binding of σ^{70} to the core enzyme allows σ to bind the promoter (Murakami, Masuda et al. 2002; Vassylyev, Sekine et al. 2002). σ_4 recognizes the -35 sequence of the promoter, while σ_2 recognizes the -10 sequence on the promoter (Hawley and McClure 1983). The -35 and -

10 are separated by a spacer region which is 16-19 base pairs long. There is also a small 4 base pair EXT region on the promoter just upstream of the -10 sequence (Figure 1.1A, red) which contacts σ_3. Just upstream of the +1 start site – is the discriminator sequence which contacts σ_1.

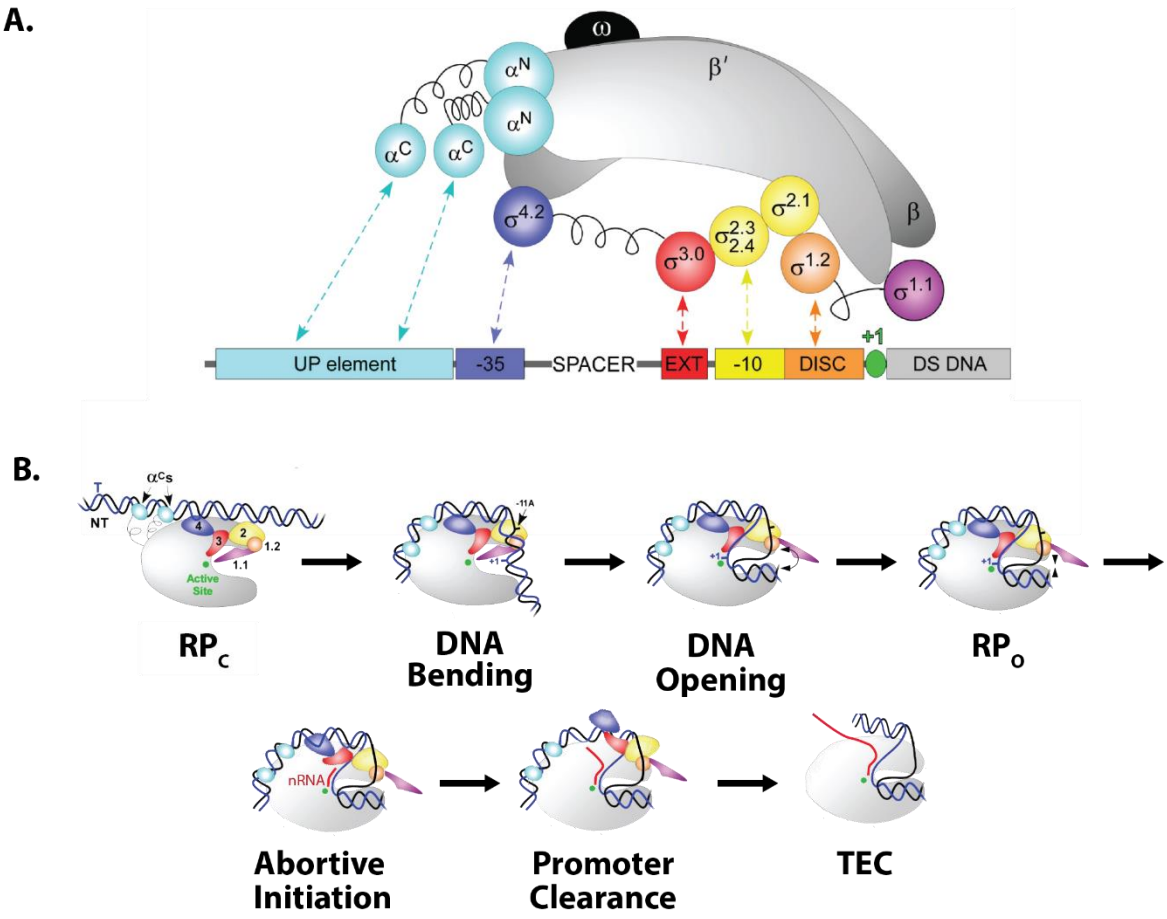

Figure 1.1: Schematic of RNAP-DNA interactions. **A**. View of domains of RNAP and of sigma factor that contact the promoter DNA. **B**. Visualization of the steps RNAP holoenzyme recruitment to promoter region of the DNA. Starting with the closed state all the way to an active transcription elongation complex. See text for details (Figure adapted from (Ruff, Drennan et al. 2015) via CC BY 4.0 with permission from publisher).

Transcription initiation

To begin transcription initiation, RNAP holoenzyme binds promoter DNA to form a closed complex (Figure 1.1B). σ_2 and σ_4 interact with the -10 and -35 region of the promoter, respectively. Aromatic residues on $\sigma_{2.3}$ are positioned to facilitate DNA melting and unwinding. This allows the template strand of DNA to bend across the active site channel of RNA polymerase (Vassylyev, Sekine et al. 2002; Saecker, Record et al. 2011). At some point during this process, $\sigma_{1.1}$ exits the RNAP active-site channel, relieving its autoinhibitory function (Murakami, Masuda et al. 2002)(Figure 1.1B). The melting of DNA will continue until a complete transcription bubble is formed (Murakami and Darst 2003). This marks the formation of the open complex. NTP substrates can now enter via a secondary tunnel, beginning the cycles of abortive initiation (Figure 1.1B). During abortive initiation, several nucleotides are added to a growing transcript until the transcript encounters the 3.2 loop of the σ factor. The transcript either displaces loop 3.2 or is displaced from the DNA-bound RNAP and another cycle of abortive initiation begins (Murakami, Masuda et al. 2002). The displacement of the 3.2 loop (at a length of roughly 12 nucleotides) marks the end of the abortive initiation. In the textbook model, the last process of transcription initiation is the dissociation of the sigma factor from the RNAP marking the transition of transcription from initiation to elongation phase. However, recent evidence has shown that some fraction of the σ factor remains bound to the polymerase, long into the transcription of a gene, and in some cases even to the end of the transcription of the gene (Mooney, Davis et al. 2009).

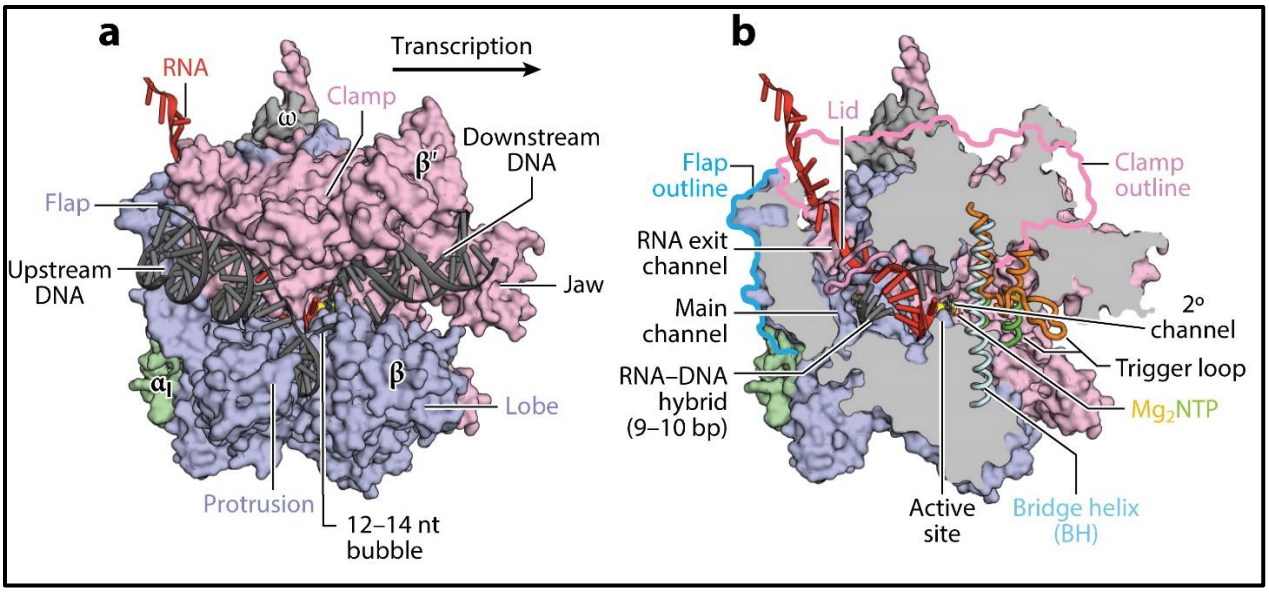

Figure 1.2: Key structural features of a TEC in both an outside view (**A**.) and a sliced view in (**B**). Adapted from (Ray-Soni, Bellecourt et al. 2016) and used with copyright permission from the publisher.

Transcription elongation

Once σ has dissociated from the transcribing polymerase, the polymerase will maintain an 8 to 9 base pair long (bp) DNA:RNA hybrid as well as a 11 to 12 bp melted DNA bubble (Belogurov and Artsimovitch 2015) (Figure 1.2A). The active site of the polymerase contains two distinct oligo-nucleotide binding sites: the *i* site (or P-site) and *i+1* site (or A-site), see figure 1.2B and figure 1.3. Right next to the *i*+1 site is a long alpha helix and a dynamic loop of the β subunit. The long alpha helix crosses the "two jaws" of the RNAP crab claw and is known as the bridge helix. The helix is critical for separating the non-template strand from the template strand of DNA. The dynamic loop next to the bridging helix is the trigger loop that is critical for nucleotide transfer reaction during the elongation of the grown RNA transcription. The *i* site contains a Mg^{2+} ion which is tightly chelated to three aspartates of the β subunit. This Mg^{2+} ion coordinates the 3'-OH of the nascent RNA activating it for a nucleophilic reaction. The nucleophilic 3'-OH attacks the alpha-phosphate of the incoming NTP-Mg^{2+} substrate (Steitz). Before insertion of the incoming nucleotide, the elongation complex is in a post-translocated state with the 3' end of the growing RNA transcript in the *i*-site of the polymerase (Figure 1.3). The trigger loop is away from the active site at this point. After the insertion of the incoming NTP-Mg^{2+} into the *i*+1 site, the trigger loop will only undergo a conformational change if the incoming nucleotide can form a Watson-Crick base pairing with nucleotide of template DNA strand in the *i*+1 site. In this conformation change the trigger loop will fold into a helix, closing the active site and allowing for the nucleotidyl transfer reaction to take place (Figure 1.3), (Kaplan, Larsson et al. 2008; Wang, Bushnell

et al. 2009; Kireeva, Kashlev et al. 2010; Yuzenkova and Zenkin 2010; Zhang, Palangat et al. 2010; Larson, Mooney et al. 2014).

When catalysis occurs a phosphodiester is formed, and the nucleotide successfully joins the growing chain of RNA. At this point the elongation complex is in the pre-translocated state with the newly extended 3' end of the transcribing RNA in the *i*+1 site (Figure 1.3). Lastly, the trigger helices transition back into the trigger loop, pyrophosphate (PPi) is released, and the elongation complex is translocated into the post-translocated state (Kang, Mishanina et al. 2018). This cycle of the bridge helix separating the down-stream DNA during translocation , the Watson-Crick base pairing of incoming NTP-Mg^{2+} with the template strand nucleotide in *i*+1 site, and the trigger loop closing to enable the formation phosphodiester repeats until transcription terminates. This cycle is known as nucleotide addition cycle (NAC) (Kang, Mishanina et al. 2019). Before the NAC is terminated the polymerase will likely encounter signals encoded in the DNA that cause it pause.

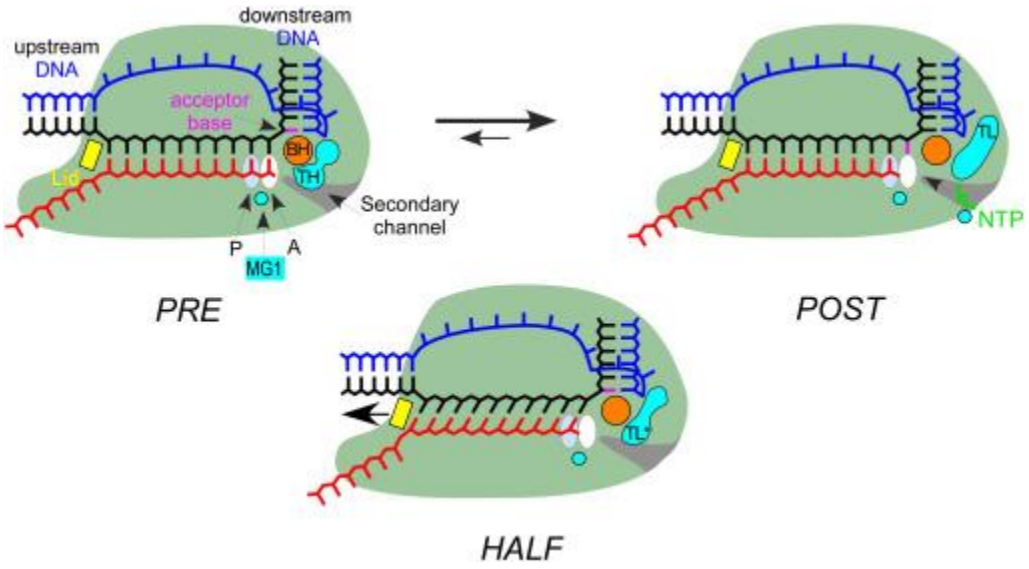

Figure 1.3: Model of translocation by the RNA polymerase. Model depicts RNA polymerase in the PRE-, POST-, and HALF- translocated state. BH is Bridge Helix, TL is Trigger Loop, TH is Trigger Helix. Used with copyright permission from Elsevier via (Belogurov and Artsimovitch 2019).

Transcription pausing

Pausing is the first necessary step for efficient termination and is mediated by different factors that influence the transcription elongation rate of the RNA polymerase (Gusarov and Nudler 1999; Yarnell and Roberts 1999). Note that pausing does not mean RNAP is always destined to terminate. In fact, there are several different mechanisms for pauses which were first identified by Artsimovitch and Landick over two decades ago (Artsimovitch and Landick 2000). In the first type of pausing (termed class 1), the formation of an RNAP-RNA hairpin within the exist tunnel of the polymerase inhibits the nucleotide addition. This is done by stabilizing the RNA 3' OH in a half-translocated position (in the *i*-site) while leaving the DNA in the *i*+1 site (Figure 1.3) (Kang, Mishanina et al. 2018). In an entirely different mechanism (termed class 2) a different type of pausing is caused by weak RNA-DNA hybrids. These weak hybrids allow the RNAP to backtrack on the DNA and to extrude the 3' end of its RNA through the nucleotide entry site into the surrounding solution. This occludes the active site and thus pauses transcription (Guajardo and Sousa 1997; Komissarova and Kashlev 1997; Gusarov and Nudler 1999). Accessory factors that bind directly to RNAP can influence the polymerase's pausing during transcription. For example, NusA and NusG, both can bind to RNAP, and effect the rate of RNA chain elongation (Burns, Richardson et al. 1998). NusA slows the rate of chain elongation and has been shown to increase termination at some transcription termination sites, while at other site it decrease termination (Lau, Roberts et al. 1982; Schmidt and Chamberlin 1987; Linn and

Greenblatt 1992). On the other hand, NusG increases the rate of chain elongation by decreasing the pause half-life of RNA polymerase (Burns, Richardson et al. 1998).

Transcription termination

At the end of an operon the RNA polymerase terminates transcription. There are two known mechanisms of termination, factor-mediated and intrinsic termination. Factor-mediated transcription termination is executed by a hexameric ATPase known as the Rho factor (Mitra, Ghosh et al. 2017). Each monomeric Rho factor subunit has two domains, an N-terminal domain (NTD) and a C-terminal domain (CTD). The NTD contains the primary RNA-binding site. The CTD contains the secondary RNA-binding site and the ATP binding site. The Rho hexamer is known to have an open and closed conformation which are controlled by several different factors. When Rho is in an open complex it looks like a spring washer, with one of the six Rho factors being disconnected from the rest. In the absence of ATP and RNA the Rho hexamer is this open complex. In the presence of ATP and RNA, Rho will undergo a conformational change to becomes the closed complex, turning the “spring washer” to an “O-ring”. During the open conformation RNA can bind to each subunit (Thomsen and Berger 2009). In the closed and active conformation, the RNA passes through the central hole formed by the six subunits and Rho can translocate along the RNA driven by ATP hydrolysis. The model for Rho factor termination has long been thought to initiate by binding of the open Rho hexamer to a *rut* site encoded in the RNA. Upon binding to the *rut* site, Rho factor closes to the “O-ring” conformation. The Rho factor would use its translocase activity to move from 5' to 3' up the nascent RNA until it reaches RNAP. Rho then causes transcription

termination, via shearing the nascent RNA of the template DNA, by forcing the RNA polymerase hypertranslocate, or by inducing conformational change of the RNAP, thus losing grip of the nascent RNA – discussed in detail below (Ray-Soni, Bellecourt et al. 2016);Lodish et al, Molecular Biology 4th edition).

New evidence that contradicts this long-standing model was presented in a series of cryo-EM structures published in 2021 (Hao, Epshtein et al. 2021; Said, Hilal et al. 2021). In the first structure, termed the engagement complex, RNAP, template and non-template DNA strands, RNA, NusG, NusA, and Rho hexamer form a complex (Figure 1.4, Engagement). The Rho hexamer is numbered one through six going counterclockwise with Rho number one being near the RNA exit tunnel of the polymerase (Figure 1.2B). The break in the Rho hexamer "spring washer" is between Rho subunit number 6 and Rho subunit number 1. In structure two (known as the priming complex – Figure 1.4)), a dramatic conformational change is seen where NusA moves under Rho subunit six while causing movement in Rho subunits four and five as well. When NusA is moving into the primed complex it moves away from the RNA exit channel of the polymerase. Going to the third complex, known as the capture complex (Figure 1.4), Rho subunit number 6 detaches from subunit 5 and joins subunit 1. At this point Rho subunit 6 contacts the upstream DNA duplex. NusA does not bind to DNA and is interacting with Rho between subunit 5 and 6. Subunit 6 of Rho binds the nascent RNA at its primary binding site while the RNA is also contacting the RNA polymerase. The conversion to structure four, known as the inhibited complex, shows NusG is released from the complex (Figure 1.4). This results in the opening of the clamp of the RNA

polymerase, exposing several more bases of upstream DNA. Finally in the last step, known as the moribund complex, the 3' of the growing nascent RNA is completely removed from the active site of RNAP (Figure 1.4). What happens afterwards is not clear, but eventually the nascent RNA must be released from the polymerase and the DNA.

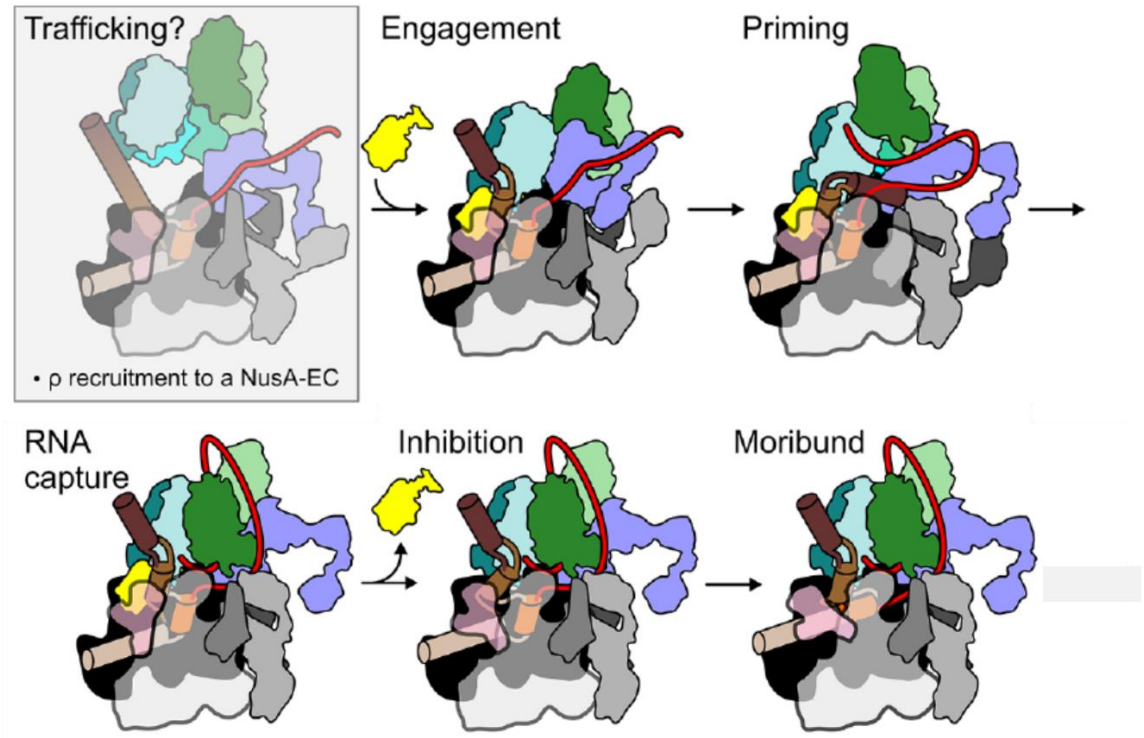

Figure 1.4: The new model for Rho-dependent termination. RNA polymerase is in shades of gray (besides the clamp of RNA polymerase which is in pink), NusG is in yellow, NusA is in purple, Rho hexamer is in green and blue tints, distal upstream DNA is in dark brown, proximal upstream DNA is in brown, downstream DNA is in light brown, DNA:RNA hybrid is in orange, RNA is in red. The different structures are listed to the top left of the corresponding structure. Originally from (Said, Hilal et al. 2021), reprinted with permission from American Association for the Advancement of Science (AAAS). Modified with permission from the corresponding authors.

Rho-dependent termination is one of the two types of transcription termination. The other type of termination is intrinsic termination. The canonical intrinsic terminator contains a GC-rich stem-loop, followed by a U-tract which contains 7 Uracil's in a stretch of 8 bases. Both the terminator hairpin and the U-tract are essential for efficient termination (Carafa, Brody et al. 1990). The first step of termination requires RNAP to pause at the 3' end of the U-tract. Because of the pausing the termination hairpin can form in the RNA exit channel (Gusarov and Nudler 1999). There are multiple models that try to explain how intrinsic termination occurs. In the hypertranslocation model, the terminator hairpin allows 2-3 base pairs of the upstream DNA-RNA hybrid to melt and causes the RNAP elongation complex to destabilize and eventually triggers dissociation of the entire elongation complex (Komissarova, Becker et al. 2002; Ray-Soni, Bellecourt et al. 2016). In the hybrid-shearing model, the extension of the termination hairpin pulls the RNA out of the RNA exit channel, shifting the nascent RNA out of register with the template DNA (Peters, Vangeloff et al. 2011). Finally, in the hairpin invasion model, the nascent RNA hairpin extends into RNAP instead moving through the exit channel which causes hybrid melting and significant steric clashes (Peters, Vangeloff et al. 2011).

Conclusion of Transcription

To summarize, bacteria contain a single multi-subunit RNA polymerase that transcribes DNA into RNA. The core enzyme of the polymerase contains two α, one β, β', and ω subunit. The binding of the σ^{70} factor to core enzyme converts the polymerase into the holoenzyme . The bound σ forms several specific interactions with the promoter

region, thus facilitating the recruitment of the polymerase to the promoter. Once to bound to the promoter region the polymerase initiates transcription. After σ dissociates from the initiating polymerase, polymerase proceeds to rapidly elongate the nascent RNA. During each nucleotide addition the RNA polymerase to undergoes multiple conformational changes propelling the polymerase from the post-translocated into pre-translocated state. The polymerase will terminate at the end of the transcription of a gene at either an intrinsic terminator site or if *rut* sites are accessible in Rho-dependent manner. While most students are taught that transcription occurs on a gene and then sometime later it is "translated", this is not the case. To better understand this "translation" of a nascent RNA, see the section below.

Translation and the Ribosome

Structure of the ribosome

Like RNA polymerase there is only one enzyme in *E. coli* that translates the information encoded on a mRNA into a protein, the ribosome. The ribosome in bacteria has a molecular mass of approximately 2.5 MDa and is comprised of two subunits, a large and a small subunit, or the 50S and 30S subunit, respectively. Each subunit is composed of at least one ribosomal RNA (rRNA) and more than twenty ribosomal proteins. The 30S subunit contains a 16S rRNA as well as 21 ribosomal proteins. The 50S ribosomal subunit contains a 23S rRNA, a 5S rRNA, and 36 ribosomal proteins in its fully matured form.

The naming convention is systematic, proteins of the large subunit start with L while those of the small subunit start with S followed by a number, starting with 1 for the largest protein going to the smallest one. For example, S2 is the second largest ribosomal protein on the small ribosomal subunit. In recent years, the naming has evolved to also include a prefix that indicates if the protein is universally conserved, prefix u, or specific to bacteria or archaea and eukaryotes, prefix b, or e, respectively (Ban, Beckmann et al. 2014). For example, the ribosomal protein S4 of the bacterial small subunit is conserved across all kingdoms of life, and thus it is now named uS4 (u for universally conserved), while ribosomal protein bS1 is specific to bacteria.

There are several key features on the large ribosomal subunit that help to orient researchers, see figure 1.5 (based on Ramakrishnan 2002). There are several protuberances on the large ribosomal subunit, including the uL1 stalk, the central

protuberance, and the bL7/L12 stalk. Because of its flexibility the L7/L12 stalk is typically not shown in structures of the ribosome. While not particularly large, there are up to four copies of the L7 protein (Diaconu, Kothe et al. 2005).

The small ribosomal subunit does not contain any large stalks but does contain several key features which are easy to recognize with enough experience. At one end is the is the head, which is more flexible than the other regions and contains many of the ribosomal proteins of the small subunit (Figure 1.5). Below the head is the neck, followed by the platform. The neck is where the mRNA will be funneled around. The entry site for the mRNA (near the A-site tRNA) is clustered around ribosomal proteins uS2-uS5 (see chapter 2 and 4 for a detailed layout of the ribosomal proteins). The small subunit's ribosomal proteins are also important in the context of transcription-translation coupling (see chapter 4).

There are three tRNA binding sites spanning across both subunits of the ribosome, the A-, P-, and E- sites (A- meaning acceptor, P- meaning peptidyl, and E- meaning exit site). The A-site tRNA is furthest away from the L1 stalk and the closest to the mRNA entry site on the 30S subunit, the P-site tRNA is between the A- and E- site, while the E-site tRNA closest to the L1 stalk and the mRNA exit site on the small subunit (Figure 1.5).

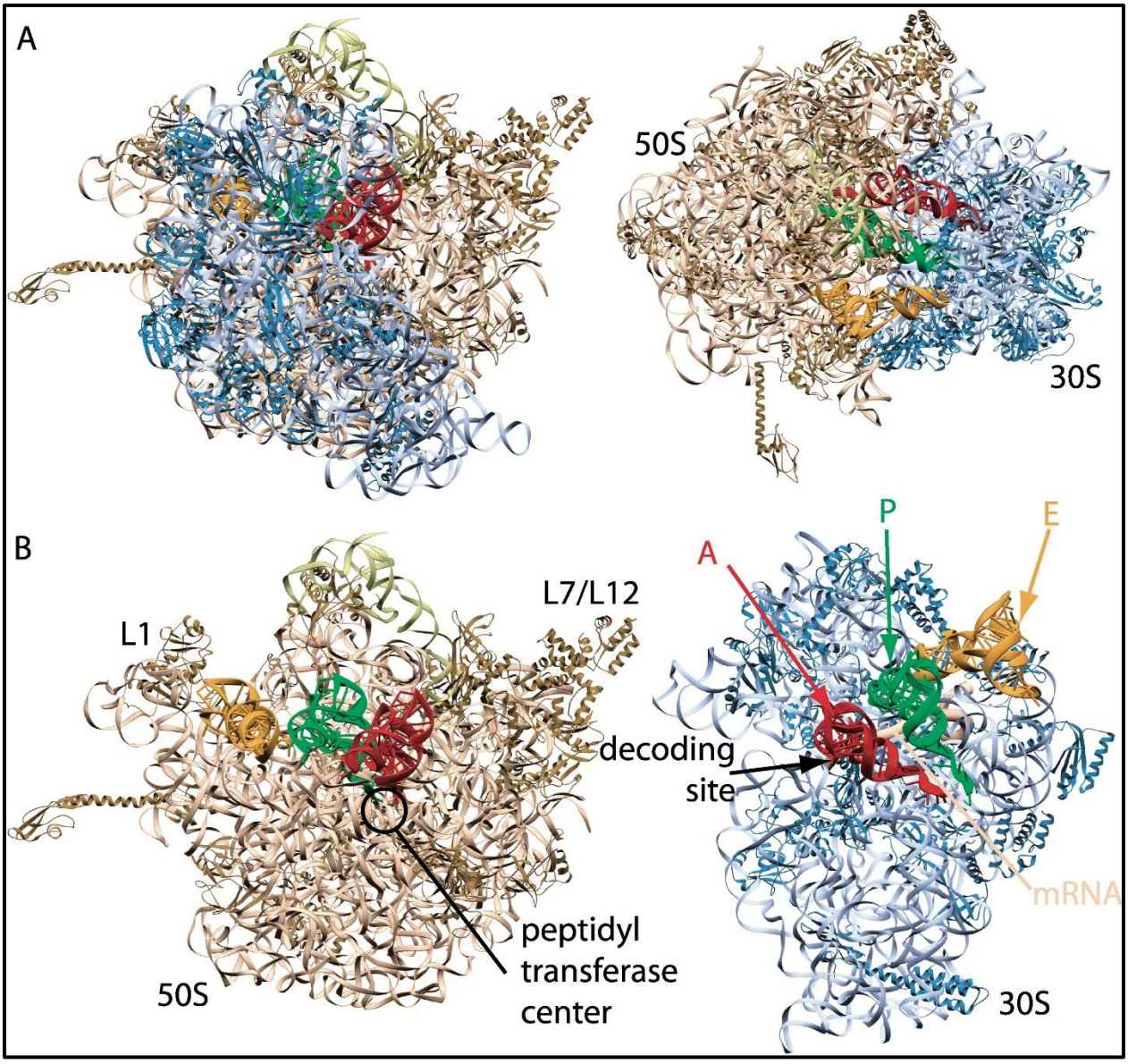
A
50S
30S
B
L1
L7/L12
50S
peptidyl
transferase
center
A
P
E
decoding
site
mRNA
30S

Figure 1.5: Structure of the 70S ribosome (A), 50S ribosomal subunit (B, left), and the 30S ribosomal subunit (B, right). Key features of the ribosomal subunits are indicated. See text for full description and details. (Figure used with permission from Elsevier, from (Ramakrishnan 2002))

Translation

The process of translating a protein from an mRNA involves three phases: initiation, elongation, and termination/recycling. During initiation, several initiation factors and the mRNA bind to the small ribosomal subunit, preparing the small ribosomal subunit to join the large ribosomal subunit. The thus formed ribosome is ready to perform the first peptidyl transfer reaction which marks the transition of translation from the initiation to the elongation phase. During elongation, tRNAs will move through the A-, P-, and E-sites of the ribosome, converting an amino acylated tRNA into a peptidyl-tRNA and finally into deacylated-tRNA in the process. Once the ribosome encounters a stop codon a release factor will bind and release the nascent polypeptide from the ribosome. The ribosome bound via two deacylated tRNAs to the mRNA is recycled by dissociating the ribosome into its two subunits. The intricate process of translation initiation, elongation, and termination/recycling is detailed below.

Translation initiation

At begin translation, initiation factor 3 (IF3) is bound to the 30S ribosomal subunit near the E-site. The binding of IF3 to the 30S subunit releases both tRNA and mRNA from a previous round of translation, thereby preventing the premature association of the 50S ribosomal subunit (Grunberg-Manago, Dessen et al. 1975; Laursen, Sørensen et al. 2005). In no particular order, IF1, IF2-GTP, fMet-tRNA^{fMet} and mRNA will bind to the 30S subunit. IF1 binds to the A-site of the 30S subunit preventing the tRNA from binding to the A-site until it dissociates from the ribosome (Carter,

Clemons et al. 2001). IF2-GTP facilitates the binding of fMet-tRNA^{fMet} and binds to the small subunit with its' N-terminal domain (near the A-site) and to the large ribosomal subunit with its' C-terminal domain (Gualerzi and Pon 2015). The C-terminal domain also contains the important GTP-binding site. Canonical initiation involves the binding of the 5' end of the mRNA to the 3' end of the 16S rRNA. In this model of translation initiation, the mRNA contains a Shine-Dalgarno sequence (aka ribosome binding site) that can base pairing with the anti-Shine-Dalgarno sequence at 3' end of the 16S rRNA. The Shine-Dalgarno sequence is an A/G rich stretch of four to six nucleotides located six to twelve nucleotides upstream from the translation start site (Shine and Dalgarno 1975; Steitz and Jakes 1975). A typical Shine-Dalgarno sequence is AGGAGG. The binding between the Shine-Dalgarno and anti-Shine-Dalgarno help the place the start codon into the P-site of the 30S subunit (Sussman, Simons et al. 1996). After the binding of the initiation factors, fMet-tRNA^{fMet}, and mRNA to the 30S subunit, the 30S subunit undergoes a conformation change to form a stable 30S initiation complex (30S-IC).

The 50S subunit can now bind to the 30S-IC to form the larger 70S initiation complex (70S-IC). Upon association of the 50S subunit, IF2 hydrolyzes its bound GTP (Tomšic, Vitali et al. 2000). Furthermore, IF3 dissociates from the ribosome (Grigoriadou, Marzi et al. 2007). The initiator tRNA is then placed into the peptidyl transfer center on the 50S subunit. Thereafter, IF2 and IF1 dissociate from the ribosome (Yamamoto, Wittek et al. 2016). With the subunits associated, the initiation factors dissociated, and the initiator tRNA in place, the ribosome is ready to begin translation.

Translation Elongation

Each round of elongating the nascent peptidyl chain involves several steps. To begin, a ternary complex which consists of EF-Tu, GTP, and an aminoacylated tRNA binds to the A-site of the ribosome. Not any ternary complex will do, though. The anti-codon on the tRNA must exhibit Watson-Crick base pairing to the codon sequence of the mRNA. A well-known exception to this is the wobble position which is the third base of the codon. The non-wobble positions are monitored via minor groove interactions with A1492 and A1493 (from the 16S rRNA) as part of a proof-reading mechanism for the ribosome. A match between the codon and anticodon triggers a conformational change in the 30S subunits shoulder. The conformational change introduces a kink into the anticodon loop of the tRNA, thereby forcing the acceptor arm of the tRNA (and the bound EF-Tu-GTP) closer to the A-site of the 50S (Schmeing, Voorhees et al. 2009). The Sarcin/Ricin loop of the 50S subunit then activates the GTPase activity of EF-Tu (Schmeing, Voorhees et al. 2009). The GTP on EF-Tu is hydrolyzed, releasing the tRNA from EF-Tu and letting the EF-Tu dissociate from the ribosome in the GDP form. The amino acyl-tRNA is accommodated into the A site of the ribosome, placing its CCA with its attached amino acyl group into the active site. There the N-terminus of incoming amino acyl group nucleophilic attacks the C-terminus of the peptidyl residue attached to the 3' OH of terminal adenine of the P-site bound tRNA (Schmeing, Huang et al. 2005). In the process the peptidyl chain from the P-site tRNA is transferred to N-terminus of the amino acyl group of the A-site tRNA. After peptidyl transfer, the polypeptidyl-tRNA is in the A-site and extended by one amino acid. The tRNA in the P-site is deacylated. Next,

the CCA end of deacylated tRNA translocates form its P-site binding site to its E-site binding site on the 50S subunit, all the while having it anticodon stem still being bound to its P-site binding site on the 30S subunit. The peptidyl-tRNA will undergo a similar translocation of its peptidyl carrying CAA end, translocating from its A-site binding site to its P-site binding site on the 50S subunit (Figure 1.6).

After a peptidyl transfer reaction, the 30S ribosomal subunit will sample different conformational states. In the process the whole 30S subunit rotate relative to the 50S subunit while the head of the 30S subunit will swivel to and from the 50S ribosomal subunit. In addition to under conformation changes the ribosome allows the bound tRNAs sample two states, the classical and the hybrid state. The classical state the tRNA binds to the same site on the 50S and 30S ribosomal subunits. This means that a tRNA bound in the P-site of the 30S is bound the P-site on the 50S. In the hybrid state, the tRNA is bound to different sites on the 30S and 50S ribosomal subunits. For example, a tRNA bound in the A-site of the 30S subunit is bound to the P-site on the 50S subunit (Figure 1.6E).

For the two tRNAs on the ribosome to adopt the hybrid state, the 30S head must swivel around the neck while the 30S is also rotated relative to the 50S subunit. The rotated and swiveled state is referred to as the ratcheted state. The ribosome will undergo conformational changes between the ratcheted state and the non-ratcheted state. Binding of the protein EF-G•GTP (a GTPase) stabilizes the ribosome in the ratcheted ribosomal state with both tRNAs in the hybrid state (Shoji, Walker et al. 2009). When the GTP on EF-G is hydrolyzed, it allows the body of the 30S subunit to relax into the non-ratcheted

state while the head remains in the ratcheted state. This results in the tRNA being linked to the A-site position on the head of small subunit and linked to the P-site position on the body, all the while in the P-site of the 50S subunit (Ratje, Loerke et al. 2010). Once EF-G is released the head relaxes back into the non-ratcheted state and the link of the tRNA to the A-site on the head of 30S subunit is transferred to the P-site. This completes translocation, freeing up the A-site for another incoming ternary complex. Multiple rounds of this elongation of nascent peptidyl will occur until a stop codon, UAG, UGA, and UAA enters the A-site. Figure 1.6 below shows a simple schematic of what is happening.

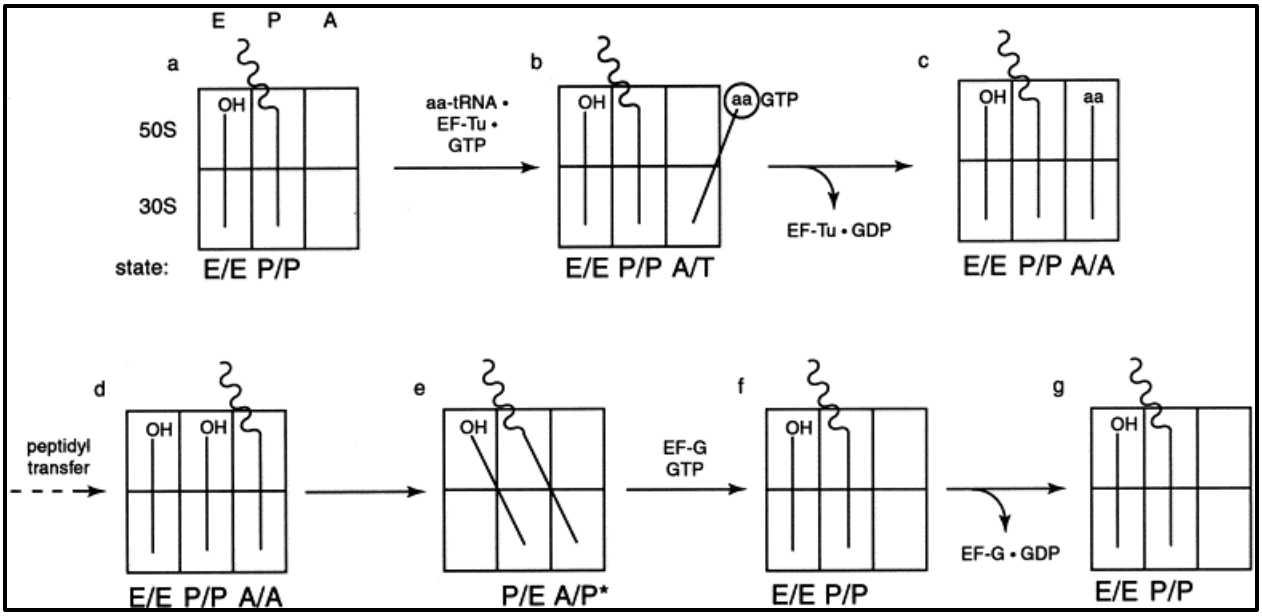

Figure 1.6: Schematic of tRNA movement during translation translocation. (Figured used with permission from publisher, figure from (Moazed and Noller 1989).

Translation Termination

Translation termination occurs when a stop codon is reaches the A-site. The polypeptide is released from the ribosome when a class I release factor cleaves the polypeptide from the P-site (Schmeing, Voorhees et al. 2009). The two class I release factors are RF1 and RF2. RF1 recognizes UAG while RF2 recognizes UGA. Both factors recognize UAA (Buckingham, Grentzmann et al. 1997). RF1 and RF2 are recognized by the GTPase RF3 which leads to both factors being released from the ribosome (Zavialov, Mora et al. 2002). Lastly, the ribosome recycling factor, RRF, binds to the ribosome and stabilizes a ratcheted state of the ribosome (Zhang, Dunkle et al. 2009). Once again EF-G binds to the ribosome. However, this time it will cause the ribosomal subunits to dissociate from each other (Karimi, Pavlov et al. 1999). IF3 is now free to bind the 30S subunit displacing the bound tRNAs and mRNA. Thus, the ribosome can begin translation renewed.

Chapter 2:

Establishing and Characterizing Ribosome and RNA Polymerase interactions

Publication:

Fan, H.*, Conn, A. B.*, Williams, P. B.*, Diggs, S.*, Hahm, J., Gamper, H. B., Jr, Hou, Y. M., O'Leary, S. E., Wang, Y., Blaha, G. M. (2017) "Transcription-Translation Coupling: Direct Interactions of RNA Polymerase with Ribosomes and Ribosomal Subunits." Nucleic Acids Research, **45**(19):11043-11055.

[PMID**:** 28977553]

* Authors contributed equally

- With copyright permission from Oxford University Press

Abstract:

In prokaryotes, RNA polymerase and ribosomes can bind concurrently to the same RNA transcript, leading to the functional coupling of transcription and translation. The interactions between RNA polymerase and ribosomes are crucial for the coordination of transcription with translation. Here, we report that RNA polymerase directly binds ribosomes and isolated large and small ribosomal subunits. RNA polymerase and ribosomes form a one-to-one complex with a micromolar dissociation constant. The formation of the complex is modulated by the conformational and functional states of RNA polymerase and the ribosome. The binding interface on the large ribosomal subunit is buried by the small subunit during protein synthesis, whereas that on the small subunit remains solvent-accessible. The RNA polymerase binding site on the ribosome includes that of the isolated small ribosomal subunit. This direct interaction between RNA polymerase and ribosomes may contribute to the coupling of transcription to translation.

Introduction:

In eubacteria, transcription and translation occur in close spatial and temporal proximity, allowing the processes to couple. In *E. coli*, most proteins are translated while their genes are still being transcribed (Bakshi, Choi et al. 2015). The inhibition of translation results in the genome-wide stalling of transcription (Zhang, Mooney et al. 2014). Stalled RNA polymerases act as a barrier for the DNA replication machinery, jeopardizing the processivity of replication, and with it, the integrity of the genome (Mirkin and Mirkin 2007; Dutta, Shatalin et al. 2011).

Functional interactions between RNA polymerase and the ribosome have been demonstrated for polycistronic operons (Yanofsky and Ito 1966; Landick, Carey et al. 1985; Yanofsky 2000). For example, a nonsense mutation in an upstream gene attenuates the transcription of downstream genes (Franklin and Luria 1961; Jacob, Monod et al. 1961). Premature translation termination causes ribosomes to dissociate from nascent RNA (Kaempfer 1970; Baggett, Zhang et al. 2017). Unhindered by ribosomes, transcription termination factor Rho proceeds along the nascent RNA to RNA polymerase, where it induces transcription termination (Richardson, Grimley et al. 1975; Adhya and Gottesman 1978);Adhya, Gottesman et al. 1976).

The functional interaction between ribosomes and RNA polymerase is also exploited in the regulation of gene expression, as exemplified by the regulation of the *trp* operon. During tryptophan starvation, ribosomes translating the operon's leader peptide stall at the two consecutive tryptophan codons. This stalling prevents the nascent RNA from forming a short stem-loop that acts as an intrinsic transcription termination signal;

without the stem-loop, RNA polymerase transcribes the downstream genes of the operon, which are necessary for tryptophan synthesis (Yanofsky and Ito 1966; Landick, Carey et al. 1985; Yanofsky 2000).

In some cases, the functional coupling of transcription and translation is thought to be promoted by physically connecting the ribosome to RNA polymerase via a small protein, such as transcription factor NusG or its paralog, RfaH (Burmann, Schweimer et al. 2010; Burmann, Knauer et al. 2012). Both factors consist of two domains, the N- and C-terminal domains. The N-terminal domain binds directly to RNA polymerase (Belogurov, Sevostyanova et al. 2010; Drögemüller, Strauß et al. 2015), while the C-terminal domain binds to ribosomal protein S10 on a surface accessible on the ribosome (Burmann, Schweimer et al. 2010; Burmann, Knauer et al. 2012). These results point to NusG and RfaH as a physical link between RNA polymerase and ribosomes (Burmann, Schweimer et al. 2010; Burmann, Knauer et al. 2012).

However, biophysical considerations of NusG's interactions with RNA polymerase and ribosomes point to a significant contribution of factor-independent interactions in the physical linking of RNA polymerase and ribosomes. Because the two domains of NusG are structurally independent of each other (Mooney, Schweimer et al. 2009), formation of the NusG-link between RNA polymerase and ribosome can be broken down into two thermodynamically separate events: the binding of NusG's N-terminal domain to the RNA polymerase and the binding of NusG's C-terminal domain to the ribosome. During exponential growth, the segregation of the nucleoid from the cytoplasm (Bratton, Mooney et al. 2011; Bakshi, Siryaporn et al. 2012; Endesfelder,

Finan et al. 2013) increases the local concentration of RNA polymerase and NusG in the nucleoid (1–2 μM (Mooney, Davis et al. 2009; Bratton, Mooney et al. 2011; Endesfelder, Finan et al. 2013)) beyond the NusG dissociation constant for RNA polymerase (0.15 μM (Turtola and Belogurov 2016)), resulting in near-saturation of the NusG binding to RNA polymerase. On the other hand, the same segregation also limits the local concentration of ribosomes in the nucleoid (2–8 μM (Bakshi, Siryaporn et al. 2012; Sanamrad, Persson et al. 2014)) to as much as an order of magnitude below NusG's dissociation constant for ribosomes (50 μM (Burmann, Schweimer et al. 2010)), implying that only a small fraction of ribosomes is engaged by NusG. These data suggest that only a modest amount of the ternary complex of RNA polymerase, NusG, and ribosomes accumulates under conditions of transcription-translation coupling, raising the question of whether additional mechanisms of coupling ribosomes to RNA polymerase exist.

We hypothesize that direct interactions between RNA polymerase and ribosome may contribute to the coupling of RNA polymerase and ribosomes during transcription-translation coupling. Early electron microscopy as well as recent functional studies demonstrate that ribosomes can directly contact RNA polymerase by translating all of the nascent mRNA being synthesized (Miller, Hamkalo et al. 1970; Proshkin, Rahmouni et al. 2010). Such proximity may be stabilized by one of several ribosomal proteins that directly bind to RNA polymerase and moonlight as transcription factors (*e.g.*, ribosomal protein S4, which binds to RNA polymerase and inhibits the premature termination of ribosomal RNA transcription (Torres, Condon et al. 2001)).

The present work tests the hypothesis of direct physical interactions between RNA polymerase and the ribosome. By applying biophysical methods and chemical crosslinking in combination with mass spectrometry, we demonstrate that these interactions occur. We expect that these direct interactions between RNA polymerase and the ribosome play an important role in the coupling of translation to transcription.

Materials and Methods:

Bacterial strains and plasmids.

E. coli MRE 600.rif was a kind gift from Dr. Knud Nierhaus, and pVS10 (T7P–α–β–β'-His_6–ω), pIA900 (T7P-α-β-β'-TEV-His10-ω), and pIA1127 (T7P-His6-TEV-σ^{70}[1-613]) were from Dr. Irina Artismovitch. Chemically competent T7 Express and BL21(DE3) *E. coli* were from New England Biolabs (Ipswich, MA, USA).

RNA polymerase and ribosome preparation.

The purification of *E. coli* RNA polymerase and ribosomes followed published protocols (Blaha, Stelzl et al. 2000; Artsimovitch, Svetlov et al. 2003; Fong, Gillies et al. 2010; Nedialkov, Opron et al. 2013) with minor modifications that were designed to reduce the co-purification of RNAs and other factors. Briefly, RNA polymerase captured on a Ni^{2+} affinity column was washed with two column volumes of 1.8 M NaCl before elution (Martin, Gillette et al. 2002); ribosomes from the lysate were pelleted through a high-salt sucrose cushion (Robertson, Paulsen et al. 1988). To remove ribosome-bound mRNAs, ribosomes were dissociated into subunits, and the purified subunits were re-

associated into vacant ribosomes following a published protocol (Blaha, Stelzl et al. 2000).

RNA polymerase•ribosome complex formation.

In a standard reaction, 2.5 µM RNA polymerase and 2.5 µM ribosomes were incubated for 15 min at 37 °C in buffer A (20 mM HEPES-KOH pH 7.5, 20 mM $Mg(OAc)_2$, and 30 mM KCl), followed by 5 min of incubation at 4 °C and a 10-min centrifugation at 19,000 × *g* at 4 °C.

Separation of free RNA polymerase from ribosome-bound RNA polymerase.

Mixtures of RNA polymerase and ribosomes were analyzed by rate zonal centrifugation or by gel filtration. For rate zonal centrifugation, samples were loaded on a 10 – 40 % sucrose or 10 – 40 % glycerol gradient in buffer A and centrifuged in an SW32.1 Ti rotor for 18 hours at 24,000 rpm at 4 °C. After centrifugation, the gradients were collected in 13 fractions starting from the bottom. The protein content of each fraction was precipitated with trichloroacetic acid (TCA) and analyzed by SDS-polyacrylamide gel electrophoresis (SDS-PAGE).

For gel filtration, samples were loaded onto a Superdex 200 10/300 GL column (GE Healthcare) equilibrated in buffer A with the KCl concentrations indicated in the text. The collected elution fractions were TCA-precipitated and analyzed by SDS-PAGE.

To probe the interactions between RNA polymerase and ribosomes, complex formation was performed in the presence of 20 µM bovine serum albumin (BSA), a 14-nucleotide-long RNA (rGrArGrUrCrUrGrCrGrGrCrGrArU) at a 5 µM concentration, 10 mM sodium phosphate pH 7.5, or additional KCl.

Separation of free ribosomes from RNA polymerase-bound ribosomes.

RNA polymerase, ribosomes, and mixtures of both were loaded onto Ni Sepharose High Performance spin columns and washed several times with increasing concentrations of imidazole before step-eluting the complex. Flowthrough, wash, and elution fractions were collected, TCA-precipitated, and analyzed by SDS-PAGE.

Capturing ribosomes with RNA polymerase immobilized on an affinity matrix.

A Ni Sepharose High Performance column was loaded with saturating amounts of His-tagged RNA polymerase before loading purified ribosomes. The column was washed with increasing concentrations of imidazole before step-eluting the complex. Fractions from all steps were TCA-precipitated and analyzed by SDS-PAGE.

Determining the RNA polymerase-ribosome binding curves.

To generate binding curves, various concentrations of ribosomes and RNA polymerase were incubated in buffer A with different concentration of KCl as indicated in the text. The content of each sample was analyzed by sucrose gradient centrifugation followed by SDS-PAGE and staining with colloidal Coomassie (Westermeier 2006). The stained gels were imaged with a ChemiDoc™ Touch Gel Imaging System (Bio-Rad), and the β/β' bands of each digital gel image were quantified using ImageJ 1.46 (Schneider, Rasband et al. 2012). The fraction of bound RNA polymerase was determined by subtracting the concentration-adjusted profile of the free RNA polymerase from that of the overall RNA polymerase profile.

The experimental data were modeled assuming that the RNA polymerase binds to one binding site on the ribosome in the presence of a dimer-monomer equilibrium of

RNA polymerase. The affinities of RNA polymerase for ribosomes were estimated by nonlinear least-square fitting of the partitioning function

$Z=[RNAP]+[70S]+K_1[RNAP]^2+K_2[RNAP][70S]+\alpha K_1K_2[RNAP]^2[70S]+$

$RNAP_{total}\ln[RNAP] - 70S_{total}\ln[70S]$

to the experimentally determined fraction of bound RNA polymerase using the "Equilibrium Expert" add-in for Microsoft Excel® (Raguin, Gruaz-Guyon et al. 2002). $[RNAP]$ and $[70S]$ are the concentrations of free RNA polymerase and ribosomes, respectively; $RNAP_{total}$ and $70S_{total}$ represent the total concentrations of RNA polymerase and ribosomes, respectively; K_1 and K_2 are the association constants for RNA polymerase dimer formation and RNA polymerase•ribosome complex formation, respectively; and α is the cooperativity factor for the binding of an RNA polymerase dimer to a ribosome. An average core enzyme•ribosome dissociation constant and its pooled standard deviation were calculated from the dissociation constants determined at 55 mM and 250 mM KCl according to (Box, Hunter et al. 2005) and yielded ~0.93 ± 0.21 μM. To calculate the holoenzyme•ribosome dissociation constant in the presence of a dimer-monomer equilibrium of the holoenzyme, we assumed a dissociation constant of 10 μM (Berg and Chamberlin 1970; Shaner, Piatt et al. 1982) and a cooperativity factor (α) of one. To calculate the complex formation in the absence of RNA polymerase dimerization (*i.e.*, holoenzyme), K_1 was set to zero. The fraction of bound RNA polymerase was set to $f_{bound} = \frac{RNAP_{bound}}{RNAP_{total}}$ for titrating the complex with increasing amounts of ribosomes and $f_{bound} = \frac{RNAP_{bound}}{70S_{total}}$ for titration with increasing amounts of RNA polymerase.

Preparation of NusG and sigma factor σ^{70}.

C-terminally His_6-tagged NusG was purified by Ni^{2+} affinity chromatography. Sigma factor σ^{70} was purified using a protein construct with an N-terminal His_6 tag and TEV protease site. After the initial capture of the protein on a Ni-NTA column, the protein was washed with two column volumes of 1 M NaCl before eluting with an imidazole gradient. The purified His_6-tagged factor was digested with TEV protease, and the free sigma factor was then separated from its cleaved His-tag and the TEV protease by passing it over a Ni-NTA column.

Formation of functional RNA polymerase complexes.

For preparation of holoenzyme, stoichiometric amounts of σ^{70} and core RNA polymerase were incubated (Gill, Weitzel et al. 1991). The transcription elongation complex was prepared following (Kashkina, Anikin et al. 2006), in which first a 14-nucleotide oligoribonucleotide (rGrArGrUrCrUrGrCrGrGrCrGrArU) and non-template DNA (GCGATTCAGACAGG) are annealed to the template DNA strand (CCTGTCTGAATCGCTATCGCCGC) to form a DNA:RNA hybrid scaffold before incubating with core RNA polymerase.

Formation of tRNA-bound ribosome complexes.

For preparation of tRNA-bound ribosomes, vacant ribosomes were incubated with an mRNA containing a Shine-Dalgarno sequence and codons for Pro and Phe (rArArArGrGrArArArUrArArArArCrCrArUrUrC), followed by sequential incubation with *E. coli* UGG $tRNA^{Pro}$ isoacceptor and yeast $tRNA^{Phe}$ (Holschuh and Gassen 1982; Schilling-Bartetzko, Franceschi et al. 1992). The UGG $tRNA^{Pro}$ isoacceptor was

transcribed *in vitro*, purified by gel electrophoresis, and *N*1 methylated at G37 with TrmD and AdoMet (Christian, Evilia et al. 2004).

Chemical crosslinking of RNA polymerase•ribosome complexes.

The RNA polymerase•ribosome complexes from *E. coli* were incubated with 5 mM 1-ethyl-3-(3-dimethyl-aminopropyl) carbodiimide (EDC) and 5 mM sulfo-*N*-hydroxysuccinimide (sulfo-NHS) at room temperature for 30 min before quenching the crosslinking reaction with 50 mM Tris-HCl. The protein content of the crosslinked sample was analyzed by SDS-PAGE with either a discontinuous 6 – 10 % Tris-glycine or a 6 – 9 % Tris-acetate gradient gel. The compositions of the SDS gel bands that occurred only in the presence of RNA polymerase and ribosomes were further analyzed by Western blot or excised and stored at 4 °C for further analysis by liquid chromatography-tandem mass spectrometry (LC-MS/MS).

Sample preparation for LC-MS/MS.

Excised SDS-PAGE bands were washed overnight before reducing and alkylating the captured protein with dithiothreitol and iodoacetamide, respectively. The alkylated proteins were subjected to tryptic digestion, followed by the extraction and desalting of the peptide fragments. The lyophilized peptides were resuspended in 0.1 % formic acid and immediately analyzed by LC-MS/MS.

LC-MS/MS for protein identification and quantification.

On-line LC-MS/MS analysis was performed on an LTQ-Orbitrap Velos mass spectrometer coupled with an EASY-nLC II HPLC system and a nanoelectrospray

ionization source (Thermo, San Jose, CA, USA). Sample injection, enrichment, desalting, and HPLC separation were conducted automatically. The HPLC was equipped with an in-house-packed ReproSil-Pur C18-AQ column. The peptides were separated using a linear gradient of 2 – 40 % acetonitrile in 0.1 % formic acid at a flow rate of 230 nL/min and electrosprayed (spray voltage 1.8 kV) into the mass spectrometer operating in positive-ion mode. Data-dependent acquisition was enabled, and the twenty most abundant ions found in the full-scan (*m/z* 300 – 1500 at a resolution of 60,000 at *m/z* 400) MS exceeding a threshold of 1000 counts were selected for collision-induced dissociation to generate the MS/MS.

LC-MS/MS data analysis.

Proteins were identified and quantified using MaxQuant software (version 1.5.3.8) (Cox and Mann 2008) to search raw LC-MS/MS data against the *E. coli* database downloaded from Uniprot (Alpi, Griss et al. 2015), which contains 4306 protein entries and additional entries for known contaminants. The fixed modification option was set to include cysteine carboamidomethylation, and the maximum number of missed cleavages was set to two per peptide. The tolerance levels in mass accuracy for MS and MS/MS were set to 4.5 ppm and 0.6 Da, respectively. The false positive rate was set to 1 %. For each protein, the spectral index (SI) was calculated as the sum of the ion intensities of all the tryptic peptides detected throughout the LC-MS/MS analysis of a sample (Griffin, Yu et al. 2010):

$$SI = \sum_{k=1}^{pn} \left(\sum_{j=1}^{sc} i_j \right)_k$$

where i_j is the ion intensity of the *j*th spectrum of peptide fragment *k* summed over all spectra *sc* for all tryptic peptides of the protein of interest, *pn*. The SI of each protein was weighted based on the length of the amino acid sequence of the protein:

$$Weighted\ SI = \frac{SI}{Protein\ Length}$$

The weighted SI values for all identified proteins were normalized to the highest weighed SI value within the sample (Griffin, Yu et al. 2010). Proteins were only considered enriched in the crosslink if they were present in all three biological replicates of the crosslinked band. We excluded proteins as potential RNA polymerase-ribosome interaction partners when they were present at the same relative mobility of the crosslinked species in either the crosslinked RNA polymerase or crosslinked ribosome sample and their SIs exceeded two-thirds of the SI observed for the crosslinked RNA polymerase-ribosome sample. The SIs of the remaining proteins were normalized to that of the protein with the highest index in each replicate. The average normalized SI values were calculated. The mass spectrometry proteomics data have been deposited to the ProteomeXchange Consortium via the PRIDE17 partner repository (Vizcaíno, Csordas et al. 2016) with the data set identifier PX006717.

Results:

E. coli RNA polymerase and ribosomes form a complex in vitro.

Eighty percent of RNA polymerase co-migrates with ribosomes when a micromolar mixture of stoichiometric amounts of RNA polymerase (core enzyme, consisting of $\alpha_2\beta\beta'\omega$ subunits) and vacant ribosomes (lacking bound mRNA and tRNAs) from *E. coli* are separated by sucrose density gradient centrifugation (Figure 2.1A). The presence of sucrose or glycerol in the density gradient does not influence the extent of complex formation (compare Figure 2.1A with 2.1B). Similar levels of complex formation are detected when the mixture is separated by size exclusion chromatography (Figure 2.1C). Density gradient centrifugation and size exclusion chromatography probe the hydrodynamic parameters of the complex, which are dominated by the sedimentation coefficient and the size of the ribosome, preventing the separation of free ribosomes from bound ribosomes.

To separate free ribosomes from bound ribosomes, we captured the complex on a Ni^{2+} affinity matrix via a C-terminal poly(Imbert, Guillemot et al.)-tag on the β' subunit of the RNA polymerase, either by pre-forming the RNA polymerase•ribosome complex or by first immobilizing the core enzyme on the matrix and then capturing vacant ribosomes from solution (Figure 2.1D). Although only an estimated 10 % of the applied RNA polymerase-ribosome complex is captured by the Ni^{2+} affinity matrix, none of the ribosomes are captured in the absence of RNA polymerase (compare 70S alone and RNAP + 70S in Figure 2.1E).

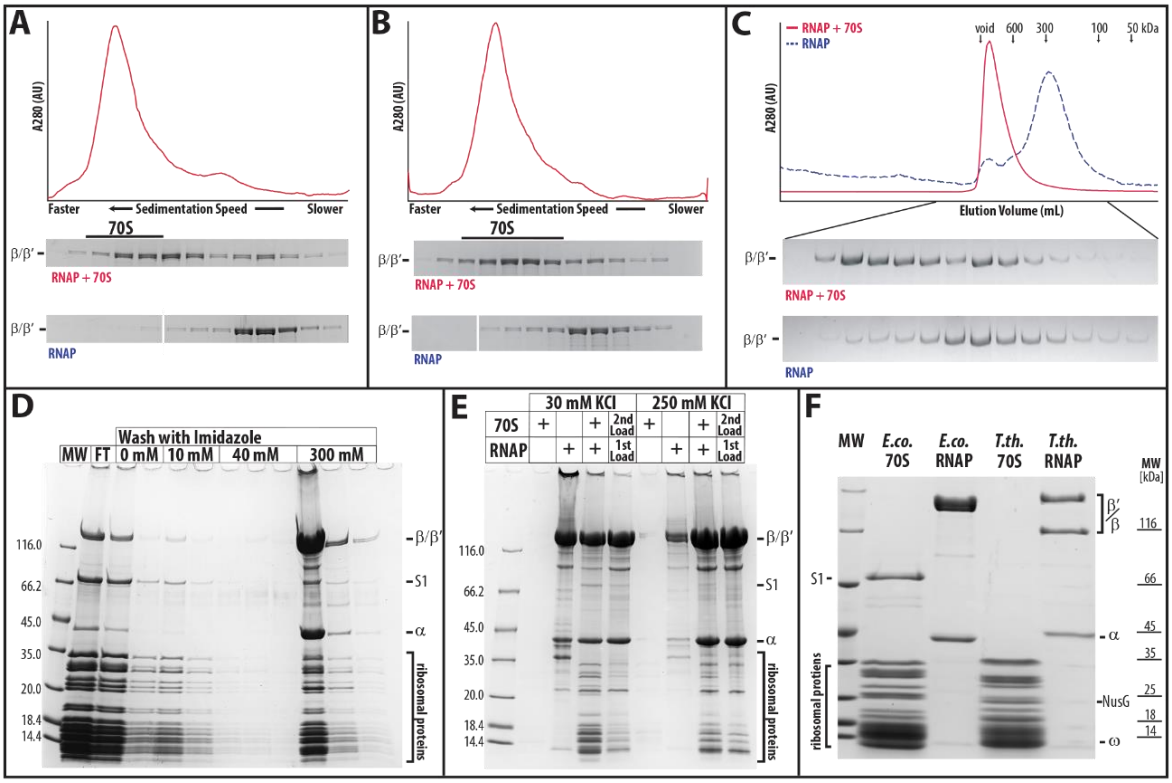
A
A280 (AU)
Faster
Sedimentation Speed
Slower
70S
β/β′
RNAP + 70S
RNAP
B
A280 (AU)
Faster
Sedimentation Speed
Slower
70S
β/β′
RNAP + 70S
RNAP
C
RNAP + 70S
RNAP
void
600
300
100
50 kDa
A280 (AU)
Elution Volume (mL)
β/β′
RNAP + 70S
β/β′
RNAP
D
Wash with Imidazole
MW
FT
0 mM
10 mM
40 mM
300 mM
116.0
66.2
45.0
35.0
20.0
18.4
14.4
β/β′
S1
α
ribosomal proteins
E
30 mM KCl
250 mM KCl
70S
RNAP
2nd Load
1st Load
116.0
66.2
45.0
35.0
20.0
18.4
14.4
β/β′
S1
α
ribosomal proteins
F
MW
E.co. 70S
E.co. RNAP
T.th. 70S
T.th. RNAP
MW [kDa]
β′
β
116
66
45
35
25
18
14
S1
α
NusG
ω
ribosomal protiens

Figure 2.1: Isolating RNA polymerase•ribosome complexes using different methods: **A**) Sucrose gradient centrifugation. The top panel displays the sedimentation profiles of RNA polymerase alone (dashed blue line) and a stoichiometric mixture of RNA polymerase and ribosomes (solid red line) recorded at 280 nm. The two bottom panels display the SDS-polyacrylamide gel electrophoresis (SDS-PAGE) result of each of the sucrose gradient fractions. The top panel shows the β/β' region of the SDS-PAGE result of the gradient centrifugation of RNA polymerase (RNAP) alone, while the bottom presents the full gel of a mixture of RNA polymerase and ribosomes (RNAP + 70S, marker lane removed for clarity). **B**) Glycerol gradient centrifugation. The panels are the same as in **A**. During ultracentrifugation, the complex of RNA polymerase and ribosome constantly re-equilibrates, causing the bound RNA polymerase to trail the ribosome in **A** and **B**. **C**) Size exclusion chromatography. The top panel shows the elution profiles of a mixture of RNA polymerase and ribosomes (solid red line) and of RNA polymerase alone (dashed blue line; for comparison, the absorption is increased by 160-fold) from a 10/30 Superdex 200 column. **D-E**) Capturing His-tagged RNA polymerase•ribosome complexes on a Ni-sepharose spin column. **D**) SDS-PAGE results of all fractions, *i.e.*, flowthrough (FT), washes with 0, 10, and 40 mM imidazole and elution with 300 mM imidazole. **E**) SDS-PAGE results of the first 300 mM imidazole elution step from Ni^{2+} affinity binding experiments. Various amounts of RNA polymerase and ribosomes are either loaded together or sequentially – first RNA polymerase ("1st Load"), followed by a stoichiometric amount of ribosomes ("2nd Load"). These experiments are performed in

the presence of 30 mM KCl and 250 mM KCl. **F**) RNA polymerase binding to ribosomes in the presence of 10 mM phosphate buffer (PO_4), 20 µM bovine serum albumin (BSA), a 14-nucleotide long RNA (RNA) at 5 µM, or 80 µg of poly(U)-RNA.

All employed methods exploit different molecular principles, yet they all consistently point to an upper limit of the apparent dissociation constant of the RNA polymerase•ribosome complex that is in the one to two micromolar range.

Non-specific competitors do not significantly impair complex formation.

While RNA polymerase consists only of protein subunits, two-thirds of the mass of the ribosome consists of RNA, implying that protein-protein and/or RNA-protein interactions may contribute to complex formation. To exclude non-specific interactions between RNA polymerase and ribosomes, we formed the complex in the presence of several potential non-specific competitors for RNA-protein and protein-protein interactions, such as phosphate buffer, a short RNA, random-sized poly(U) RNA, or BSA. The extent of complex formation is not significantly impaired by the presence of either an eight-fold excess of BSA or by 10 mM phosphate buffer at pH 7.4 (Figure 2.1F). At higher phosphate buffer concentrations, ribosomes dissociate into subunits, *i.e.*, in the presence of 10 mM phosphate buffer, none of the ribosomes dissociate, whereas with 100 mM phosphate buffer, approximately 40 % of the ribosomes dissociate into subunits. The presence of poly(U) RNA or a 14-nucleotide-long RNA reduces the extent of complex formation by approximately one-third. A fraction of RNA polymerase, ribosomes, and the RNA polymerase•ribosome complex appears to bind poly(U), causing it to sediment faster during sucrose gradient centrifugation. The nominal effect of these non-specific competitors for binding argues in favor of a specific interaction between the RNA polymerase core enzyme and the vacant ribosome. Thus, we hypothesize that the interactions between RNA polymerase and the ribosome are direct and specific.

Stoichiometry and dissociation constants of the RNA polymerase•ribosome complex.

Specific interactions between macromolecules cause the formation of defined stoichiometric complexes. Depending on the ionic conditions, the RNA polymerase core enzyme exists in an equilibrium of multiple oligomeric states (Stevens, Emery et al. 1966; Shaner, Piatt et al. 1982; Harris, Williams et al. 1995; Kansara and Sukhodolets 2011). To distinguish between the binding of an oligomer and the binding of multiple monomers, titration experiments were performed at salt concentrations that favor either the oligomeric or monomeric state of the RNA polymerase.

The titration of the core enzyme with vacant ribosomes in 55 mM KCl saturates at a one-to-one stoichiometry, while two equivalents of RNA polymerase bind to one equivalent of ribosomes under saturating conditions (Figure 2.2A and 2.2B, 55 mM KCl). At 250 mM KCl, a one-to-one complex is formed between the RNA polymerase and ribosomes at a saturating concentration of RNA polymerase (Figure 2.2B, 250 mM KCl). The similar sedimentation coefficients of ribosomes and of RNA polymerase•ribosome complexes indicate that only one ribosome is bound in each of the observed complexes. Ribosome dimers would sediment much faster than monomers, *i.e.*, 100 Svedbergs versus 70, respectively (Stöffler, Hasenbank et al. 1973; Morrison, Tischendorf et al. 1977; Kato, Yoshida et al. 2010).

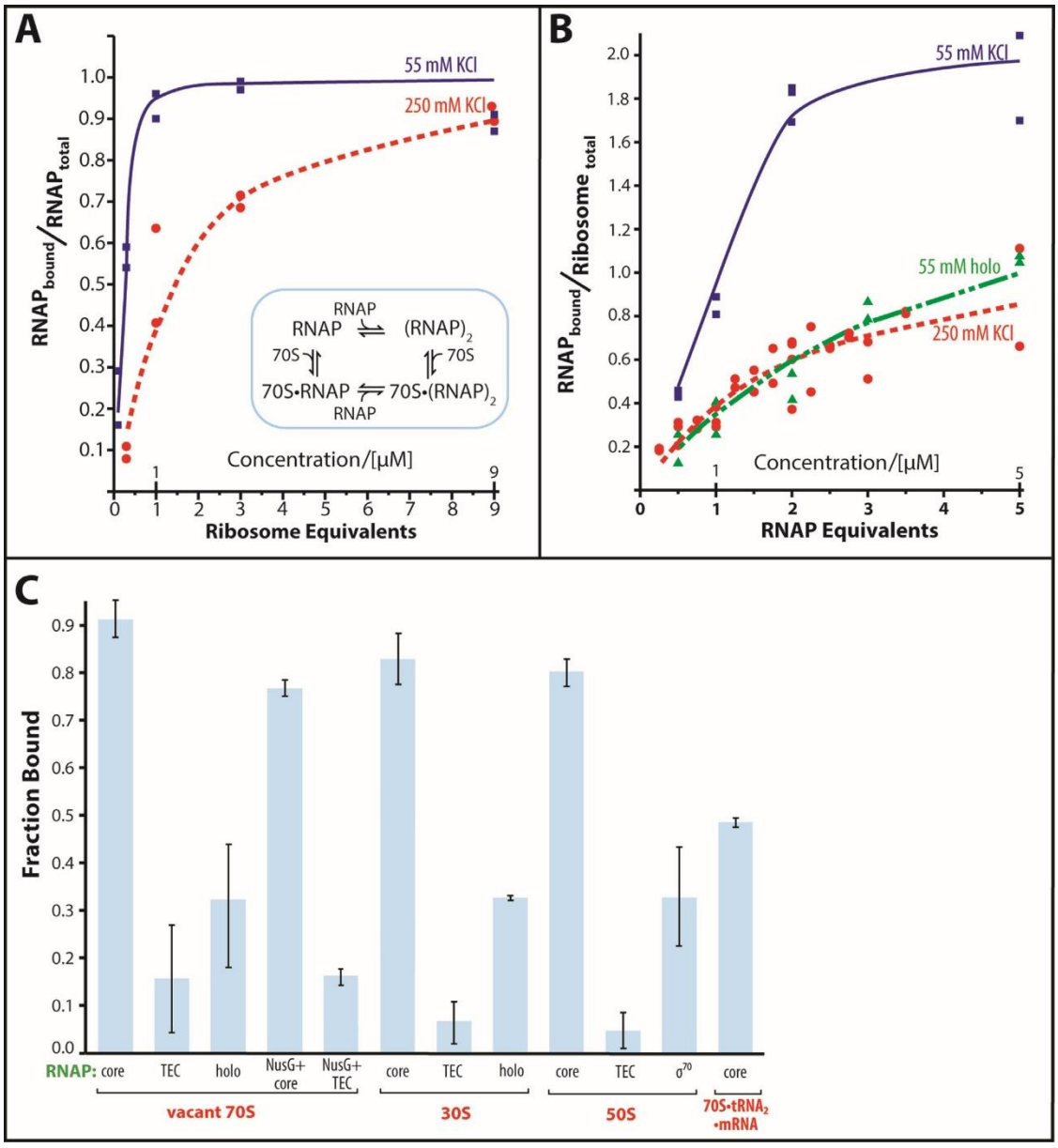
A
55 mM KCl
250 mM KCl
RNAP
RNAP ⇌ (RNAP)2
70S
70S•RNAP ⇌ 70S•(RNAP)2
RNAP
RNAPbound/RNAPtotal
Concentration/[μM]
Ribosome Equivalents
B
55 mM KCl
55 mM holo
250 mM KCl
RNAPbound/Ribosometotal
Concentration/[μM]
RNAP Equivalents
C
Fraction Bound
RNAP: core TEC holo NusG+ core NusG+ TEC core TEC holo core TEC σ70 core
vacant 70S
30S
50S
70S•tRNA2 •mRNA

Figure 2.2: Titration of RNA polymerase with ribosomes and vice versa. **A)** Binding of ribosomes to RNA polymerase. RNA polymerase (1 μM) is incubated with increasing concentrations of ribosomes in the presence of 55 mM KCl (blue squares) or 250 mM KCl (red circles). The inset displays the proposed binding model of complex formation. **B)** Binding of RNA polymerase to ribosomes. Ribosomes (1 μM) are incubated with increasing concentrations of RNA polymerase core enzyme (blue squares) or holoenzyme (green triangles) in the presence of 55 mM KCl or 250 mM KCl (red circles, core enzyme only). The lines connecting the data in **A** and **B** are the binding curves calculated as described in the Materials and Methods section of the text. For the holoenzyme, the simulated binding curve in the presence of dimer-monomer equilibrium is shown. **C**) Influence of the functional state of the RNA polymerase and of the ribosome on the RNA polymerase•ribosome complex formation. The complex formation of ribosomes (70S), small subunits (30S), large subunits (50S), and tRNA-bound ribosomes ($70S•tRNA_2•mRNA$) with RNA polymerase core enzyme (core), transcription elongation complex (TEC), holoenzyme (holo), core enzyme and transcription elongation complex in the presence of NusG (NusG + core and NusG + TEC) was analyzed by sucrose gradient centrifugation.

We were able to model the formation of the RNA polymerase•ribosome complex assuming the presence of one binding site on the vacant ribosome and a dimer-monomer equilibrium of the core enzyme (with estimated dissociation constants of 0.02 μM and 0.2 mM for 55 and 250 mM KCl, respectively, based on (Harris, Williams et al. 1995), inset in Figure 2.2A). This model yields a nearly identical RNA polymerase•ribosome dissociation constant of 0.93 ± 0.21 μM. However, upon transitioning from 55 to 250 mM KCl, the presence of ribosomes ceases to skew the RNA polymerase towards dimer formation, as reflected by a drop in the cooperativity factor, α, from 50 to 1. The significantly lower ratio of ribosomes to RNA polymerase captured on the Ni-affinity matrix at 250 mM KCl compared to 30 mM KCl supports the results from sucrose gradient centrifugation (compare experiments at 30 mM with 250 mM KCl in Figure 2.1E).

The observed dissociation constant for the RNA polymerase•ribosome complex constitutes an upper limit, as the presence of a nascent RNA that connects both interaction partners further reduces the dissociation constant. Despite being an upper limit, the one micromolar dissociation constant of the RNA polymerase•ribosome complex is by itself similar to those seen for other processes that regulate RNA polymerase or ribosome activity (*i.e.*, 0.9 μM for RNA polymerase binding to ribosomes versus 0.1 μM for transcription factor NusA binding to RNA polymerase (Gill, Weitzel et al. 1991) or 0.2 μM for EF-G (Katunin, Savelsbergh et al. 2002) and 0.5 μM for EF-Tu•GTP•Phe-tRNA^{Phe} (Maracci, Peske et al. 2014) binding to ribosomes.)

Characterization of the interaction between RNA polymerase and the ribosome.

The RNA polymerase adopts multiple functional states in the course of transcribing a gene. Therefore, in addition to testing the core enzyme, we also tested RNA polymerase with bound sigma factor σ^{70} (holoenzyme) and RNA polymerase with a bound DNA:RNA scaffold (transcription elongation complex, TEC) as examples of the initiation and elongation states, respectively. The sigma factor, as well as the radioactively labeled RNA of the DNA:RNA scaffold, co-migrates with the RNA polymerase-ribosome complex (Figure S2.2A and B), indicating that actively transcribing RNA polymerase may also participate in complex formation. Both states display reduced affinity for the ribosome, albeit to different extents – 31 % of the holoenzyme and 15 % of the TEC bind to the ribosome versus 90 % of the core enzyme (Figure 2.2C).

Nonlinear regression to best fit the measured binding data results in a computed dissociation constant of 1.4 ± 0.2 μM for the holoenzyme•ribosome complex when modeled for the dimer-monomer equilibrium, as predicted for our experimental conditions (Berg and Chamberlin 1970; Shaner, Piatt et al. 1982). An assumption of pure monomer reduces the quality of the fit but yields a dissociation constant of 1.2 ± 0.2 μM, which is still consistent with a weaker binding of the holoenzyme than of the core enzyme (K_d of core enzyme complex 0.9 ± 0.2 μM).

Like RNA polymerase, ribosomes adopt multiple functional states when translating a gene. Therefore, in addition to testing the vacant ribosomes, we tested tRNA-bound ribosomes. The tRNA-bound ribosomes display a weaker affinity for the core RNA polymerase (Figure 2.2C). The modulation of the dissociation constant by the

functional states of the RNA polymerase and ribosome may indicate that certain combinations of functional states permit tight binding, possibly synchronizing transcription and translation during transcription-translation coupling.

The ribosome consists of a small and a large ribosomal subunit. To identify the contribution of each subunit to the binding of the RNA polymerase, we investigated the interaction of the RNA polymerase with each subunit individually. The RNA polymerase core enzyme interacts with both subunits (Figure 2.2C), and the non-specific competitors have similar effects on the complex formation as on the RNA polymerase•ribosome complex formation (Figure S2.3). These results suggest that either each ribosomal subunit interacts with a different part of the RNA polymerase or that one RNA polymerase binding site is blocked upon subunit association. To distinguish between these two possibilities, we identified the RNA polymerase binding interfaces on the ribosome and on each of its subunits using chemical crosslinking.

Chemical crosslinking of RNA polymerase and ribosomes.

In the presence of sulfo-NHS, the zero crosslinker 1-ethyl-3-(3-dimethyl-aminopropyl) carbodiimide (EDC) produces a ribosome-dependent crosslink of the core enzyme (Figure 2.3A, 30 mM KCl). The effect of non-specific competitors on the crosslinking efficiency mirrors the effect of these competitors on RNA polymerase•ribosome complex formation (Figure S2.4A). In addition, the crosslinking efficiency correlates with the affinity of the RNA polymerase for the ribosome. The holoenzyme and TEC, which have lower affinity for ribosomes, display no increase in crosslink formation in the presence of ribosome (Figure S2.4A inset).

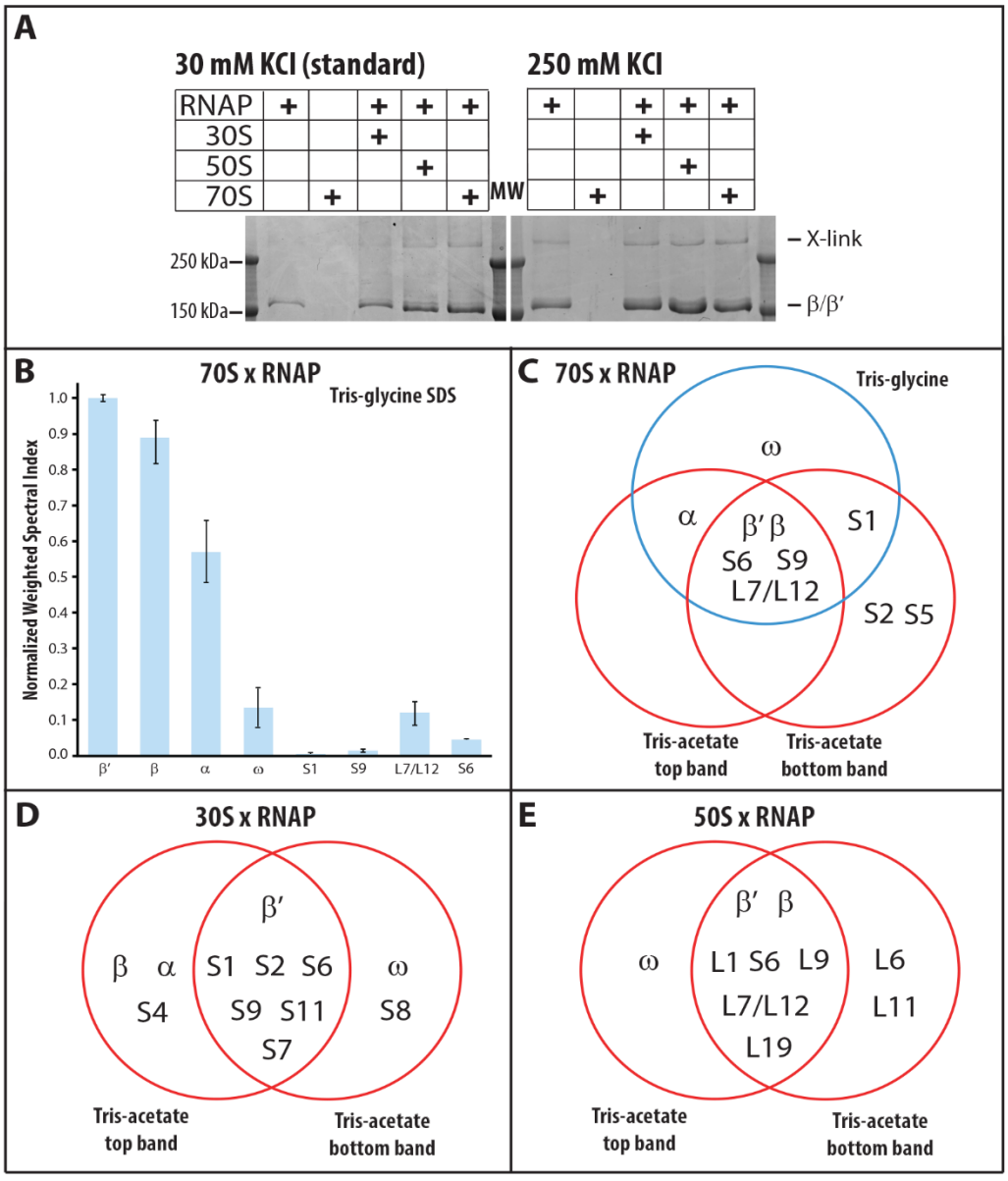
A
30 mM KCl (standard)
250 mM KCl
RNAP
30S
50S
70S
MW
250 kDa
150 kDa
X-link
β/β′
B
70S x RNAP
Tris-glycine SDS
Normalized Weighted Spectral Index
β′ β α ω S1 S9 L7/L12 S6
C 70S x RNAP
Tris-glycine
ω
α
β′ β
S1
S6 S9
L7/L12
S2 S5
Tris-acetate top band
Tris-acetate bottom band
D
30S x RNAP
β′
β α
S1 S2 S6
ω
S4
S9 S11
S8
S7
Tris-acetate top band
Tris-acetate bottom band
E
50S x RNAP
β′ β
ω
L1 S6 L9
L6
L7/L12
L11
L19
Tris-acetate top band
Tris-acetate bottom band

Figure 2.3: EDC crosslinking of RNA polymerase-ribosome complexes. **A)** EDC crosslinking of RNA polymerase in the presence of the small ribosomal subunit (30S), large ribosomal subunit (50S), and ribosome (70S) with 30 mM and 250 mM KCl. **B**) Normalized weighted spectral index of LC-MS/MS analysis of the Tris-glycine SDS-PAGE purified RNA polymerase-ribosome crosslink. **C)** Venn diagram of crosslinked proteins after exposing a mixture of RNA polymerase and ribosomes to EDC and isolating the unique crosslinked species by 6 – 10 % Tris-glycine (single band) and by 6 – 9 % Tris-acetate SDS-PAGE (two bands). **D** and **E)** Venn diagram of the proteins in the two species isolated from 6 – 9 % Tris-acetate PAGE, which are specific to the EDC crosslinking of RNA polymerase in the presence of the small and the large ribosomal subunits.

However, an LC-MS/MS analysis of the SDS-PAGE-purified crosslink reveals a significant enrichment of the RNA polymerase subunits α, β, and β' in the crosslink (Figure 2.3A). The presence of the RNA polymerase subunits in the crosslink was confirmed by Western blot analysis (Figure S2.4B). Therefore, we conclude that upon ribosome binding, the core enzyme adopts a conformation that promotes EDC-induced crosslinking within the polymerase. A similar crosslink is produced with the core enzyme alone in the presence of 250 mM KCl (Figure 2.3A, 250 mM KCl). RNA polymerase can be coaxed into different functional states by manipulating the solvent conditions (Ruff, Kontur et al. 2015; Ruff, Record et al. 2015). The similarity of the two crosslinks may point to a similar conformation of the RNA polymerase when bound to the ribosome and in the presence of 250 mM KCl.

EDC induces a limited number of crosslinks between RNA polymerase and the ribosome.

MS analysis of the crosslink identified several ribosomal proteins that co-migrate with the intramolecularly crosslinked polymerase. These ribosomal proteins are less abundant than the α, β, or β' subunits in the crosslinked band (Figure 2.3B), implying that only a fraction experienced an additional crosslinking event to a ribosomal protein. Except for minuscule amounts of β and β' subunits, no other protein can be identified at the relative mobility of the crosslinked species in the absence of the chemical crosslinker (Table S1). The crosslinked species resolve into at least three bands on Tris-acetate SDS gels (Figure S2.5). LC-MS/MS analysis of two of these bands confirms that the single crosslinked species on our standard Tris-glycine gel indeed contains multiple components. Common to all three analyzed crosslinks are β, β', S6, S9, and L7/L12

(Figure 2.3C; L7 is the acetylated form of L12. The ratio of L7 to L12 varies with the cell's growth phase (Gordiyenko, Deroo et al. 2008)). The observed crosslinks place the ribosome-bound RNA polymerase on the cytosolic site of the small ribosomal subunit, covering the mRNA exit and entry sites (Figure 2.4C). The restricted number of ribosomal proteins in the crosslinks further hints at a defined arrangement between the RNA polymerase and the ribosome, which also supports our observation of a stoichiometric complex between RNA polymerase and ribosomes in solution.

Crosslinks between RNA polymerase and ribosomal subunits overlap with those between RNA polymerase and the ribosome.

The same crosslinked species are present on a Tris-acetate gel when the RNA polymerase is crosslinked to the small and to the large ribosomal subunits. LC-MS/MS analysis of two crosslinked species of the small and of the large ribosomal subunit indicates that the ribosomal proteins have a similar abundance relative to that of the RNA polymerase subunit, as they do when the RNA polymerase is crosslinked to the ribosome. Common to the two RNA polymerase-small subunit crosslinks are the RNA polymerase β' subunit and the small ribosomal subunit proteins S1, S2, S6, S9, S11, and S7 (Figure 2.3D). All of the identified ribosomal proteins cluster next to the mRNA exit site on the small ribosomal subunit (Figure 2.4A).

Common to the two RNA polymerase-large ribosomal subunit crosslinks are the β and β' RNA polymerase subunits and the ribosomal proteins L1, S6, L9, L7/L12, and L19 (Figure 2.3E). The proteins of the large ribosomal subunit are clustered at the tRNA entry (L7/L12) and exit sites (L1 and L9). L19 is the only ribosomal protein on the

interface between the small and large ribosomal subunits (Figure 2.4B), which, upon association of these subunits, is buried within the ribosome. These identified crosslinks position the RNA polymerase on the ribosomal subunit interface of the large subunit, indicating that only the RNA polymerase interface of the small ribosomal subunit contributes to RNA polymerase binding to the ribosome.

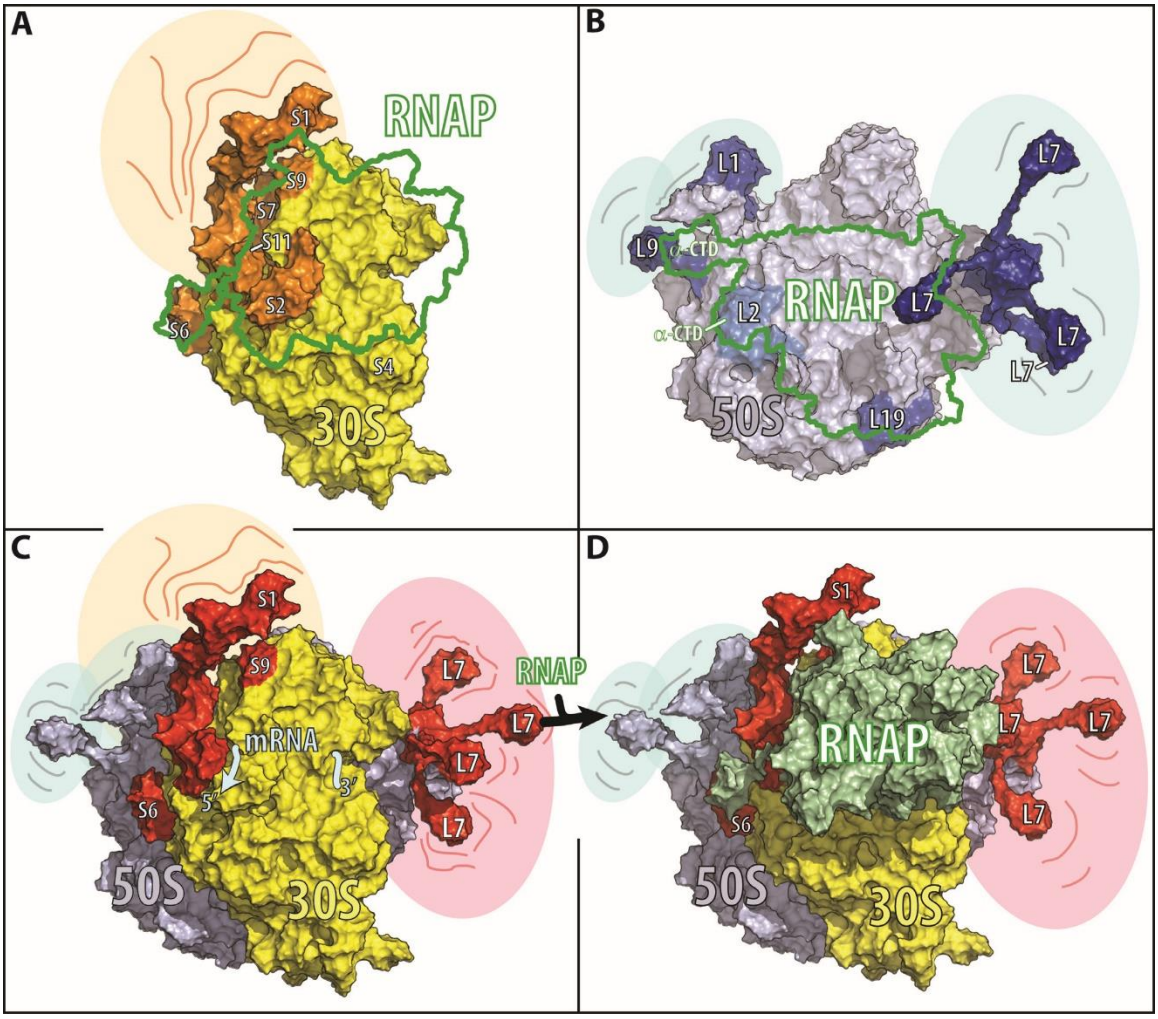
A
RNAP
S1
S9
S7
S11
S2
S6
S4
30S
B
L1
L7
L9
α-CTD
RNAP
L2
L7
α-CTD
L7
L7
50S
L19
C
S1
S9
L7
RNAP
L7
mRNA
L7
3'
5'
S6
L7
50S
30S
D
S1
L7
L7
RNAP
L7
S6
L7
50S
30S

Figure 2.4: Models for RNA polymerase binding to the small ribosomal subunit, the large ribosomal subunit, and the ribosome. Ribosomal proteins crosslinked to RNA polymerase (RNAP, in green) are indicated in orange for the small ribosomal subunit (30S, in yellow), in blue for the large ribosomal subunit (50S, in gray), and red for the whole ribosome (70S). The model of the full-length RNA polymerase is based on the cryo-EM structure of *E. coli* RNA polymerase (PDB: 5UPC (Kang, Olinares et al. 2017)) and the NMR structure of the C-terminal domain of the α subunit (PDB: 2MAX (Borin, Tang et al. 2014)). The models of the ribosome and its subunits are based on the cryo-EM structure of *E. coli* ribosomes (PDB: 4V6Q (Agirrezabala, Liao et al. 2012)). To complete the ribosome model, the L1 stalk is modeled based on the crystal structure of the L1 stalk (PDB: 1U63 (Nevskaya, Tishchenko et al. 2005)), the L7/L12 stalk is based on the NMR structure of L10•$(L7/L12)_4$ (PDB 1RQU (Bocharov, Sobol et al. 2004)), the C-terminal residues of ribosomal protein S6 are modeled according to the full-length S6 in the cryo-EM structure of the ribosome (PDB: 4V6P (Agirrezabala, Liao et al. 2012)), and ribosomal protein S1 is modeled based on the crystal structure of domain I in complex with ribosomal protein S2 (PDB 4TOI (Byrgazov, Manoharadas et al. 2012)) and the NMR structures of domains 4 and 6 (PDB 2KHI and 2KHJ (Salah, Bisaglia et al. 2009)). The relative position of the RNA polymerase on the small ribosomal subunit and ribosome is restrained by the identified crosslinks as well as by the assumption that the nascent RNA between the RNA polymerase and ribosome has the shortest length during transcription-translation coupling. The shaded areas surrounding different components of the ribosome in **A**-**D** indicate spatial flexibility. On the small ribosomal subunit the

flexible region involves ribosomal protein S1; on the large ribosomal subunit it involves the L1 stalk, the L7 stalk, and of the ribosomal protein L9; and on the ribosome the L1 stalk, the L7 stalk, and the ribosomal proteins S1 and L9. **A)** The small ribosomal subunit viewed from the cytosolic site with crosslinked ribosomal proteins S6, S2, S11, S7, S9, and S1 in orange. The green boundary outlines the RNA polymerase position on the small ribosomal subunit. **B)** The large subunit viewed from the ribosomal subunit interface. In blue are the crosslinked proteins L1, L9, and L19, and in light blue is L2, a known binding partner of the RNA polymerase α-subunit. **C)** Ribosome with identified crosslinked proteins S6, S9, and L7 in red. **D)** Model of RNA polymerase-ribosome interactions based on the chemical crosslinks identified in this study. The figures were prepared in PyMOL (Schrödinger, LLC) using a solvent radius of 5 Ångstrom.

Discussion:

In *E. coli*, the translation rate is the same as the transcription rate (Proshkin, Rahmouni et al. 2010). The first ribosome trailing the transcribing RNA polymerase directly assists the polymerase during elongation (Proshkin, Rahmouni et al. 2010) and suppresses transcription termination within coding regions (Lesnik, Sampath et al. 2001; de Smit, Verlaan et al. 2009; Li, Zhang et al. 2016). Recent ribosome profiling studies show that translational elongation speed is not uniform (Li, Oh et al. 2012; Mohammad, Woolstenhulme et al. 2016). Prolonged pausing of translation decouples RNA synthesis from protein synthesis, causing the premature termination of transcription (Elgamal, Artsimovitch et al. 2016). Prolonged pausing of transcription turns the RNA polymerase into a roadblock for the leading ribosome. Any barrier encountered by the translating ribosome promotes the loss of its reading frame (Caliskan, Katunin et al. 2014; Chen, Petrov et al. 2014; Kim, Liu et al. 2014; Yan, Wen et al. 2015), which, in turn, results in the premature termination of translation. Premature translation termination causes premature Rho-dependent and Rho-independent transcription termination (Adhya and Gottesman 1978; Elgamal, Artsimovitch et al. 2016; Li, Zhang et al. 2016). Consequently, the synchronization of transcription and translation is essential for gene expression in eubacteria.

The direct interaction between the RNA polymerase and the ribosome results in stoichiometric complex formation. The strength of the interaction is modulated by the functional state of the RNA polymerase and the ribosome (Figure 2.2C), with the vacant ribosome binding more tightly to the core polymerase and holoenzyme than to the

transcription elongation complex. Although this analysis was performed with stable functional states, the results suggest that the different states the RNA polymerase and ribosome adopt during transcription and translation will modulate the interaction between them. For instance, the binding of DNA to the RNA polymerase restricts the number of conformations the polymerase can sample, while binding of σ^{70} does not affect the conformational dynamics of the polymerase (Chakraborty, Wang et al. 2012). Therefore, when bound to the ribosome, the core and holoenzyme may adopt a conformation that is not attainable by the transcription elongation complex, but enables a better interaction with the ribosome, thus explaining the observed difference in the binding affinities.

The spatial arrangement of the polymerase and ribosome is reflected in the proteins that are crosslinked within the complex and allows us to triangulate the location of the RNA polymerase on the surface of the subunits and the ribosome. The interface between the polymerase and the large subunit is located on the face that binds the small subunit, which, upon association with the small subunit, is buried within the ribosome (Figure 2.4B and 2.4C). Modeling the binding of RNA polymerase on the large ribosomal subunit places the RNA polymerase in close proximity to the ribosomal protein L2, which is known to bind the α subunit of RNA polymerase (Rippa, Cirulli et al. 2010). The set of proteins crosslinked in the complex with ribosomes overlaps with that of the small ribosomal subunit complex (Figure 2.3C and 2.3D), clustering around the mRNA exit site of the ribosome (Figure 2.4A and 2.4C), hinting at the possible coordination between the transcription and translation initiation of the nascent RNA.

During the initial phase of translation initiation, the mRNA binds to a ‘‘standby’’ site on the ribosome that encompasses the entire mRNA exit site (Yusupova, Jenner et al. 2006). The binding of translation initiation factors repositions the mRNA on the small ribosomal subunit, permitting translation initiation to progress (Gualerzi and Pon 2015). *In vivo*, transcription pauses near the promoter (Mooney, Davis et al. 2009; Larson, Mooney et al. 2014). This pausing of the RNA polymerase seems to allow the ribosome to initiate translation and catch up with the polymerase. The “standby” position of the mRNA may interfere with the interaction of the RNA polymerase with the mRNA exit site, thus coordinating the accommodation of the nascent RNA and the subsequent initiation of translation with the resumption of transcription. During eukaryotic translation initiation, initiation factor eIF3 also engages with the mRNA in the exit site while it is bound to both the mRNA entry and exit sites, thereby coordinating mRNA accommodation with the downstream steps of translation initiation (Aylett, Boehringer et al. 2015; Aitken, Beznosková et al. 2016).

Common to the identified RNA polymerase interfaces on the ribosome and small ribosomal subunit are ribosomal proteins S6 and S9; additionally, S1 is present in all but one of the identified crosslinked species (Figure 2.3C). Ribosomal protein S1 binds to RNA polymerase near the exit site of the nascent RNA (Sukhodolets and Garges 2003; Liu, Zuo et al. 2015) and promotes the recycling of the RNA polymerase after transcription termination (Sukhodolets, Garges et al. 2006). Similar to the C-terminal domains of ribosomal protein S1, the two to six glutamic acid residues of the C-terminal tail of S6 extend away from the ribosome, reaching into the surrounding solution. This

local accumulation of glutamic acid residues may form the same salt bridges with the RNA polymerase as free glutamate at high cellular concentrations, when it releases the RNA polymerase stalled at the *osmY* promoter DNA (Lee and Gralla 2004). Although ribosomal protein S9 is farther from the mRNA exit site, its long C-terminal tail reaches through the head of the subunit to the mRNA channel. In the mRNA channel, the tail stabilizes the tRNA-mRNA interactions at the P-site (Selmer, Dunham et al. 2006), contributing to the fidelity of translation initiation and the maintenance of the reading frame (Arora, Bhamidimarri et al. 2013) (Figure 2.4A and 2.4D).

The potential mechanistic implications of the observed interaction of the RNA polymerase with the large ribosomal subunit are difficult to reconcile with our current understanding of the coupling of transcription and translation. However, this interaction might hint at the potential coordination of ribosomal RNA transcription and ribosome assembly during ribosome biogenesis. Ribosome assembly factors can, like RNA polymerase, bind to mature ribosome particles *in vitro* and *in vivo* (Sharma, Barat et al. 2005; Qin, Polacek et al. 2006; Jain 2008; Gibbs, Moon et al. 2017).

In summary, our binding studies suggest that during transcription-translation coupling, the RNA polymerase binds to the cytosolic site of the small ribosomal subunit, extending from the mRNA exit to the mRNA entry site. This binding allows the polymerase to monitor the translation rate of the ribosome while providing it with more nascent RNA. The coordination of transcription and translation may be conferred via the interaction with ribosomal protein S9. The tightest interaction between RNA polymerase

and the ribosome arises from an RNA polymerase conformation that is distinct from that of the TEC.

While revising our manuscript, Cramer, Landick, and colleagues published a 9 A cryo-EM structure of the RNA ˚ polymerase•ribosome complex (Kohler, Mooney et al. 2017). Although the stoichiometry and the ribosomal interface components of our model agree well with that of the EM structure, the relative orientation of the polymerase and ribosome are distinct. The EM structure places the polymerase more towards the mRNA entry site of the ribosome, with the nascent RNA exit site of the polymerase in closer contact with the mRNA entry site of the ribosome and the RNA polymerase rotated more towards the cytosol. Further studies will be required to understand the origins of these differences.

Our biochemical study, as well as the recently published EM structure of the RNA polymerase•ribosome complex (Kohler, Mooney et al. 2017), demonstrates the existence of a direct interaction between RNA polymerase and ribosomes, and points to its functional relevance during transcription–translation coupling. However, the here determined equilibrium constants only reflect the strength of the interaction between two the molecules, but not the time that interaction will persist in a dynamic setting, such as during on-going transcription and translation. Consequently, detailed kinetic studies will be needed to fully understand the feedback between the RNA polymerase and ribosome during transcription–translation coupling. The mechanistic insights derived from such studies will add to this new paradigm of how gene expression is controlled.

Funding: National Institutes of Health [R21 ES025392 to Y.W.]; University of California, Riverside (to G.B. and Y.W.). Funding for open access charge: University of California, Riverside.

Conflict of interest statement. The authors declare that there are no conflicts of interest.

Acknowledgements: We thank Mr. Carlos Rodriguez and Ms. Gabriela Sanchez for technical assistance during sample preparation, Dr. Jacques Barbet for unwavering technical support with the "Equilibrium Expert" add-in for Microsoft Excel®, Dr. Whitney Yin for critical discussion, and Mr. Tim Rowsell, Mr. Timothy Tam and Ms. Kacey Kilpatrick for assisting in the preparation of the manuscript.

Supplementary Data:

Material & Methods:

Chemicals.

RNase-free sucrose and, ultra-pure Tris were from Amresco (Solon, OH, USA), HEPES and imidazole were from Calbiochem (San Diego, CA, USA), 1-ethyl-3-(3-dimethylaminopropyl) carbodiimide (EDC) was from Pierce (Waltham, MA, USA), sulfo Nhydroxysuccinimide (sulfo-NHS) was from Chem-Impex Int'l (Wood Dale, IL, USA), and βmercaptoethanol was from Bio-Rad (Hercules, CA, USA). Poly(U)-RNA and all other chemicals were purchased from Sigma Aldrich (St. Louis, MO, USA). The oligoribonucleotide and oligodeoxyribonucleotides were from IDT (Coralville, IA, USA). All buffers were prepared with DEPC-treated water. Polyvinylidene difluoride membranes, antibodies, and Western blot luminol reagent were from Santa Cruz Biotechnology (Santa Cruz, CA, USA). The ReproSil C18-AQ resins (300 Å pore size) with 3-μm and 5-μm particle sizes used to pack the LC-MS/MS separation and trapping columns, respectively, were purchased from Dr. Maisch HPLC GmbH, Germany.

Quality assessment of purified ribosomes.

The amount of NusG present in our ribosome preparations was assessed by tandem mass spectrometry analysis. As internal standards for our assessment, ribosome samples were spiked with one-tenth or with equimolar amounts of NusG. Samples were loaded onto a 6 % SDS-polyacrylamide gel and run a few millimeters into the gel. The band containing all of the ribosomal proteins was excised from the gel. The proteins captured in the excised gel band were reduced, alkylated, and in-gel digested with

trypsin. The resulting peptide mixture was extracted and subjected to liquid chromatography-tandem mass spectrometry (LC-MS/MS) analysis as described below.

Ribosomal RNA from purified and crude ribosomes was extracted using an E.Z.N.A. Bacterial RNA kit (Omega Bio-tek, Norcross, GA, USA) according to the protocol provided by the manufacturer. The quality of the extracted ribosomal RNA was assessed after separation by microfluidic chip gel-electrophoresis with an RNA 6000 Nano kit (Agilent, Santa Clara, CA, USA).

Preparative isolation of the RNA polymerase•ribosome complex.

One milliliter of 10 µM RNA polymerase and 2.5 µM ribosomes were incubated for 15 min at 37 °C in buffer A (20 mM HEPES-KOH pH 7.5, 20 mM Mg(OAc)2, and 30 mM KCl). The mixture was loaded onto a 36- mL 10 – 40 % sucrose gradient prepared in buffer A and centrifuged in a SW32 Ti rotor for 16 hours at 24,000 rpm and 4 °C. After centrifugation, the gradient was collected in 1.8-mL fractions. The protein content of each fraction was determined by SDS-polyacrylamide gel electrophoresis. Fractions containing ribosomes with co-migrated RNA polymerase were pooled, concentrated, and buffer-exchanged into buffer A. The concentrated complex was aliquoted, flash frozen in liquid nitrogen, and stored at -80 °C until further use.

To test the stability of the complex, a frozen aliquot of the complex was diluted with buffer to a final concentration of 1 µM and incubated for 15 min at 37 °C, before analyzing the RNA polymerase-ribosome content by sucrose gradient centrifugation as described in “Separation of free RNA polymerase from ribosome-bound RNA polymerase.” To determine the quality of the ribosomal RNA, we extracted ribosomal

RNA from the purified complex and, as a positive control, from crude ribosomes, both of which were analyzed using an RNA 6000 Nano kit (Agilent).

Western blot analysis.

Proteins were electro-blotted onto a polyvinylidene difluoride membrane, probed with mouse antibodies against individual RNA polymerase subunits, incubated with horseradish peroxidase-conjugated goat anti-mouse antibodies, and visualized via a chemiluminescence reaction, which was documented with the ChemiDoc™ Touch Gel Imaging System (Bio-Rad).

Results:

*Establishing conditions for the analysis of RNA polymerase-ribosome interaction*s.

The effect of different cations and anions on ribosomes and RNA polymerase has been extensively documented (Miskin, Zamir et al. 1970; Zamir, Miskin et al. 1971; Shaner, Piatt et al. 1982; Suh, Leirmo et al. 1992). We chose to perform our studies with KCl in the presence of magnesium ions either as chloride or acetate, as these ions are compatible with both transcription (So, Davie et al. 1967) and translation (Zamir, Miskin et al. 1974).

The stability of the RNA polymerase-ribosome complex decreases with increasing concentrations of potassium chloride. Compared to 30 mM KCl in the sucrose gradient, only half the amount of the complex is detected with 125 mM KCl, and none was detected with 250 mM KCl (Figure S2.2A). RNA polymerase-ribosome complexes appear to be more stable at low salt conditions during sucrose gradient centrifugation. To prevent the dissociation of RNA polymerase-ribosome complexes during sucrose

gradient centrifugation, all analyses of complex formation were performed with sucrose gradients under low-salt conditions of 30 mM KCl and 20 mM magnesium acetate or chloride.

Supplemental Figures:

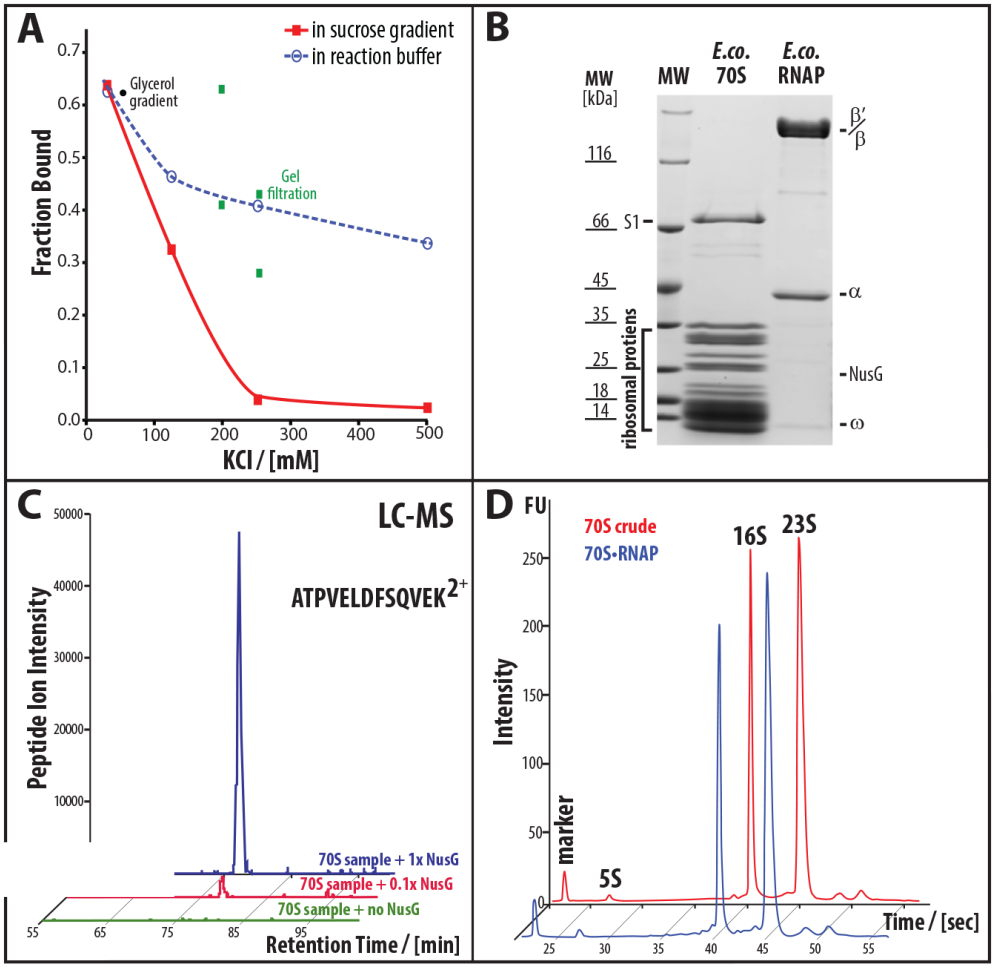
A
in sucrose gradient
in reaction buffer
Glycerol gradient
Gel filtration
Fraction Bound
KCl / [mM]
B
MW [kDa]
MW
E.co. 70S
E.co. RNAP
116
66
45
35
25
18
14
S1
ribosomal protiens
β′
β
α
NusG
ω
C
LC-MS
ATPVELDFSQVEK2+
Peptide Ion Intensity
70S sample + 1x NusG
70S sample + 0.1x NusG
70S sample + no NusG
Retention Time / [min]
D
FU
70S crude
70S•RNAP
16S
23S
Intensity
marker
5S
Time / [sec]

Figure S2.1: Characterization of the RNA polymerase, ribosomes and complexes thereof. **A)** Establishing experimental conditions for analysis of the complex formation. Titration of RNA polymerase-ribosome mixtures with KCl during the reaction (blue) and during sucrose gradient centrifugation (red). In black is the fraction of bound RNA polymerase as determined by glycerol gradient centrifugation at a low salt concentration. In green are the fractions of bound RNA polymerase as determined by gel filtration. **B)** SDS-polyacrylamide gel electrophoresis (SDS-PAGE) analysis of purified RNA polymerase (RNAP) and ribosome (70S) samples from Escherichia coli (E.co.). The positions of ribosomal protein S1 and additional ribosomal proteins are indicated on the left of the gel image, and RNA polymerase subunits α, β, β', and ω and the expected position of NusG are indicated on the right. The molecular weights of the protein ladder are to the left side of the gel. **C)** Determination of the amount of NusG contamination of E. coli ribosomes by LC-MS/MS. Ion intensity of one tryptic-digest peptide fragment of NusG (ATPVELDFSQVEK2+). The blue and red traces are ribosome samples with NusG added in stoichiometric and sub-stoichiometric amounts. The green trace is the ribosome sample alone. **D)** Ribosomal RNA quality determined by micro-chip capillary electrophoresis. The red trace is ribosomal RNA extracted from ribosomes from cell lysates that were pelleted through a high-salt sucrose cushion. The blue trace is ribosomal RNA extracted from the purified RNA polymerase ribosome complex.

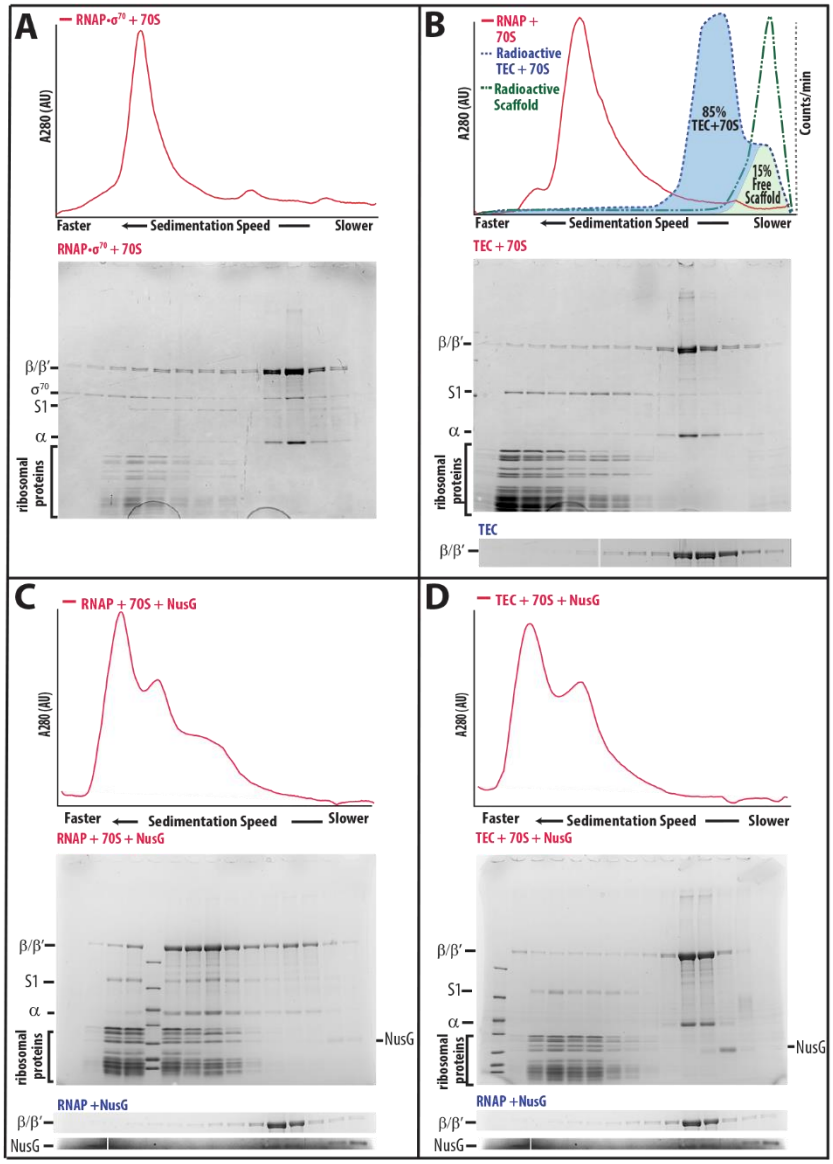
A
RNAP•σ70 + 70S
A280 (AU)
Faster
Sedimentation Speed
Slower
RNAP•σ70 + 70S
β/β′
σ70
S1
α
ribosomal proteins
B
RNAP + 70S
Radioactive TEC + 70S
Radioactive Scaffold
A280 (AU)
Counts/min
85% TEC+70S
15% Free Scaffold
Faster
Sedimentation Speed
Slower
TEC + 70S
β/β′
S1
α
ribosomal proteins
TEC
β/β′
C
RNAP + 70S + NusG
A280 (AU)
Faster
Sedimentation Speed
Slower
RNAP + 70S + NusG
β/β′
S1
α
ribosomal proteins
NusG
RNAP +NusG
β/β′
NusG
D
TEC + 70S + NusG
A280 (AU)
Faster
Sedimentation Speed
Slower
TEC + 70S + NusG
β/β′
S1
α
ribosomal proteins
NusG
RNAP +NusG
β/β′
NusG

Figure S2.2: Sucrose gradient analysis of the interactions of the vacant ribosome (70S) with A) the holoenzyme (RNAP•σ70), B) transcription elongation complex (TEC), C) the core enzyme in the presence of NusG, and D) the TEC in the presence of NusG. **A)** Analysis of the interactions between ribosome with the holoenzyme. The top panel displays the sedimentation profile of the complex recorded at 280 nm. The bottom panel displays the SDS-PAGE gel of the sucrose gradient fractions. **B)** Analysis of the interactions between the ribosome and TEC. The top panel displays the sedimentation profiles of the RNA polymerase-ribosome complex recorded at 280 nm (shown as a red solid line, left ordinate axis) and of the radioactively labeled DNA:RNA hybrid scaffold in the presence of ribosomes and alone (shown as a dashed blue line and dashdotted green line, respectively, right ordinate axis). The center panel displays the SDS-PAGE gel of the sucrose gradient analysis of the RNA polymerase•TEC complex formation. The bottom panel displays the SDS-PAGE gel of sucrose gradient analysis of the TEC alone, covering the β/β' molecular weight range. **C)** Analysis of the interactions between the ribosome, RNA polymerase, and NusG. The top panel displays the sedimentation profile of the complex recorded at 280 nm. The center panel presents the SDS-PAGE gel of the sucrose gradient fractions. The bottom panels show the SDS-PAGE gel of the sucrose gradient analysis of a mixture of RNA polymerase and NusG displaying only the regions covering β/β' and the NusG molecular weight ranges. The contrast of the NusG region has been enhanced to better visualize the NusG band. **D)** Analysis of the interactions between the ribosome, TEC, and NusG. Panels are the same for C).

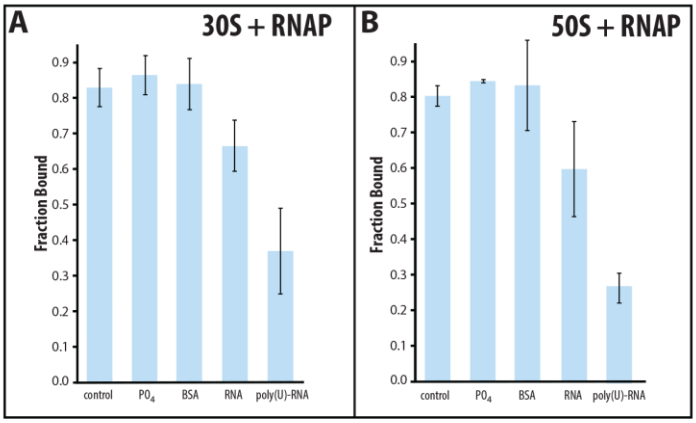

Figure S2.3: Characterizing the interactions between RNA polymerase and ribosomal subunits from E. coli. A and B) RNA polymerase binding to small ribosomal subunit (30S) and large ribosomal subunit (50S) in the presence of 10 mM phosphate buffer (PO4), 20 µM bovine serum albumin (BSA), a 14-nucleotide long RNA (RNA) at a 5 µM concentration, and 80 µg of poly(U)-RNA.

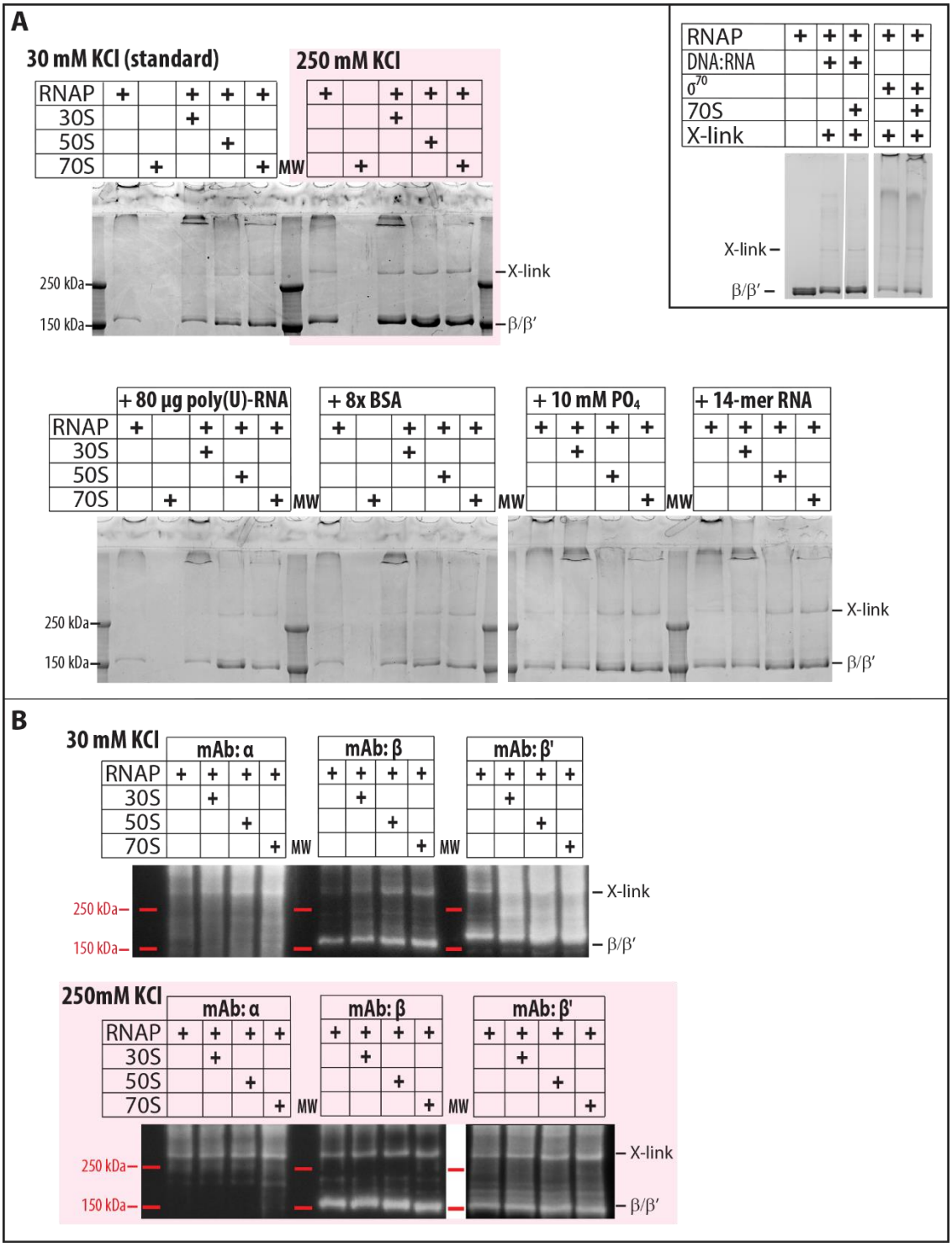
A
30 mM KCl (standard)
250 mM KCl
RNAP
30S
50S
70S
MW
250 kDa
150 kDa
X-link
β/β′
DNA:RNA
σ70
+ 80 µg poly(U)-RNA
+ 8x BSA
+ 10 mM PO4
+ 14-mer RNA
B
30 mM KCl
250mM KCl
mAb: α
mAb: β
mAb: β'

Figure S2.4: EDC crosslinking of RNA polymerase-ribosome complexes. **A)** EDC crosslinking of RNA polymerase in the presence of small ribosomal subunits (30S), large ribosomal subunits (50S), and ribosomes (70S) in 30 mM and 250 mM KCl buffer (light red background). Crosslinking experiments at 30 mM KCl were also performed in the presence of 80 μg of poly(U)-RNA, 40 μM bovine serum albumin (BSA), 10 mM phosphate buffer (PO4), and a 14- nucleotide long RNA (RNA) at a concentration of 10 μM. Inset in A) EDC crosslinking of holoenzyme and transcription elongation complex in the absence and presence of ribosomes. **B)** Western blot analysis of EDC crosslinked RNA polymerase in the presence of 30 mM KCl and 250 mM KCl (light red background) probed with monoclonal antibodies against α, β, and β'.

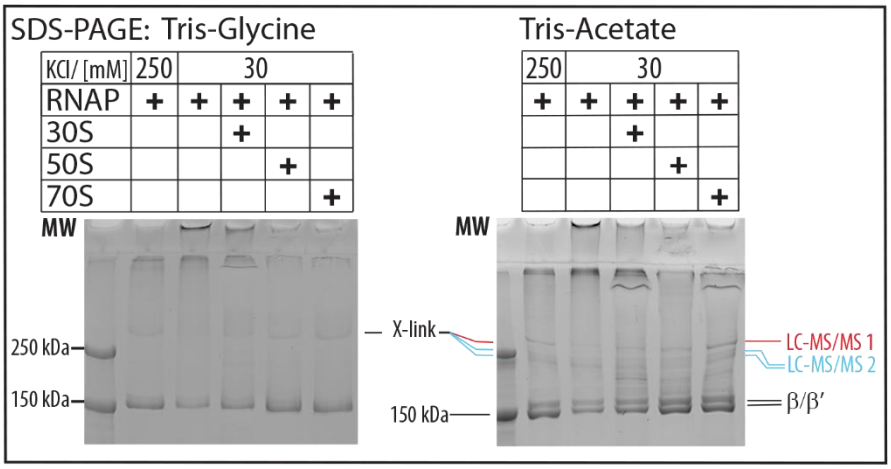

Figure S2.5: EDC crosslinking of RNA polymerase-ribosome complexes analyzed by Tris-glycine and Tris-acetate SDS-PAGE. Indicated on the right of the Tris-acetate SDS-PAGE are the bands which were extracted from the gel for further analysis by LC-MS/MS. The two bands indicated in blue were extracted as one sample for further LC-MS/MS analyses.

Protein Name - Purity of RNA polymerase

RNA polymerase, alpha subunit
RNA polymerase, beta subunit
RNA polymerase, beta prime subunit
RNA polymerase, omega subunit
predicted methltransferase, enzyme of biotin synthesis gb|ACB01978.1
hydrogenase 4, membrane subunit gb|ACB03634.1|
DNA-binding transcriptional dual regulator gb|ACB04972.1|
S-adenosyl-dependent methyltransferase activity on membrane-located substrates gb|ACB01263.1|
transcription elongation factor pTEF-b gb|ACB04465.1|
RNA polymerase, sigma 70 (sigma D) factor gb|ACB04152.1|
CPZ-55 prophage; predicted integrase gb|ACB03593.1|
predicted pilus assembly protein gb|ACB04454.1|
DNA helicase IV gb|ACB02162.1|
UDP-N-acetyl-D-mannosaminuronic acid (ManNAcA) transferase gb|ACB04824.1|
murein lipoprotein gb|ACB02879.1|

Table S2.1.1: LC-MS/MS analyses of the protein composition of purified RNA polymerase

Protein Name - Purity of 70S

50S ribosomal subunit protein L1
30S ribosomal subunit protein S5
50S ribosomal subunit protein L7/L12
50S ribosomal subunit protein L10
50S ribosomal subunit protein L2
50S ribosomal subunit protein L6
50S ribosomal subunit protein L14
50S ribosomal subunit protein L9
30S ribosomal subunit protein S4
50S ribosomal subunit protein L15
50S ribosomal subunit protein L3
30S ribosomal subunit protein S7
50S ribosomal subunit protein L11
50S ribosomal subunit protein L4
30S ribosomal subunit protein S13
50S ribosomal subunit protein L13
50S ribosomal subunit protein L22
30S ribosomal subunit protein S6
50S ribosomal subunit protein L19
30S ribosomal subunit protein S9
50S ribosomal subunit protein L16
50S ribosomal subunit protein L5
50S ribosomal subunit protein L18
30S ribosomal subunit protein S10
50S ribosomal subunit protein L17
30S ribosomal subunit protein S11
30S ribosomal subunit protein S20
50S ribosomal subunit protein L21
30S ribosomal subunit protein S8
30S ribosomal subunit protein S2
50S ribosomal subunit protein L31
30S ribosomal subunit protein S15
30S ribosomal subunit protein S18
50S ribosomal subunit protein L33
50S ribosomal subunit protein L24
30S ribosomal subunit protein S21
30S ribosomal subunit protein S19
50S ribosomal subunit protein L29
50S ribosomal subunit protein L20
30S ribosomal subunit protein S16
50S ribosomal subunit protein L25
50S ribosomal subunit protein L28
30S ribosomal subunit protein S14
30S ribosomal subunit protein S1
50S ribosomal subunit protein L30
50S ribosomal subunit protein L27
50S ribosomal subunit protein L23
50S ribosomal subunit protein L34
50S ribosomal subunit protein L32
membrane anchored protein involved in growth of wall at septum gb|ACB01274.1
30S ribosomal subunit protein S17
peptidyl-tRNA hydrolase gb|ACB02374.1|
RNA polymerase, alpha subunit
50S ribosomal subunit protein L35
RNA polymerase, beta subunit
RNA polymerase, beta prime subunit

ribose 1,5-bisphosphokinase gb|ACB05090.1|
gb|ACB04341.1| predicted amino-acid transporter subunit; ATP-binding component of ABC superfamily
gb|ACB04257.1| predicted RNA-binding protein
exonuclease
murein lipoprotein

Table S2.1.2: LC-MS/MS analyses.

	RNAP-70S_Glycine_Control_No X-Link			**RNAP-70S_X-linked_Glycine**		
Protein Name	Spectral Index - Trial 1	Spectral Index - Trial 2	Spectral Index - Trial 3	Spectral Index - Trial 1	Spectral Index - Trial 2	Spectral Index - Trial 3
RNA polymerase, beta subunit	72.67	112.66	71.44	56620.47	235181.24	37973.7
RNA polymerase, beta prime subunit	4.34	65.75	51.99	46463.49	225156.48	33893.44

	RNAP-70S_X-linked_AcOH_top_band			**RNAP-70S_X-linked_AcOH_bottom**		
Protein Name	Spectral Index - Trial 1	Spectral Index - Trial 1	Spectral Index - Trial 1	Spectral Index - Trial 1	Spectral Index - Trial 2	Spectral Index - Trial 3
RNA polymerase, beta subunit	78002.98	41994.78	41994.78	41994.78	35043.22	35257.82
RNA polymerase, beta prime subunit	109090.26	79303.48	79303.48	79303.48	43685.15	39953.09

	RNAP-50S_X-linked_AcOH_top			**RNAP-50S_X-linked_AcOH_bottom**		
Protein Name	Spectral Index - Trial 1	Spectral Index - Trial 2	Spectral Index - Trial 3	Spectral Index - Trial 1	Spectral Index - Trial 2	Spectral Index - Trial 3
RNA polymerase, beta subunit	17992.55	35043.22	35257.82	32234.72	35587.06	13090.16

RNA polymerase, beta prime subunit	32036.25	43685.15	39953.09	72885.57	35297.32	18090.26

	RNAP-30S_X-linked_AcOH_top			**RNAP-30S_X-linked_AcOH_bottom**		
Protein Name	Spectral Index - Trial 1	Spectral Index - Trial 2	Spectral Index - Trial 3	Spectral Index - Trial 1	Spectral Index - Trial 2	Spectral Index - Trial 3
RNA polymerase, beta subunit	10108.05	16827.87	20774.96	N/A	11634.13	20929.21
RNA polymerase, beta prime subunit	8850.75	20453.45	27675.2	10285	9342.57	23164.18

Table S2.1.3: LC-MS/MS analyses of the background at the relative mobility of the crosslinked band in Tris-glycine SDS PAGE (RNAP-70S_Glycine_Control), and the different crosslinked species isolated using Tris-glycine and Tris-acetate SDS-PAGE.

Protein Name - RNAP-70S_X-linked_Glycine	**Average Normalized Spectral Index**	**Standard Deviation**
RNA polymerase, beta prime subunit	1.0000	0.0000
RNA polymerase, beta subunit	0.8902	0.0684
RNA polymerase, alpha subunit	0.5693	0.1082
RNA polymerase, omega subunit	0.1346	0.0474
30S ribosomal subunit protein S1	0.0049	0.0039
30S ribosomal subunit protein S9	0.0145	0.0033
50S ribosomal subunit protein L7/L12	0.1203	0.0303
30S ribosomal subunit protein S6	0.0442	0.0060

Table S2.1.4: Average normalized Spectral index of crosslinked RNA polymerase and ribosomal proteins.

Chapter 3:

The Intrinsic Effects of Universally Conserved Ribosomal Proteins uS2, uS3, and uS4 on Transcription

Unpublished work

Abstract:

In bacteria, transcription and translation are coupled and ribosomes directly contact RNA polymerase. The contacts are formed between the RNA exit site of the RNA polymerase and ribosomal proteins uS2, uS3, or uS4. Here, we gauged the intrinsic effects uS2, uS3, and uS4 exert on transcription. We determined their effects on transcription termination and pausing as well as their ability to bind to the polymerase. All three ribosomal proteins reduced ρ-dependent and intrinsic termination to a different degree. They all increased the time the polymerase required to escape the *his* pause. While uS2 bound directly to the polymerase, it had the least effect on transcription, whereas uS3 had the most prominent. We suggest that during coupling of transcription and translation, uS2 acts as an anchor of the ribosome for the polymerase. uS3 and uS4 appear to affect transcription depending on the length of the nascent RNA between the ribosome and polymerase. All three ribosomal proteins may coordinate the transcription of ribosomal RNA with its assembly into a ribosomal subunit. We speculate that the intrinsic effects of ribosomal proteins on transcription are the reason for the tight regulation of their expression in the cell.

Introduction:

Escherichia coli has a single multi-subunit RNA polymerase (RNAP) that transcribes all cellular RNA. The cellular level of many RNAs is regulated while the RNA is being transcribed. This regulation depends on DNA-encoded pause, arrest, and termination signals. Factors that bind the polymerase can modify its response to these signals (Belogurov and Artsimovitch 2015). On protein-encoding genes, the RNAP's response is also affected by the ribosome. Because bacteria lack a nuclear membrane, ribosomes can directly interact with RNAP (Fan, Conn et al. 2017; Conn, Diggs et al. 2019; Irastortza-Olaziregi and Amster-Choder 2021). This allows the ribosome to influence RNAP's response to DNA-encoded signals. The direct interaction also allows the RNAP to affect the ribosome. For instance, when RNAP pauses close to a promoter site (Mooney, Davis et al. 2009), it impels the ribosome to bind and translate the RNAP-bound nascent RNA. The translating ribosome allows the paused polymerase to resume transcription (Chatterjee, Chauvier et al. 2021) and even resuscitate arrested RNAPs (Stevenson-Jones, Woodgate et al. 2020). In vivo, inhibition of translation results in the genome-wide arrest of transcription (Zhang, Mooney et al. 2014). Arrested RNAPs are a barrier for the DNA replication machinery, jeopardizing the processivity of DNA replication and with it the integrity of the genome (Mirkin and Mirkin 2007; Dutta, Shatalin et al. 2011).

When transcribing a protein-encoding gene, RNAP is usually trailed by a ribosome (Miller, Hamkalo et al. 1970). The trailing ribosome suppresses the RNAP from prematurely terminating transcription. Both Rho (ρ) factor-dependent and ρ-

independent (aka intrinsic) termination are suppressed. However, when the gap between RNAP and the first, leading ribosome is too large, transcription will terminate (de Smit, Verlaan et al. 2008; de Smit, Verlaan et al. 2009; Li, Zhang et al. 2016). A gap can open because the first ribosome may be too slow or terminate translation prematurely. Once the ribosome undergoes translation termination, it will dissociate from the nascent RNA. This will allow the ρ factor to translocate unhindered along the nascent RNA towards the RNAP. At the RNAP, the ρ factor will induce transcription termination, thus curtailing the transcription of downstream sequences and genes. In short, the first, pioneering round of translation by the first, leading ribosome ensures the quality of the resulting transcript. The discovery of this control mechanism, aka polarity effect, was early evidence that mRNAs are translated while they are being transcribed (Adhya and Gottesman 1978).

The close trailing of RNAP by the ribosome in vivo supports the hypothesis of a direct interaction between them. The recent burst of structural work seems to confirm this view ((Demo, Rasouly et al. 2017; Fan, Conn et al. 2017; Kohler, Mooney et al. 2017; Webster, Takacs et al. 2020) reviewed in (Conn, Diggs et al. 2019) and (Irastortza-Olaziregi and Amster-Choder 2021)). The latest structures reveal that transcription factors NusA and NusG can bridge RNAP and the ribosome (O'Reilly, Xue et al. 2020; Wang, Molodtsov et al. 2020; Washburn, Zuber et al. 2020). In most of these structures, RNAP directs its nascent RNA towards the mRNA entry site of the ribosome. The direct contacts between RNAP and the ribosome that are shared among these different structures, are formed between the RNA exit site on the RNAP and ribosomal proteins

uS2, uS3, and uS4 on the ribosome (Kohler, Mooney et al. 2017; Wang, Molodtsov et al. 2020; Webster, Takacs et al. 2020).

The ribosomal proteins lining the RNAP-binding interfaces have compact, globular structures (Brodersen, Clemons et al. 2002). This suggests that they adopt a similar compact structure off the ribosome in solution or when bound to the RNAP. Off the ribosome, uS4 adopts the same compact structure in solution (Markus, Gerstner et al. 1998) and can suppress ρ-dependent transcription termination (Torres, Condon et al. 2001). uS4 is not the only ribosomal protein with an intrinsic effect on transcription. Ribosomal protein bS1 promotes the recycling of polymerases that have terminated transcription (Sukhodolets, Garges et al. 2006). Ribosomal protein uL2 directly binds the alpha subunit of the polymerase and promotes transcription initiation from ribosomal promoter sites (Rippa, Cirulli et al. 2010). Ribosomal proteins L3 and L14 reduce ρ-dependent termination (Torres, Condon et al. 2001). Ribosomal protein uS10, aka NusE, can bind RNAP directly (Mason and Greenblatt 1991; Sukhodolets and Garges 2003; Drögemüller, Strauß et al. 2015). As part of a larger RNAP complex, uS10 enables the RNAP to transcribe faster and suppress termination. The known components of this complex are RNAP, NusA, NusB, NusE (aka uS10), NusG, and depending on the biological context, other factors (DeVito and Das 1994; Nudler and Gottesman 2002; Said, Krupp et al. 2017; Huang, Said et al. 2019; Krupp, Said et al. 2019). Not all ribosomal proteins promote transcription. For example, an excess of ribosomal protein uL4 will downregulate its own expression (Zengel, Mueckl et al. 1980). The expression of most ribosomal proteins is regulated at the translational level (Mikhaylina, Nikonova

et al. 2021). uL4 not only regulates the translation but also the transcription of its operon. Its operon, the uS10 operon, contains next to uL4 ten other ribosomal genes. Binding of uL4 to the 5'-UTR of its operon terminates transcription in the presence of NusA.

Our knowledge of the direct interaction between RNAP and ribosome is mainly based on structure work. The effect of these interactions on transcription and translation remains less explored. We decided to explore the effect of these interactions on transcription. Each interaction consists of several RNAP-ribosome contacts. Each contact is formed between RNAP and a ribosomal protein. In most structures, ribosomal proteins uS2, uS3, and uS4 contact RNAP. Proteins that interact with RNAP may affect the polymerase's activity. They may increase or decrease the likelihood of the polymerase to terminate or pause transcription (Burns, Richardson et al. 1998; Sevostyanova, Belogurov et al. 2011). Here we set out to determine the intrinsic effect(s) uS2, uS3, and uS4 exert on transcription termination and pausing.

Materials and Methods

All chemicals were purchased from Sigma–Aldrich (St. Louis, MO, USA). The genomic DNA of E. coli K12 was obtained from the American Type Culture Collection (Manassas, VA, USA), pETite N-His and pETite N-His Sumo plasmids were from Lucigen (Middleton, WI, USA), and all oligonucleotides from Integrated DNA Technologies (Coralville, IA, USA). Chemically competent T7 Express and BL21(DE3) cells were purchased from New England Biolabs (Ipswich, MA, USA). DNA sequencing was performed at GENEWIZ (La Jolla, CA, USA).

3.1. Protein production and purification

Overexpression vectors for the many proteins required for this work were kind gifts from several generous colleagues. Vectors for the ribosomal proteins uS2, uS3, uS4, and uS10 were provided by Dr. Harry Noller, for ρ factor by Dr. James Berger, for RNAP and σ^{70}, i.e., pVS10 (T7P-α-β-β′-His6-ω) and pIA1127 (T7P-His6-TEV-σ70[1-613]), by Dr. Irina Artsimovitch, and NusB by Dr. Markus C. Wahl.

All operations were carried out on ice or at 4ºC unless specified otherwise. All cells were lysed by passing the resuspended cells three to five times through an EmulsiFlex-C3 homogenizer set at 5,000-15,000 psi. All samples were concentrated using either 15 or 50 mL Amicon ultrafiltration units with appropriate MW cutoffs at 4,000x g. Centrifugation was carried out in an SS34 rotor unless otherwise specified. For ease of tracking the ionic and buffering conditions of each buffer, we named all buffers using a combination of abbreviations and subscripts. Each abbreviation identified a component of the buffer and then the concentration in millimolar of the component in solution. Tris, HEPES, sodium acetate, imidazole, and phosphate buffer are abbreviated with T, H, NaAc, I, and P; NaCl, KCl, (NH4)2SO4, NH4Cl, and MgCl2 with Na, K, Am, N, and M; β-mercaptoethanol, Dithiothreitol, Glycerol, Sucrose, and EDTA with SH, DTT, Gol, Suc, and E.

Purification of σ^{70}

Transcription factor σ^{70} was overexpressed with a C-terminal TEV protease site followed by a His-tag (σ^{70}-TEV-His6). For expression, the cells were grown in Terrific

Broth media to an OD of 0.6 before protein expression was induced with 0.5 mM IPTG. Five hours after induction at 30°C, cells were harvested, flash frozen in liquid N2, and stored at -80°C until further use.

Approximately 5 g of cells were resuspended in a buffer containing T20Na100 (20 mM Tris-HCl pH 8.0 and 100 mM NaCl) and lysed. Lysed cells were centrifuged at 16,000 rpm for 1 hour. The soluble fraction was loaded onto a 20 mL Ni-NTA column. The column was washed with 20-60 mL of a buffer containing T20Na500I20 (20 mM Tris-HCl pH 8.0, 500 mM NaCl, and 20 mM imidazole-HCl pH 8.0). The protein was eluted from the column with a linear gradient from T20Na100 to T20Na100I1000 (20 mM Tris-HCl pH 8.0, 100 mM NaCl, and 1,000 mM imidazole-HCl pH 8.0). Gradient fractions containing pure σ70-TEV-His6 were pooled and dialyzed into T20Na100. Dialyzed σ70-TEV-His6 was mixed with 1.5 mg of TEV protease and incubated overnight with constant stirring at 100 rpm. The next day the sample was diluted to 50 mL with T20Na100 and loaded onto a 20 mL Ni-NTA column. The flow-through containing σ70 was concentrated, aliquoted, frozen in liquid N2, and stored at -80°C until further use.

Purification of RNA polymerase core enzyme

E. coli RNA polymerase was purified using a well-established protocol with minor changes (Svetlov and Artsimovitch 2015). In brief, BL21(DE3) cells containing pVS10, a plasmid that contains all subunits of the RNA polymerase under the control of a single T7 promoter [T7P-α-β-β'-His6-ω]. For expression, the cells were grown in LB

media to an OD of 1.2 before protein expression was induced with 1.0 mM IPTG. Five hours after induction, cells were harvested, flash frozen in liquid N2, and stored at -80°C until further use.

5-8 grams of harvested cells were resuspended in 50 mL lysis buffer T20Na150E2SH2 (20 mM Tris-HCl pH 8.0, 150 mM NaCl, 2 mM EDTA, and 2 mM β-mercaptoethanol). Just before lysis, PMSF was added to a final concentration of 1.4 mM. Lysed cells were then centrifuged at 13,000 rpm for 30 minutes, and the soluble fraction was collected. 4 mL of a 10% polyethyleneimine (Wu, Peng et al.) neutralized with HCl was slowly added to the soluble fraction under constant stirring. The sample was then centrifuged at 13,000 rpm for 30 min. The pellet was washed twice with 25 mL of T20Na200E2SH2 (20 mM Tris-HCl pH 8.0, 200 mM NaCl, 2 mM EDTA, and 2 mM β-mercaptoethanol). The pellet was extracted twice using 20 mL of T20Na1000E2SH2 (20 mM Tris-HCl pH 8.0, 1,000 mM NaCl, 2 mM EDTA, and 2 mM β-mercaptoethanol). Under constant stirring, solid ammonium sulfate was slowly added to the 40 mL of clarified extract to a final concentration of 0.3 g/mL and incubated overnight. The ammonium sulfate pellet was collected by centrifugation at 13,000 rpm for 30 minutes. The collected pellet was resuspended in 20 mL T20Na1000E2SH2Am2000 (20 mM Tris-HCl pH 8.0, 1,000 mM NaCl, 2 mM EDTA, 2 mM β-mercaptoethanol, and 2,000 mM (NH4)2SO4), centrifuged at 13,000 rpm for 30 min, before resuspending the collected pellet in 20 mL T20E2SH1Gol5% (20 mM Tris-HCl pH 8.0, 2 mM EDTA,1 mM β-mercaptoethanol, and 5% [v/v] Glycerol). The resuspended pellet was dialyzed three times against 1 L of T20Na30E2SH2Gol5% (20 mM Tris-HCl pH 7.3, 30 mM NaCl, 2

mM EDTA, 2 mM β-mercaptoethanol, and 5% [v/v] Glycerol) for at least 45 minutes each time. This suspension was clarified by ultracentrifugation for 30 min at 30,000 rpm in a Beckman Type 45 Ti rotor. The collected supernatant was spilt in half. Each half was loaded onto a 20 mL SP Sepharose column and the protein was eluted by using a linear gradient from T10Na50E1SH1Gol5% (10 mM Tris-HCl pH 7.3, 50 mM NaCl, 1 mM EDTA, 2 mM β-mercaptoethanol, and 5% [v/v] Glycerol) to T10Na500E1SH1Gol5% (10 mM Tris-HCl pH 7.3, 500 mM NaCl, 1 mM EDTA, 2 mM β-mercaptoethanol, and 5% [v/v] Glycerol) over ten column volumes. Before loading the second half of the 45 Ti-clarified protein solution onto the 20 mL SP Sepharose column, the column was washed with 10 column volumes of T10Na1500E1SH1Gol5% (10 mM Tris-HCl pH 7.3, 1500 mM NaCl, 1 mM EDTA, 2 mM β-mercaptoethanol, and 5% [v/v] Glycerol). The fractions containing RNA polymerase core enzyme (~25-30 mL) were combined and diluted to 140 mL with T20E1SH1Gol5% (20 mM Tris-HCl pH 8.0, 1 mM EDTA, 1 mM β-mercaptoethanol, and 5% [v/v] Glycerol). The sample was then loaded onto a 6 mL Resource Q column and eluted using the same buffer and protocol as for SP Sepharose column separation. Fractions containing RNAP core enzyme at a purity of at least 95% were combined, buffer exchanged into T20Na200DTT2 (20 mM Tris-HCl pH 8.0, 200 mM NaCl, and 2 mM DTT) and concentrated to 250 µL (>10 mg/mL). This sample was immediately used to prepare holoenzyme.

Formation of RNA polymerase holoenzyme

Purified core RNA polymerase and purified σ70 were mixed in a 1:3 molar ratio (Murakami 2013). The mixture was incubated in T20Na200DTT2Gol2% (20 mM Tris-

HCl pH 8.0, 200 mM NaCl, 2 mM DTT, and 2% [v/v] Glycerol) at room temperature for 15 minutes, before centrifuging for five minutes at 19,000x g and loading onto a 320 mL Superdex 200 column equilibrated in T20Na200DTT2Gol2%. The fractions containing pure stoichiometric amounts of RNA polymerase holoenzyme were combined and concentrated to more than 10 mg/mL (or 25 μM), aliquoted, flash frozen in liquid N2, and stored at -80°C.

Purification of ribosomal proteins

Ribosomal proteins were overexpressed and purified according to (Culver and Noller 1999) with minor modifications, i.e., T7 express cells were used instead of BL21(DE3) for protein overexpression.

The T7 express cells transformed with an expression vector for a single ribosomal protein were grown in LB media. At an OD of 0.6-1.2, protein expression was induced with 0.5-1.0 mM IPTG. Four hours after induction, cells were harvested, flash frozen in liquid N2, and stored at -80°C until further use.

Purification of uS2

3-5 grams of cells containing overexpressed ribosomal protein uS2 were resuspended in H20K20SH6 (20 mM HEPES-KOH pH 7.5, 20 mM KCl, and 6 mM β-mercaptoethanol) and lysed. Lysed cells were then ultracentrifuged at 41,000 rpm for 1 hour in a Beckman Type 45 Ti rotor. The pellet was resuspended in NaAc20K20SH6U6000 (20 mM sodium acetate pH 5.6, 20 mM KCl, 6 mM β-mercaptoethanol, and 6,000 mM urea) before clarifying by ultracentrifugation for 1 hour

at 41,000 rpm in a Beckman Type 70 Ti rotor. The supernatant was loaded onto a 6 mL Resource S column before being eluted via a salt gradient from NaAc20K20SH6U6000 to NaAc20K1000SH6U6000 (20 mM sodium acetate pH 5.6, 1,000 mM KCl, 6 mM β-mercaptoethanol, and 6,000 mM urea). Fractions containing pure uS2 were pooled and dialyzed overnight against 1 L of T20K1000 (20 mM Tris-HCl pH 8.0 and 1,000 mM KCl). uS2 was concentrated to 2 mL with concentration of ~1.4 mM, aliquoted, flash frozen in liquid N2, and stored at -80°C.

Purification of uS3

3-5 grams of cells containing overexpressed ribosomal protein uS3 were resuspended in H20K20SH6 (20 mM HEPES-KOH pH 7.5, 20 mM KCl, and 6 mM β-mercaptoethanol) and lysed. Lysed cells were then ultracentrifuged at 41,000 rpm for 1 hour in a Beckman Type 45 Ti rotor. The pellet was resuspended in T20K20SH6U6000 (20 mM Tris-HCl pH 7.3, 20 mM KCl, 6 mM β-mercaptoethanol, and 6,000 mM urea) before clarifying in a Beckman Type 70 Ti rotor at 41,000 rpm for 1 hour. The supernatant was loaded onto a 6 mL Resource S column before being eluted via a salt gradient from T20K20SH6U6000 to T20K1000SH6U6000 (20 mM Tris-HCl pH 7.3, 1,000 mM KCl, 6 mM β-mercaptoethanol, and 6,000 mM urea). Fractions containing pure uS3 were pooled and dialyzed overnight against 1 L of T20K1000. uS3 was concentrated to 750 µL with a concentration of 45 µM, aliquoted, flash frozen in liquid N2, and stored at 80°C.

Purification of uS4

3-5 grams of cells containing ribosomal protein uS4 were resuspended in T40K40SH12 (40 mM Tris-HCl pH 8.0, 40 mM KCl, and 12 mM β-mercaptoethanol). Just before lysis, PMSF and Benzamidine HCl were added to a final concentration of 1 to 5 mM. Lysate was clarified by ultracentrifugation in a Beckman Type 45 Ti rotor at 42,000 rpm for 2 hours. Urea powder was added to the collected supernatant to a final concentration of 6 M. The solution was filtered, loaded onto a 6 mL Resource S column, and eluted in the same manner as ribosomal protein uS3. Fractions containing purified uS4 were concentrated to 800 µM, dialyzed (against T20K1000), aliquoted, flash frozen, and stored at -80°C.

Purification of Nus factors

NusA was cloned into the pETite N-His plasmid, while NusE was cloned into the pETite N-His Sumo plasmid. NusA, Sumo-tagged NusE, and NusG were overexpressed in BL21(DE3) cells, NusB was overexpressed in T7 express cells. Cells transformed with an expression vector for a Nus factor were grown in LB media. At an OD of 0.6-1.2, protein expression was induced with 0.5-1.0 mM IPTG. Four hours after induction, cells were harvested, flash frozen in liquid N2, and stored at -80°C until further use.

Purification of NusA

3-5 grams of cells containing overexpressed NusA were resuspended in T20Na100. Just before lysis, PMSF and Benzamidine HCl was added to a final concentration of 1 to 5 mM. Lysed cells were ultracentrifuged at 42,000 rpm for 2 hours

in a Beckman Type 45 Ti rotor. The supernatant was loaded on a 20 mL Ni-NTA column before being washed with high salt buffer T20Na500 (20 mM Tris-HCl pH 8.0 and 500 mM NaCl) and finally eluted with a linear gradient from T20Na100I20 (20 mM Tris-HCl pH 8.0, 100 mM NaCl, and 20 mM imidazole-HCl pH 8.0) to T20Na100I300 (20 mM Tris-HCl pH 8.0, 100 mM NaCl, and 300 mM imidazole-HCl pH 8.0). Fractions containing purified NusA were pooled, concentrated to ~900 µM, dialyzed against T20Na100Suc100 (20 mM Tris-HCl pH 8.0, 100 mM NaCl, and 100 mM Sucrose), aliquoted, flash frozen, and stored at -80°C until further use.

Purification of NusB

3-5 g of cells containing overexpressed NusB were resuspended in T20Na25SH3 (20 mM Tris-HCl pH 7.3, 25 mM NaCl, and 3 mM β-mercaptoethanol). Lysed cells were centrifuged at 16,000 rpm for 45 minutes. The supernatant was loaded onto a 20 mL SP-Sepharose column before being eluted via a salt gradient from T20Na25SH3 to T20Na1000SH3 (20 mM Tris-HCl pH 7.3, 1,000 mM NaCl, and 3 mM β-mercaptoethanol). Fractions with pure NusB were pooled, concentrated, and loaded onto a 24 mL Superdex 200 column equilibrated in T20Na120SH3 buffer. Fractions containing NusB were pooled, concentrated to ~500 µM, and dialyzed against 1 L of T20Na100Gol50% (20 mM Tris-HCl pH 7.3, 100 mM NaCl, and 50% [v/v] Glycerol) and stored at -80°C until further use.

Purification of NusB-NusE complex

NusE (aka uS10) requires the presence of NusB to form a soluble complex of NusB-NusE (Nus B/E). Therefore, NusB was purified prior to NusE being purified in the form of a Nus B/E complex. The steps of the protocol had to be performed in the exact order as described to maximize the yield of soluble NusB-NusE complex. 3-5 grams of cells containing overexpressed Sumo-NusE were resuspended in T20Na100. Lysed cells were centrifuged at 16,000 rpm for 30 min. The supernatant was loaded onto a 20 mL Ni-NTA column. After a high salt wash using T20Na500I20, the protein was eluted with an gradient from T20Na100 to T20Na100I1000. Fractions containing Sumo-NusE were pooled and concentrated. Sumo-NusE was then incubated with a stoichiometric amount of NusB. After 1-2 hours, Sumo protease was added and the cleavage reaction was allowed to proceed overnight. Fractions containing pure NusB-NusE complex were pooled, dialyzed against T20Na100DTT1, concentrated to ~120 μM, aliquoted, and stored at -80°C until further use.

Purification of NusG

5-7 g of cells containing overexpressed NusG were resuspended in T20Na100 (20 mM Tris-HCl pH 8.0 and 100 mM NaCl). Just before lysis, PMSF was added to a final concentration of 1 to 5 mM. Lysed cells were ultracentrifuged at 44,000 rpm for 2 hours in a Beckman Type 45 Ti rotor. After ultracentrifugation, the supernatant was filtered through a 250 mL Corning™ disposable vacuum filter (pore size 0.22 μm). The filtrate was diluted to 150 mL with T20Na100 buffer and was loaded onto a 20 mL Ni-NTA

column. A low imidazole wash was used to wash away nonspecifically bound proteins using T20Na100I20 (20 mM Tris-HCl pH 8.0, 100 mM NaCl, and 20 mM imidazole-HCl, pH 8.0). NusG was eluted via an imidazole gradient from T20Na100I20 to T20Na100I300 (20 mM Tris-HCl pH 8.0, 100 mM NaCl, and 300 mM imidazole-HCl, pH 8.0). Fractions containing pure NusG were pooled, concentrated to ~320 µM, buffer exchanged three times against T20Na100 buffer, aliquoted, and stored at -80°C.

Purification of ρ factor

Purification of ρ factor was based on (Skordalakes and Berger 2003). T7 express cells transformed with ρ factor expression vector were grown in LB media. At an OD of 0.6-1.2, protein expression was induced with 1.0 mM IPTG. Four hours after induction, cells were harvested, flash frozen in liquid N2, and stored at -80°C until further use.

3-5 grams of cells containing overexpressed ρ factor were resuspended in 75 mL of T20K50DTT1Gol10% (20 mM Tris-HCl pH 7.5, 50 mM KCl, 1 mM DTT, and 10% [v/v] Glycerol). Lysed cells were centrifuged at 16,000 rpm for 1 hour. The supernatant was collected, and the protein was loaded onto a 20 mL SP-Sepharose column and eluted with a gradient from T20K50DTT1Gol10% to T20K1000DTT1Gol10% (20 mM Tris-HCl pH 7.5, 1,000 mM KCl, 1 mM DTT, and 10% [v/v] Glycerol). Fractions containing ρ factor were pooled (~20 mL), diluted to a total of 75 mL with T20K50DTT1Gol10%, and loaded onto a 6 mL Resource S column. The protein was eluted from the column with a linear gradient from T20K50DTT1Gol10% to T20K1000DTT1Gol10%. Fractions containing ρ factor were pooled, concentrated to 500 µL, and loaded onto a 24 mL

Superdex 200 column that was equilibrated in T20K200Gol10% (20 mM Tris-HCl pH 7.5, 200 mM KCl, 1 mM DTT, and 10% [v/v] Glycerol). Fractions containing pure ρ factor were pooled, buffer exchanged into T20K200DTT1Gol20%, concentrated, aliquoted, and stored at -20°C until further use. The final concentration of ρ factor preparations were typically 5-10 μM.

In vitro transcription assays

The vector carrying the template for the *his* pause assay, pIA267, was a kind gift of Dr. Irina Artsimovitch. The vector carrying the template for the ρ-dependent termination assay uses the pIA267 backbone, but has the *his* pause sequence replaced by a boxBAC element followed by the tR' terminator as in (Huang, Said et al. 2019). Individual nucleotides were purchased from GE Healthcare (Chicago, IL, USA). ApU dinucleotide was purchased from TriLink Biotechnologies (San Diego, CA, USA). MspI-digested pBR322 DNA and T4 Polynucleotide Kinase were from New England Biolabs (Ipswich, MA, USA). Radioactive [α32P]GTP and [γ32P]ATP with a specific activity of 6,000 Ci/mmol were from Perkin Elmer (Santa Clara, CA, USA).

General outline of all transcription assays

The design of our transcription assays was guided by (Artsimovitch and Henkin 2009). The DNA template for both assays contained a strong λPR promoter followed by C-less region and DNA sequence specific to each assay. The sequence of each template is given in Table 3.1 and schematic representations for ρ-dependent termination is shown in

Figure 3.1A and for RNAP pausing at the *his* pause site in Figure 3.3A. Each DNA template was prepared by PCR amplification from plasmid DNA.

For the RNAP activity assay, RNAP was loaded onto the DNA template in the form of a holoenzyme. Transcription was initiated with a ApU dinucleotide and ribonucleotide triphosphate mixture without CTP, thus halting the RNAP after transcribing the C-less region. This transcription complex was stable for several hours on ice. The polymerase was released from the halt by addition of a full complement of ribonucleotide triphosphate. To prevent re-initiation of transcription, rifampicin was added with the chase nucleotides. Samples were withdrawn, quenched, and analyzed on a denaturing polyacrylamide gel. The denaturing gel (~35 x 43 cm with 0.4 mm spacers) was prepared within 24 hours of use and contained either 4% or 10% polyacrylamide for the ρ-dependent termination and *his* pause assay, respectively. MspI-digested pBR322 DNA was used as a molecular weight ladder for all denaturing PAGE after being 5' radiolabeled with T4 Polynucleotide Kinase and [γ32P]ATP. The developed gel was exposed to a phosphor imager screen, before scanning the recorded gel image with a Typhoon 9410 (GE Healthcare). The digitalized image was quantified using ImageQuant (GE Healthcare).

The quantification of the half-life of pausing of RNAP at the *his* pause site was based on (Landick, Wang et al. 1996) and that of % run through product was calculated by dividing the intensity of the run-off band by the intensity of the entire lane starting with the first ρ-dependent termination site. To quantify intrinsic termination, the lanes from the ρ-dependent termination were redrawn to start at the intrinsic termination band

(+400) and went up to the read-out band (+426). Both bands had their intensity quantified and backgrounds subtracted before obtaining a "band %" for the intrinsic terminator and the read-out product. The "band %" for the band representing the intrinsic terminator is what was used and reported. Conversely, to obtain the % read-out the number recorded would be "100 – intrinsic terminator band %".

Preparation of DNA template. All plasmid constructs used as source for DNA template were verified by sequencing and the DNA templates were prepared according to (Artsimovitch and Henkin 2009). In brief, the templates were amplified from plasmid constructs by standard PCR amplification (see Table 3.1 for nucleotide sequence of DNA templates and Table 3.2 for primers for PCR amplification). The PCR products were purified using a QIAquick PCR Purification kit (Qiagen, Hilden, Germany) following the instructions of the manufacturer. The resulting templates were ethanol precipitated, resuspended in TE buffer or nuclease free water, and the concentration was determined by nanodrop.

ρ-dependent termination assay

The DNA template contained a λPR promoter, followed by an anti-termination motif (boxBAC), ρ entry sites (rutA/rutB), five consecutive ρ-dependent termination site clusters, and an intrinsic terminator (tR'; see Figure 3.1A). The boxBAC motif is also known as the antitermination sequence (AT), at which N-utilizing (or Nus) factors bind to the RNAP (Berg, Squires et al. 1989; Quan, Zhang et al. 2005). This is followed by the trp t' termination sites, which facilitate ρ-dependent termination (Platt 1981). The first

termination site occurs after +200 nucleotides with several others occurring downstream of the boxBAC motif and rutA/rutB sequence (see Figure 3.1A and Table 3.1).

Halted complexes were formed by mixing nuclease free water, 10X T40K50M5DTT0.1Gol3% (final ion condition 40 mM Tris-HCl pH 7.5, 50 mM KCl, 5 mM MgCl2, 0.1 mM DTT, and 3% [v/v] Glycerol), 10X initiating NTPs (final nucleotide concentration 1 µM GTP, 5 µM ATP and UTP, and 100 µM ApU), [α32P]GTP, template DNA, and RNAP holoenzyme. The mixtures were incubated at 37°C for 15 minutes. The buffer conditions used here are those used in (Said, Hilal et al. 2021). After the halted complex was formed, ρ factor and various combinations of accessory protein factors were added and incubated for 3 minutes at 37°C. This was followed by the addition of a 5X chase solution (1,000 µM ATP, UTP, CTP, GTP, and 250 µg/mL Rifampicin are the concentrations of the 5X solution). The final concentration of holoenzyme was 50 nM, DNA template 40 nM, ρ hexamer 25 nM, NusA 0.2 µM, NusG 0.5 µM, NusB-NusE complex 1 µM, uS2 1µM, uS3 0.5 µM, and uS4 1 µM; all values were gleaned from previously published studies (Torres, Condon et al. 2001; Artsimovitch and Henkin 2009; Said, Hilal et al. 2021). The transcription reaction was terminated after 360 seconds by addition of an equal volume of 2X STOP buffer and heating at 95°C for 2 minutes. STOP buffer composition is from (Artsimovitch and Henkin 2009) and is 8 M urea, 130 mM Tris, 45 mM boric acid, 12.5 mM EDTA, 3 mM Bromophenol blue (100 mg/50 mL), and 3.7 mM Xylene cyanol (100 mg/50 mL).

his pause escape assay

To study pausing, we utilized the well-studied *his* pause system (Chan and Landick 1993) (see Figure 3.3A and Table 3.1). The final buffer conditions to form halted complexes are those used in (Artsimovitch and Henkin 2009) (T20Na20M2DTT1E0.1Gol5%, 20 mM Tris-HCl pH 7.5, 20 mM NaCl, 2 mM MgCl2, 1 mM DTT, 0.1 mM EDTA, and 5% [v/v] Glycerol). The final concentration of holoenzyme was 50 nM, DNA template 40 nM, NusG 0.5 µM, NusB-NusE complex 0.75 µM, uS2 0.75 µM, uS3 0.75 µM, and uS4 0.75 µM; all values were gleaned from published studies (Torres, Condon et al. 2001; Artsimovitch and Henkin 2009; Said, Hilal et al. 2021). After the halted complex was formed as in the ρ-dependent termination assay, accessory factors were added and incubated for 3 minutes at 37°C. This was followed by the addition of a 5X chase solution (750 µM ATP, UTP, and CTP, 50 µM GTP, and 125 µg/mL Rifampicin concentrations for the 5X chase solution). Samples were drawn from this stock at 12, 24, 36, 48, 60, 80, 120, 160, 300, and 600 seconds and the transcription reactions were halted by adding an equal volume of 2X STOP buffer and heating at 95°C for 2 minutes.

3.3. Size exclusion Chromatography

RNAP complex formation with ribosomal proteins was monitored by gel filtration over a Superdex 200 10/300 GL column (24 mL). The column was equilibrated in running buffer T20K250 (20 mM Tris-HCl pH 7.5 and 250 mM KCl). A 1:30 stoichiometric mixture of RNA polymerase to uS2 was incubated at room temperature in

T20K250 in a volume of 60 µL. Before loading the complex onto the gel filtration column, the sample was diluted to 400 µL with T20K250. A 1:30 stoichiometric mixture of RNA polymerase to uS3 and to uS4 underwent the same incubation and dilution strategy. Transcription elongation complexes were formed using the oligonucleotides found in Table 3.2 and following previously published protocols (Kashkina, Anikin et al. 2006; Fan, Conn et al. 2017). Once elongation complexes were formed the same incubation-dilution protocol as for assaying the core RNAP-uS3 complex formation was performed. All binding mixtures were centrifuged for 1 to 5 min at 19,000x g before being loaded onto the column. 1 mL fractions were collected beginning with the elution of the void volume. These 1 mL fractions were subjected to a TCA precipitation (with a 95% acetone wash) before resuspending in 1x SDS loading buffer and loaded onto a 7x8 cm large and 1 mm thick 6-25% SDS-polyacrylamide gel and run for 80 min at 120V. Gels were Coomassie stained and destained with several exchanges of hot distilled water before imaging with a BioRad ChemiDoc system.

Results:

To determine the intrinsic effects ribosomal proteins uS2, uS3, and uS4 exert on transcription, we employed several well-known assays. The ribosomal proteins' effects i) on ρ-dependent termination were assessed on the trp t' terminator; ii) on ρ-independent, intrinsic termination at the tR' terminator site; and iii) on pausing and pause escape at the *his* pause site. Finally, we gauged if the proteins bound directly to core RNAP by gel filtration.

All transcription assays were also performed in the presence of NusA and NusG and in the presence of all Nus factors (Nus A/B/E/G). Both, NusA and NusG, are found bound to RNAP on most protein-encoding genes (Mooney, Davis et al. 2009). They are also an integral part of the most recent structures of RNAP in complex with the ribosome and with ρ factor (O'Reilly, Xue et al. 2020; Wang, Molodtsov et al. 2020). All Nus factors are present in several RNAP complexes that enable the RNAP to transcribe faster and suppress termination (DeVito and Das 1994; Nudler and Gottesman 2002; Said, Krupp et al. 2017; Huang, Said et al. 2019; Krupp, Said et al. 2019).

1. Transcription anti-termination assays using read-through at the ρ-dependent termination sites

The effects of ribosomal proteins on ρ-dependent transcription termination were determined by the efficiency of RNAP to read-through (RT) a series of ρ-dependent termination sites. The DNA template used for this assay is under the control of the λPR promoter. The promoter is followed by a C-less region. The C-less region is followed by an anti-termination motif (boxBAC), ρ entry sites (rutA/rutB), and the trp t' ρ-dependent termination sites (positions from ~200-300). The template ends with an intrinsic terminator (tR') (Figure 3.1A). To quantify the RT efficiency, the assay was performed in a single-round format (Artsimovitch and Henkin 2009). First, RNAP holoenzyme was incubated with DNA template in the presence of a nucleotide mixture. This mixture contained ApU dinucleotide to help initiate transcription and radioactive [α32P]GTP to produce labelled transcription products for imaging, but was devoid of CTP to stall RNAP at the C-less region. The polymerase formed a halted complex at position +26.

Next, protein factors were added and incubated with the reaction mixture. After incubation, transcription was resumed by adding a large excess of all four, unlabeled nucleotide triphosphates. To prevent re-initiation of transcription, rifampicin was also added. The transcription reaction was quenched, and the transcription products were separated on a denaturing polyacrylamide gel. The developed gel was imaged and the transcription products were quantified as detailed in Material and Methods.

1.1 Validation of transcription assay to determine read-through at the ρ-dependent termination sites

To establish the quality of the data produced in our hands, we recapitulated a set of published ρ-dependent termination results (Torres, Condon et al. 2001; Said, Hilal et al. 2021). These control assays measured not only RNAP's efficiency to read-through (RT) ρ-dependent termination sites but also identified the size range of the termination products. Changes in the size range can point to changes in the mode that ρ terminates transcription (Squires, Greenblatt et al. 1993; Burns, Richardson et al. 1998; Torres, Condon et al. 2001; Hao, Epshtein et al. 2021; Said, Hilal et al. 2021). These assays were also performed in the presence of different combinations of Nus factors.

Our preparation of RNAP on its own had an RT of 62.3%. The addition of ρ factor sharply decreased the polymerase's RT to 20.7% (see Figure 3.1B, lanes 1 and 2). These observations agree well with those reported. (See for comparison Figure 1.6C or panel labelled wild type in Figure S10A of (Said, Hilal et al. 2021)). The RT of ρ-dependent termination only slightly increased in the presence of NusG to 23.5% (Figure

3.1B, lane 3), while it decreased modestly in the presence of NusA to 17.6% (Figure 3.1B, lane 4). As expected, the size range of termination products in the presence of NusG shifted towards shorter transcripts, while that of NusA shifted towards longer transcripts (Squires, Greenblatt et al. 1993; Burns, Richardson et al. 1998; Torres, Condon et al. 2001; Hao, Epshtein et al. 2021). Because NusE (aka uS10) is only soluble in the presence of NusB, we determined the effect of the complex of NusE and NusB (Nus B/E) on RT of ρ-dependent termination. The Nus B/E complex affected the RT to a lesser degree than NusA and was only 19.1% (Figure 3.1B, lane 5). The presence of all Nus factors (Nus A/B/E/G) reduced the RT at ρ-dependent termination sites to 15.5% (Figure 3.1B, lane 6).

In summary, the RT and the shift in the size range of the termination products for the different combinations of Nus factors agreed well with those reported (Squires, Greenblatt et al. 1993; Burns, Richardson et al. 1998; Torres, Condon et al. 2001; Hao, Epshtein et al. 2021; Said, Hilal et al. 2021). This reassured us to continue our studies of the intrinsic effects of ribosomal proteins on ρ-dependent termination.

1.2 Ribosomal proteins' effects on ρ-dependent termination on their own

First, we tested if ribosomal proteins uS2, uS3, and uS4 disrupted ρ-dependent termination on their own. They all reduced ρ-dependent termination, resulting in an increased RT product formation (Figure 3.1B lanes 2, 10, 11, and 12 and Figure 3.1C). In the presence of uS2, the RT increased insignificantly to 30.9%, while in the presence of uS4 and uS3 the RT significantly increased to 52.8% and 68.8%, respectively (see Figure

3.1C, P-value ~0.001 and ~0.01 for uS4 and uS3, respectively). The RT levels in the presence of uS4 and of uS3 are similar if not higher than the RT for RNAP alone in the absence of ρ. The size range of ρ-dependent termination products appears to be unaffected by the presence of either uS2, uS3, or uS4 (Figure 3.1B, lane 2 vs lanes 10-12). Our data suggest that the presence of uS2 on its own had only marginal effect on ρ-dependent termination, while uS3 and uS4 seem to completely suppress ρ-dependent termination.

1.3 Ribosomal proteins' effects on ρ-dependent termination in the presence of NusA and NusG

Next, we tested the effects of the ribosomal proteins on ρ-dependent termination in the presence of NusA and NusG (without NusB and NusE, aka uS10). The addition of only NusA and NusG (Nus A/G) to our ρ-dependent termination only slightly reduced the RT from 20.7% to 16.7% (Figure 3.1B, lane 13). This reduction followed the same trend observed by others (Said, Hilal et al. 2021).

The addition of uS2 to the ρ-termination assay in the presence of NusA and NusG left the RT virtually unaffected, i.e., 17.8% in the presence of uS2 vs 16.7% in its absence. uS3 and uS4 exerted much larger effects when added to the ρ-dependent termination assay in the presence of NusA and NusG. The addition of uS4 increased the RT to 37%, while the addition of uS3 increased the RT to 41.1% (Figure 3.1B, lanes 13-16). Assays containing uS3 or uS4 exhibited a nearly two-fold increase of RT compared to ρ-termination in the absence and in the presence of NusA and NusG. Although the

yield of termination was diminished due the presence of ribosomal proteins, the size range of the termination products remained unaffected (Figure 3.1B, lane 13 vs lanes 14-16). We conclude that the presence of NusA and NusG overwrote uS2's intrinsic effects on ρ-dependent termination and significantly reduced uS3's and uS4's effect.

1.4 Ribosomal proteins' effects on ρ-dependent termination in the presence of all Nus factors (Nus A/B/E/G)

Because uS3 and uS4 reduced ρ-dependent termination by themselves and in the presence of Nus A/G, we were interested in their effect on ρ-dependent termination in the presence of all Nus factors (Nus A/B/E/G). The addition of uS3 to our ρ-dependent termination in the presence of all Nus factors significantly increased the polymerase's RT from 15.5% to 56.1% (Figure 3.1B, lane 9 vs lane 6, P-value ~0.001). This increase appears to be mainly due to the presence of uS3, as uS3 on its own allowed for an RT of 68.8% at the ρ-dependent termination sites (Figure 3.1B, lane 12 vs lane 9). Like uS3, the addition of ribosomal protein uS4 significantly increased the RT of RNAP in the presence of all Nus factors (47.9% vs 15.5% with and without uS4, respectively; see Figure 3.1B, lane 8 vs lane 6, P-value ~0.0001). Also, like uS3, the increase in RT is mainly due to the presence of uS4 (Figure 3.1B, lane 8 vs lane 11). In contrast to uS3 and uS4, the presence of all Nus factors completely abolishes the effect of uS2 (Figure 3.1B, lane 10 vs lane 7). The size range of termination products in the presence of all Nus factors remained unchanged by the addition of either uS2, uS3, or uS4. The presence of all Nus factors overwrites uS2's intrinsic effect on ρ-dependent termination but leaves uS3's and uS4's unaffected.

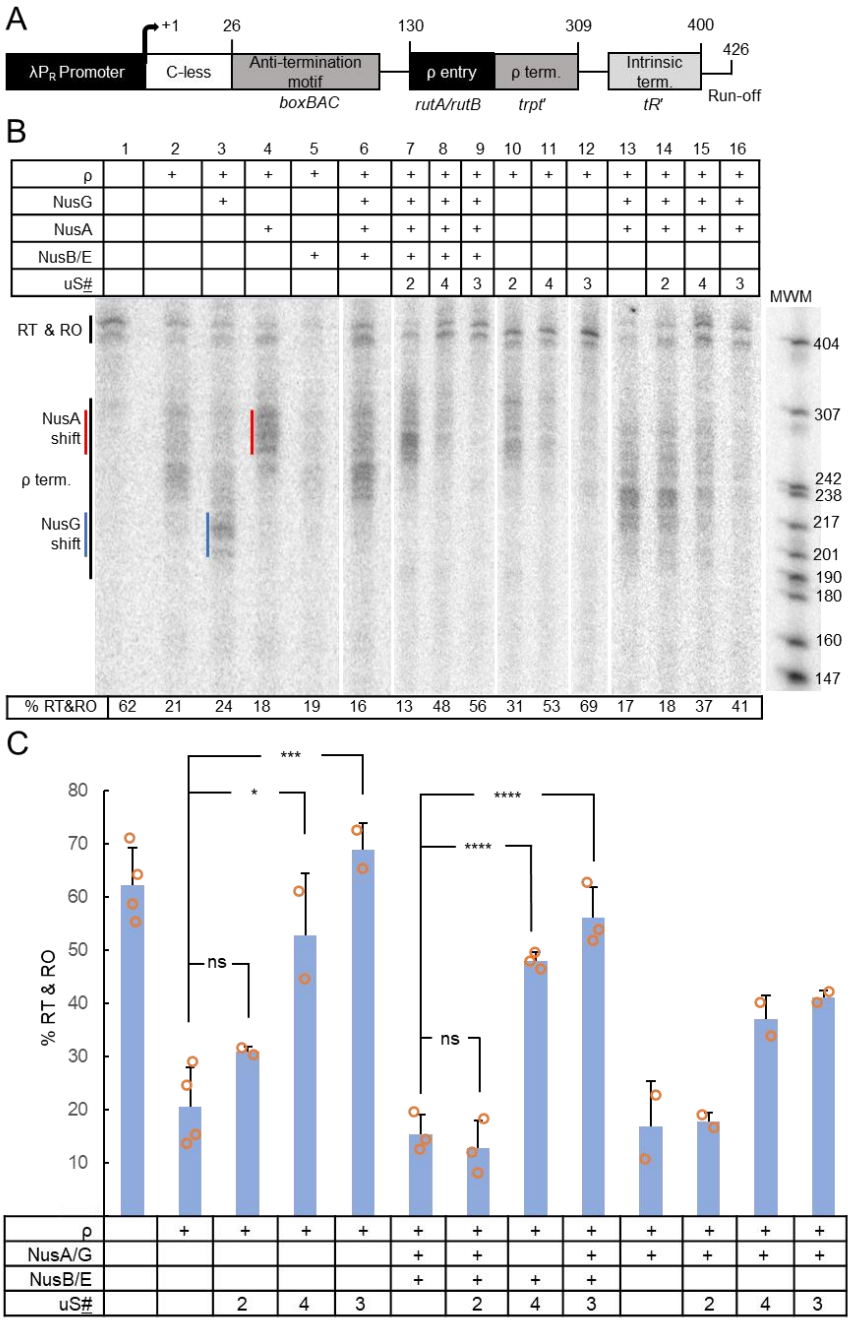
A
+1
26
130
309
400
426
λP$_R$ Promoter
C-less
Anti-termination motif
boxBAC
ρ entry
ρ term.
rutA/rutB
trpt'
Intrinsic term.
tR'
Run-off
B
1 2 3 4 5 6 7 8 9 10 11 12 13 14 15 16
ρ + + + + + + + + + + + + + + +
NusG + + + + + + + + + + + + +
NusA + + + + + + + + + + + + +
NusB/E + + + + + + + + + + + + +
uS# 2 4 3 2 4 3 2 4 3
MWM
RT & RO
NusA shift
ρ term.
NusG shift
404
307
242
238
217
201
190
180
160
147
% RT&RO 62 21 24 18 19 16 13 48 56 31 53 69 17 18 37 41
C
% RT & RO
80
70
60
50
40
30
20
10
***
*
****
****
ns
ns
ρ + + + + + + + + + + + + + +
NusA/G + + + + + + + + + +
NusB/E + + + + + + +
uS# 2 4 3 2 4 3 2 4 3

Figure 3.1. Intrinsic effect of ribosomal proteins on ρ-dependent termination. (A) Schematic representation of the DNA template used. Key features of the DNA template are displayed as labelled boxes and important nucleotide positions are indicated above the schematic representation of the template. See Materials and Methods for the origin and the complete nucleotide sequence of the DNA template. (B) Representative denaturing gel. The table above the gel indicates the combination of factors present in each transcription assay. An assay corresponds to a single column in the table and is matched to the lane of the denaturing gel of the transcription products. The last row of the table indicates the ribosomal protein added to each reaction (for example, 3 indicates that uS3 was added to the reaction). The percentage of RT & RO of each experiment is displayed on the bottom of the gel and is based on the average of at least two trials, except the RT percentage in the presence of Nus B/E (lane 5), which is based on a single trial. The molecular weight marker in the right most lane is from NEB (MspI digested pBR322 DNA). (C) Histogram of RT in the presence of different combinations of Nus factors and ribosomal proteins. RT is shown as a percentage and plotted along the Y-axis. The average for each experiment is shown as a blue histogram bar and the value of each trail as a small orange circle. The standard deviation of each experiment is shown with a plus-sided error bar. The different combinations of factors present in the transcription experiment are listed below each bar. Significance was determined using an unpaired two-sided t-test, with the indicators as follows: ns for not significant, * for $p \leq 0.05$, ** for $p \leq 0.01$, *** for $p \leq 0.005$, **** for $p \leq 0.001$.

2. Intrinsic termination assays

Considering the intriguing data obtained for the ρ-dependent termination, we next determined if any combination of RNAP, ρ, Nus factors, and ribosomal proteins would influence intrinsic termination. The presence of ρ during intrinsic termination is reflective of the situation RNAP encounters in the cell. To determine the efficiency of intrinsic termination, we exploited the fact that our construct contained in addition to the trp t' ρ-dependent terminator an intrinsic tR' terminator (position +400). By comparing the product of the run-off (426 nucleotide length) vs. that of tR'-termination (400 nucleotide length) we were able to assess the effect of the ribosomal proteins on intrinsic termination. Here we report the efficiency of intrinsic termination relative to the sum of intrinsic termination and run-off. (For more details on determining the yield of intrinsic termination, see Material and Methods.)

2.1 Validation of the intrinsic termination assay

Although we determined intrinsic termination in the presence of ρ factor, its presence had no significant effect on transcription termination. RNAP on its own terminated 34.5% of the time at the intrinsic terminator site while in the presence of ρ factor 35.1% of the time. The presence of NusA nearly doubled the intrinsic termination to 62.6%. The addition of the other Nus factors to NusA modulated the NusA-mediated effect on the intrinsic termination only by a small amount. For example, the combination of NusA and NusG terminated transcription 70.5% of the time, while the combination of NusA, NusB, NusE, and NusG terminated 61.3% of the time (see Figure 3.2A). Because

the data obtained in our hands agreed well with those published (Farnham, Greenblatt et al. 1982; Schmidt and Chamberlin 1987; Gusarov and Nudler 2001; Mandell, Oshiro et al. 2021), we set out to determine the effect ribosomal proteins exert on intrinsic termination.

2.2 Ribosomal proteins' effects on intrinsic termination

We set out to determine if the presence of ribosomal proteins changed the efficiency of intrinsic termination. The presence of uS2 only marginally decreased the intrinsic termination to 34.6%, an insignificant difference of 0.5% compared to RNAP in the presence of ρ factor alone. A similar insignificant decrease of 5% of intrinsic termination to 31% was detected in the presence of uS4. The presence of ribosomal protein uS3 also produced a modest decrease of intrinsic termination to 25%, but different to the other ribosomal proteins, this change was statistically significant (P-value ~0.027, see Figure 3.2B).

Next, we determined the effects ribosomal proteins uS2, uS3, or uS4 exerted on intrinsic termination in the presence of NusA and NusG. RNAP terminated 70.5% of the time in the presence of ρ, NusA, and NusG while only 60% of time with the additional presence of uS2. In the presence of uS4 or uS3 the termination efficiency reduced even further to 52.9% and 48.3%, respectively. However, only the uS3-induced decrease of intrinsic termination was statistically significant (P-value ~0.03; see Figure 3.2C). The drop from 70.5% to 48.3% due to the presence of uS3 was almost proportional to the

drop of intrinsic termination uS3 induced by itself in the absence of all Nus factors (35% to 25%).

Lastly, we determined the effect uS2, uS3, or uS4 had on intrinsic termination in the presence of all Nus factors (Nus A/B/E/G). The efficiency of termination increased from 61.3% to 71.1% due to the presence of uS2, however, it decreased to 44.3% and 55.8% due to the presence of uS3 and uS4, respectively (Figure 3.2D).

In summary, uS2 has only a marginal effect on intrinsic termination. Although uS4 affected the intrinsic termination insignificantly, the trend of its effects matched that of uS3's. The presence of all Nus factors modulated the extent but not the effect the ribosomal proteins exert on intrinsic termination.

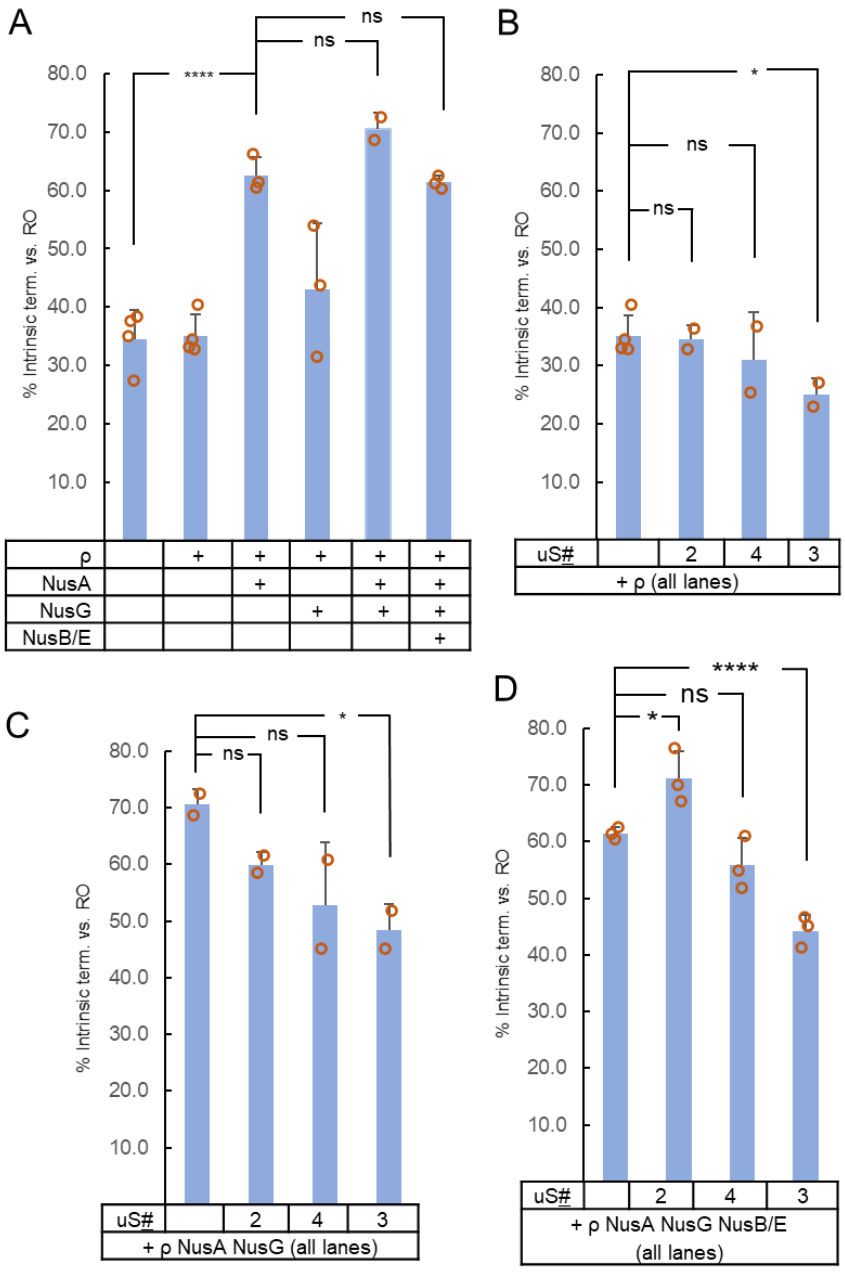
A
ns
ns
****
80.0
70.0
60.0
50.0
40.0
30.0
20.0
10.0
% Intrinsic term. vs. RO
ρ + + + + +
NusA + +
NusG + + +
NusB/E +
B
*
ns
ns
80.0
70.0
60.0
50.0
40.0
30.0
20.0
10.0
% Intrinsic term. vs. RO
uS# 2 4 3
+ ρ (all lanes)
C
*
ns
ns
80.0
70.0
60.0
50.0
40.0
30.0
20.0
10.0
% Intrinsic term. vs. RO
uS# 2 4 3
+ ρ NusA NusG (all lanes)
D
****
ns
*
80.0
70.0
60.0
50.0
40.0
30.0
20.0
10.0
% Intrinsic term. vs. RO
uS# 2 4 3
+ ρ NusA NusG NusB/E
(all lanes)

Figure 3.2. Intrinsic effect of ribosomal proteins on intrinsic termination. Shown are percentage of intrinsic termination as histograms for validation of assay in the absence (A) and in the presence of ribosomal proteins (B-D). The effect of ribosomal proteins on intrinsic termination is shown in the presence of ρ (B), in the presence of ρ, NusA, and NusG (C), and in the presence of ρ and all Nus factors (D). Histogram displays the average percentage of each intrinsic termination experiment as a blue bar, the value of each trial of each experiment is shown as a small open orange circle, and the standard deviation as a black positive error bar. Percentage of intrinsic termination was calculated by dividing the amount of termination product by the sum of termination and run-off product. Significance was determined using an unpaired two-sided t-test, with the indicators as follows: ns for not significant, * for $p \leq 0.05$, ** for $p \leq 0.01$, *** for $p \leq 0.005$, **** for $p \leq 0.001$.

3. RNAP pausing at and escape from the his pause site

To further our understanding of the intrinsic effects of ribosomal proteins uS2, uS3, and uS4 on transcription, we determined their effects on the polymerase at the *his* pause site. The DNA template used for this assay consists of the λPR promoter which is followed by a C-less region, the *his*-pause, and a stretch of 75 nucleotides (Figure 3.3A). As in our termination assay, we first prepared a stalled transcription complex by incubating the DNA template with holoenzyme and low concentration of ribonucleotides containing [α32P]GTP and devoid of CTP. To this stalled transcription complex proteins were added as needed and incubated for an additional three minutes. Transcription was resumed by addition of a large excess of all four ribonucleotides. Re-initiation of transcription was suppressed with rifampicin, which was added with the full set of ribonucleotides. At different timepoints aliquots were drawn from the reaction mixture and quenched. The transcripts of the reaction were separated on a denaturing polyacrylamide gel. The efficiency of pausing and the average rate of escaping from the *his* pause site were calculated as detailed in Material and Methods.

3.1 Validation of the his pause assay

As was the case for the transcription termination assays, we first validated our pausing assay by recapitulating published results. This also included the effect the addition of NusG has on the pausing of RNAP at the *his* pause site. With our preparation of RNAP, we determined a half-life of pausing of RNAP at the *his* pause site of 26 seconds (Figure 3.3B and 3.3C and Table 3.3). This value is shorter than the reported

half-life of 56 seconds (Belogurov, Mooney et al. 2009). However, our assay conditions were designed to accommodate the high salt conditions of the ribosomal protein (i.e., 20 mM Tris-HCl and 1M KCl), resulting in three-fold more KCl present during the reaction. Increases in the KCl concentration shortens the time RNAP requires to escape the pause site (Chan and Landick 1997). The half-life of the polymerase pausing decreased even further in the presence of NusG to 18.2 seconds. The relative drop of half-life in the presence and absence of NusG matches that observed by Artsimovitch and colleagues (Belogurov, Mooney et al. 2009). After establishing that our RNAP preparation performed similarly to those reported, we set out to determine the effect ribosomal proteins uS2, uS3, uS4, and uS10 (aka NusE in the form of the Nus B/E complex) exerted on pausing of the RNAP at the *his* pause site.

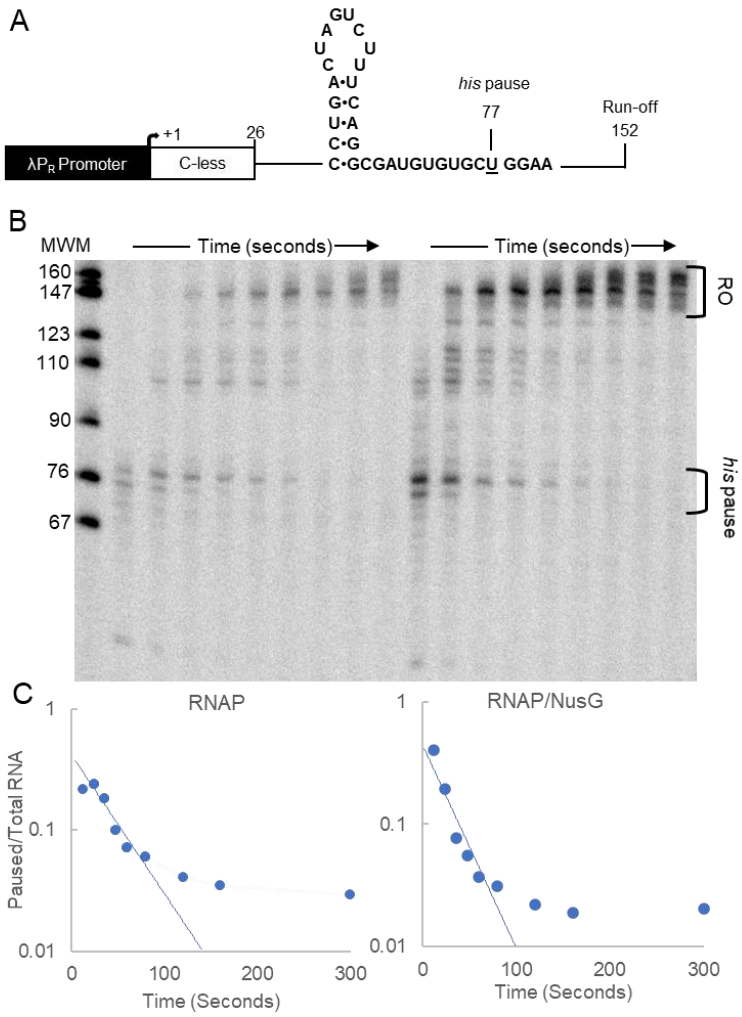
A
GU
A C
U U
C U
A•U
G•C
U•A
C•G
C•GCGAUGUGUGCU GGAA
his pause
77
Run-off
152
+1
26
λP$_R$ Promoter
C-less
B
MWM
Time (seconds)
Time (seconds)
160
147
123
110
90
76
67
RO
his pause
C
RNAP
RNAP/NusG
Paused/Total RNA
1
0.1
0.01
0
100
200
300
Time (Seconds)

Figure 3.3. Validation of *his* pause assay. (A) Schematic representation of *his* pause DNA template. Key features are displayed inside boxes, and nucleotide milestones are indicated above the template. (B) Representative denaturing gel. The gel image displays the RNA transcript products for different timepoints of RNAP by itself (left half) and in the presence of NusG (right half). The RNA lengths corresponding to RNAP paused at the *his* pause site and to the RNAP run-off product (RO) are indicated by black brackets. (C) Graphs depicting the portion of paused over total RNA plotted against time in seconds. All data points used to generate the trendline in these graphs are listed in Table 3.3. Graphs and calculations were performed as described in (Landick, Wang et al. 1996).

3.2 Pausing of RNAP at the his pause site in the presence of ribosomal proteins

Ribosomal proteins uS2, uS3, and uS4 all increased the time the RNAP required to escape the *his* pause site, but each to a different extent. uS2 prolonged the pausing of RNAP at the *his* pause site the least, with a half-life of 53 seconds. uS4 and uS3 prolonged the half-life of RNAP pausing to 114 and 347 seconds, respectively (Figure 3.4A and 3.4B and Table 3.3). Interestingly, ribosomal protein uS10 (in the form of a Nus B/E complex) had little to no effect on the half-life of RNAP pausing, with a 24.7 second half-life.

Given the intriguing effects the ribosomal proteins had on the half-life of pausing, we also determined their effects on the efficiency with which the polymerase pauses. RNAP by itself pauses at the *his* pause with an efficiency of 80%, which is in line with the results from (Artsimovitch and Landick 2000; Herbert, La Porta et al. 2006). The efficiency with which the polymerase paused in the presence of NusG was only 65%, which is lower than that reported (Artsimovitch and Landick 2000). uS2 and uS10 (in the form of Nus B/E complex) increased the pausing efficiency to 85% and 90%, respectively. uS3 and uS4 on the other hand decreased the pausing efficiencies even more than NusG, to only 60% (see Table 3.3).

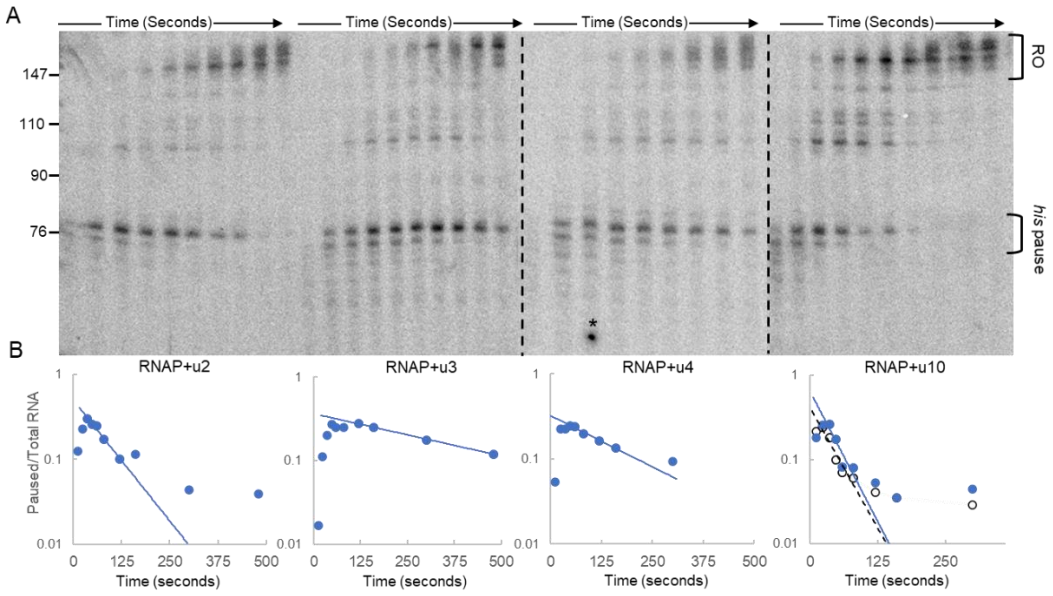
A
Time (Seconds)
Time (Seconds)
Time (Seconds)
Time (Seconds)
147
110
90
76
RO
his pause
*
B
RNAP+u2
RNAP+u3
RNAP+u4
RNAP+u10
Paused/Total RNA
1
0.1
0.01
0
125
250
375
500
Time (seconds)

Figure 3.4. Intrinsic effect of ribosomal proteins on *his* pause escape of RNAP. (A) Gel images displaying the RNA transcript products for different timepoints of RNAP escape from the *his* pause site in the presence of different ribosomal proteins; from left to right: in the presence of uS2, uS3, uS4 and uS10 (in form of Nus B/E complex). The RNA lengths corresponding to RNAP paused at the *his* pause site and of RNAP run-off product are indicated by black brackets. (B) The gel images are graphs depicting the portion of paused over total RNA plotted against time in seconds. For comparison, the data of RNAP escape by RNAP itself (open gray circles) is overlayed onto the data of the RNAP escape in the presence of uS10 (in the form of Nus B/E complex; filled blue circles).

4. Initial rate of run-off product formation for the his pause construct

We also determined the time it took for the formation of the first full-length product. This time is reflective of the transcription rate of the polymerases that avoided pausing. The more time the product formation requires the slower the transcription rate. The initial rate of product formation can be estimated by dividing the length of the transcribed RNA by the time required to transcribe it. (Here, the length of transcribed RNA is 126 nts. This is the length of the transcribed template minus the length of the C-less region.)

4.1 Initial rates of product formation in the presence and absence of ribosomal proteins

RNAP on its own completed the first transcripts in 17.6 seconds. The corresponding rate of 7.1 nt/sec matched well the rates reported by others at similar nucleotide concentrations (Ederth, Mooney et al. 2006; Svetlov, Belogurov et al. 2007; Mooney, Schweimer et al. 2009). The presence of NusG decreased the time for formation of the first full-length product to 11.4 seconds. The corresponding increase of rate to 11.0 nt/sec follows the trend previously seen (Mooney, Schweimer et al. 2009). Therefore, the time of appearance of the first full-length transcript allows us to assess the effects of ribosomal proteins on the transcription rates.

All tested ribosomal proteins increased the time required for the first full-length product, suggesting the ribosomal proteins decreased the rate of transcription. Ribosomal protein uS10 delayed the production formation to 21 seconds (corresponding to 6.0

nt/sec), uS2 to 21.5 seconds (5.6 nt/sec), uS4 to 22.1 seconds (5.7 nt/sec), and uS3 to 27.7 seconds (4.5 nt/sec) (see Table 3.4).

Previous studies have noticed that the slower the transcription rate the greater chance of RNAP to pause (Herbert, La Porta et al. 2006). This correlation holds true for NusG and ribosomal proteins uS2 and uS10. The presence of NusG increased the rate of transcription and decreased the efficiency of pausing, while uS2 and uS10 decreased the rate of transcription and increased the efficiency of pausing. However, it should be noted that pausing efficiencies are difficult to measure accurately, especially with slow RNAPs. This may have affected the here measured efficiencies for uS3 and uS4 (Svetlov, Belogurov et al. 2007).

5. RNAP binding assays

In previous work, we established that physical interactions of RNAP to transcription factors and to ribosomes can be assessed by gel filtration (Fan, Conn et al. 2017). We set out to test by gel filtration if ribosomal proteins uS2, uS3, and uS4 bound to RNAP.

Ribosomal proteins are prone to oligomerize and even precipitate in buffers with less than 100 mM of monovalent ions ((Dodd and Hill 1987) and references therein). Therefore, purified ribosomal proteins are stored under high salt conditions, i.e., 1 M KCl (Culver and Noller 1999). To ensure that the ribosomal proteins remained monomeric during gel filtration, we optimized the ionic conditions for each ribosomal protein. We optimized the buffer conditions by progressively reducing the KCl concentration from 1

M to 250 mM. Ribosomal proteins uS2 and uS3 remained monomeric at 250 mM KCl, while uS4 required a higher salt concentration of 350 mM KCl.

5.1 Ribosomal proteins binding to RNAP

Our data suggest that ribosomal protein uS2 formed a 1:1 complex with RNAP that could be isolated by gel filtration (Figure 3.5A). However, when we tried to form an RNAP complex with ribosomal protein uS3, we were not able to detect any stable complex, not even in the presence of a 30-fold stoichiometric excess of uS3 (Figure 3.5B). Repeating the experiment with RNAP with bound short, nascent RNA, we were still unable to detect any complex formation (Figure 3.5C). We also attempted to use gel filtration to isolate a RNAP-uS4 complex under conditions where both RNAP and uS4 are monomeric (i.e., 350 mM KCl). However, RNAP did not form a stable complex with uS4 in 30-fold excess (Figure 3.5D). We conclude that under the ionic conditions described above, uS3 and uS4 do not form a RNAP complex that can be isolated by gel filtration, suggesting that uS3 and uS4 do not bind RNAP by themselves.

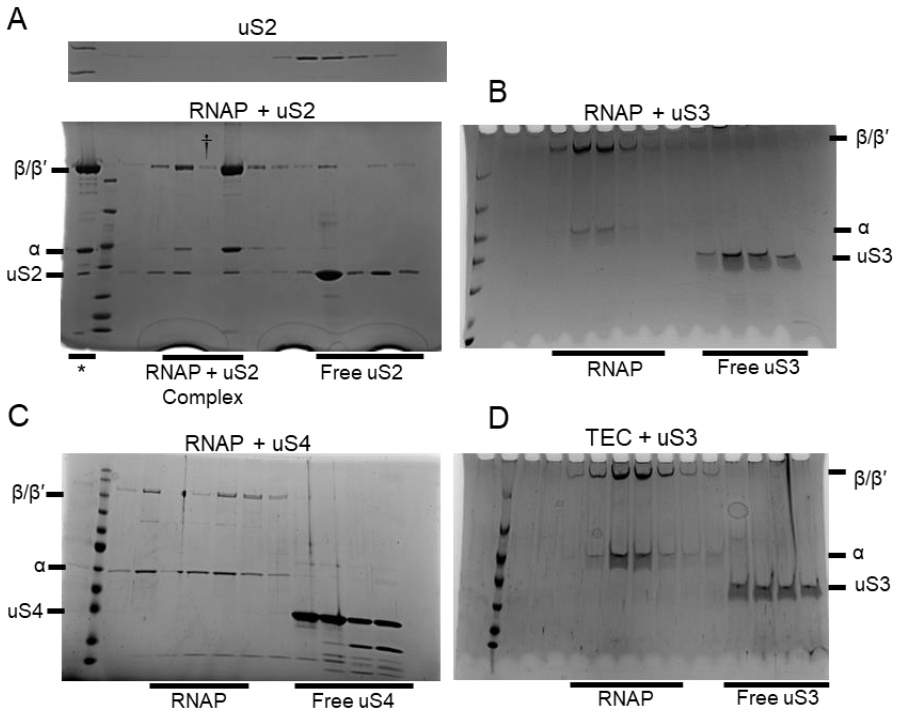
A
uS2
RNAP + uS2
β/β′
α
uS2
†
*
RNAP + uS2
Complex
Free uS2
B
RNAP + uS3
β/β′
α
uS3
RNAP
Free uS3
C
RNAP + uS4
β/β′
α
uS4
RNAP
Free uS4
D
TEC + uS3
β/β′
α
uS3
RNAP
Free uS3

Figure 3.5. Binding of ribosomal proteins to RNAP and to RNAP with bound nascent RNA. Shown are the SDS polyacrylamide gels of all fractions of the size exclusion chromatography of mixtures of RNAP with 30-fold excess of (A - bottom) ribosomal protein uS2, (B) uS3, and (C) uS4. Also shown are the SDS polyacrylamide gels for the size exclusion chromatography of uS2 alone (A - top) and of RNAP with bound nascent RNA (TEC) in the presence of uS3 (D). In (A) the lane marked with an asterisk below the gel is a 1:1 mixture of uS2 and RNAP. The lane labeled with † in (A) marks the partial loss of sample during SDS sample preparation.

Discussion:

In this work, we determined the effects of the universally conserved ribosomal proteins uS2, uS3, and uS4 on transcription (see Table 3.5). We investigated the intrinsic effect of these proteins on transcription, as they are at the RNAP-interface of the ribosome in recently published structures of the ribosome in complex with RNAP (Kohler, Mooney et al. 2017; Wang, Molodtsov et al. 2020; Webster, Takacs et al. 2020).

Our results showed that ribosomal protein uS2 bound directly to RNAP. It only modestly reduced ρ-dependent termination, but the presence of all Nus factors (Nus A/B/E/G) abolished this effect. uS2 was unable to alter the efficiency of intrinsic termination by itself. Yet, it decreased termination by 10% when NusA and NusG were both present (Nus A/G) and increased termination by 10% when all Nus factors (Nus A/B/E/G) were present. At the *his* pause site, uS2 increased the time RNAP required to escape the site.

Unlike uS2, uS3 did not bind directly to RNAP, yet it reduced the rate of transcription by a third. It also decreased ρ-dependent and intrinsic termination, regardless of the presence of Nus factors. Although the change in ρ-dependent termination was significant, the presence of uS3 left the size range of the termination products unaffected. The time RNAP required to escape from the *his* pause site in the presence of uS3 was especially long (half-life of the *his* pause was 347 sec versus 26.3 sec for RNAP alone).

Like uS2 and uS3, uS4 increased the time RNAP required to escape the *his* pause site. Akin to uS3, uS4 did not directly bind to RNAP, but exerted a large effect on ρ-dependent termination regardless of the presence of Nus factors (although the effect was less pronounced than that of uS3). As reported previously, uS4 had an insignificant effect on intrinsic termination (Torres, Condon et al. 2001).

Do the ribosomal proteins affect transcription by simply binding to nascent RNA or downstream DNA?

uS2, uS3, and uS4 exert their intrinsic effects on transcription independent of the Nus factors. This suggests that their mode of affecting the RNAP persists even in the presence of Nus factors.

Our data suggest that ribosomal protein uS2 directly binds RNAP and thus mediates its intrinsic effect on transcription. Although uS3 and uS4 had a more pronounced effect on transcription than uS2, we were not able to observe a direct binding to RNAP. Because both uS3 and uS4 are basic (with a pI of 10.27 and 10.05, respectively), they may bring about their effects on transcription by non-specifically coating the DNA or nascent RNA.

Non-specific coating of the downstream DNA may produce enough of a barrier to hamper RNAP's progression along the DNA, i.e., reducing the rate of transcription. Such a reduction of transcription rate will increase the time window for the ρ factor to catch up with the polymerase and terminate transcription. The slower transcription rate will also give the nascent RNA more time to form a stable stem-loop in the RNA exit channel of

polymerase. This will result in a higher likelihood of intrinsic termination and pausing at the *his* pause site, requiring a longer time for the polymerase to escape. Although uS3 and uS4 substantially increased the time the polymerase pauses at the *his* pause, they both reduce the likelihood of the polymerase to pause or to terminate in a ρ-dependent manner.

Non-specific coating of the nascent RNA may promote or hamper the formation of RNA stem loops on the polymerase. During transcription, this effect might even vary with the length of the nascent RNA. However, the molecular motor of ρ is strong enough to displace non-specific proteins from the nascent RNA (Schwartz, Margeat et al. 2007). (Rho produces enough force while translocating along the RNA that it even dislodges streptavidin from biotin. The Streptavidin-biotin interaction has a Kd of ~10-13 M, one of the strongest known affinities for a protein-ligand interaction.) This would suggest that proteins that non-specifically bind RNA may delay but not prevent ρ-dependent termination. For ribosomal proteins uS15 and uL4 (with a pI of 10.4 and 9.72, respectively) this is the case; they are unable to delay or reduce ρ-dependent termination (Torres, Condon et al. 2001).

Recent structure work shows NusA can mediate the binding of ρ factor to RNAP. This suggests that RNAP, NusA, and ρ factor are in contact even before ρ factor terminates transcription (Said, Hilal et al. 2021). This challenges the prevailing view that ρ factor has to be recruited to the nascent RNA and translocate all the way to RNAP to terminate transcription (Roberts 2019). In either case, simple coating of the nascent RNA would not hamper ρ-dependent termination. Because uS3 and uS4 reduce the ρ-

dependent termination, they have to directly interact with the polymerase to exert this effect.

Although non-specific interactions to the DNA and RNA cannot explain uS3's and uS4's effect on the polymerase, these interactions may assist both proteins in overcoming their low affinity for the polymerase. In the structure of the factor-mediated complex of RNAP and ribosome, the nascent RNA tethering the ribosome to the polymerase runs along the surface of uS3 before entering the ribosome through a tunnel. Running along the surface of uS3, the nascent RNA tracks a stretch of basic residues. Only single-stranded RNA can engage with all the residues at once, suggesting they may act as an RNA helicase during translation (Zhang, Hong et al. 2018; Amiri and Noller 2019). Upon entering the ribosome, the nascent RNA is exposed to another set of basic residues of uS3 and of uS4. However, these residues are critical for the helicase activity of the ribosome during translation (Takyar, Hickerson et al. 2005).

uS4 directly influences RNAP on its own

In the structure of RNAP in complex with ribosomal protein uS4, all Nus factors (Nus A/B/E/G), and SuhB, uS4 is only attached via NusA to the complex and does not contact RNAP (Huang, Hilal et al. 2020). This complex assembles at the 5' end of rRNA operons and suppresses ρ-dependent termination. The structure of this complex casts doubt on the previous study of uS4's effects on transcription (Torres, Condon et al. 2001). Here, we confirm that uS4 by itself suppresses ρ-dependent termination. However, in our hands, uS4 does not bind directly to RNAP nor affect product range of the ρ-

dependent termination (Figure 3.1B and Figure 3.5D). Based on the structure of the RNAP complex we expected that uS4 would not be able to directly influence RNAP in the presence of Nus factors. Yet, to our surprise, uS4 significantly suppressed ρ-dependent termination even in the presence of all Nus factors (Nus A/B/E/G). Further work will be required to address if this observation points, for example, to SuhB being the lynchpin for the suppression of ρ-dependent termination on rRNA operons (Dudenhoeffer, Schneider et al. 2019; Huang, Hilal et al. 2020).

Potential implication for cellular processes

We can envision that the direct interaction of ribosomal protein(s) with RNAP may play a critical role during at least two cellular processes: gene expression and ribosome biogenesis. Because of the lack of a nuclear membrane, ribosomes can start translating RNAs that are still being transcribed (Conn, Diggs et al. 2019; Irastortza-Olaziregi and Amster-Choder 2021). During ribosome biogenesis, the assembly of the ribosomal proteins on the ribosomal RNA occurs while the ribosomal RNA is still being transcribed (Davis and Williamson 2017). In either case, a mature/maturing ribosome is tethered to RNAP. This tethering increases the local concentration of ribosomes around the polymerase, thus promoting interactions of the surface-exposed ribosomal proteins to the polymerase (Conn, Diggs et al. 2019). Ultimately, these interactions can influence RNAP's activity, thus coupling transcription to translation and to ribosome assembly (Davis and Williamson 2017). Therefore, we will discuss the potential contributions of uS2, uS3, and uS4 on transcription-translation coupling and on ribosome assembly (see Figure 3.6).

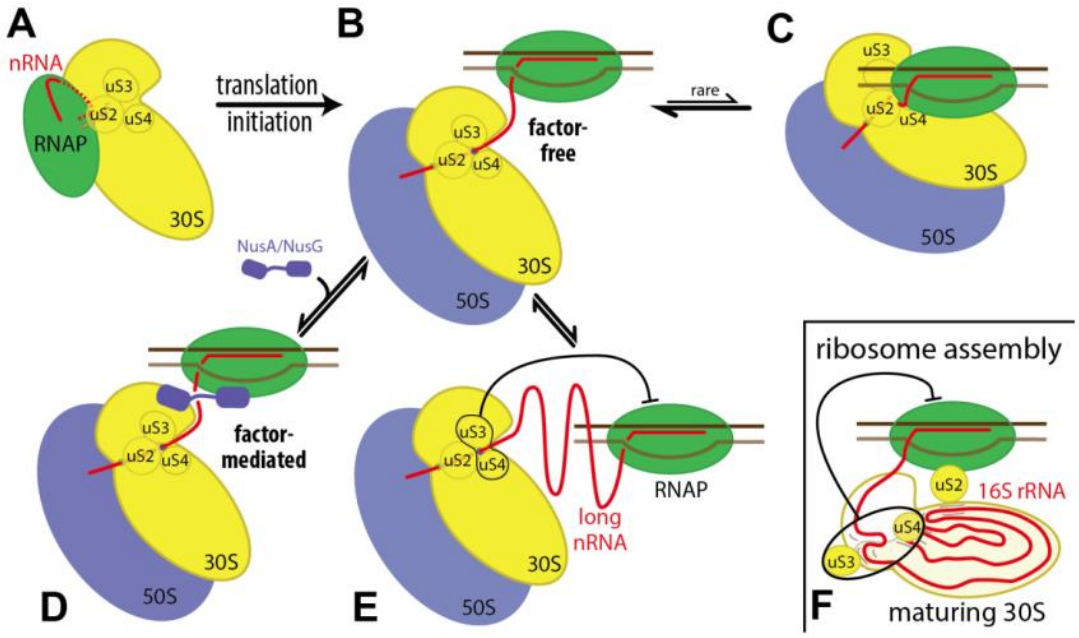

Figure 3.6. RNA polymerase-ribosome arrangements when transcription is coupled to translation or to ribosome assembly. (A-D) Arrangements for transcription-translation coupling are based on current structures. (E-F) Arrangements that may allow ribosomal proteins uS2, uS3, or uS4 to exert their intrinsic effects on transcription during transcription-translation coupling (E) and ribosome assembly (F).

Ribosomal protein uS2 may act as an anchor for RNAP during transcription-translation coupling

The recent burst of structure work has produced models for RNAP bound to the small ribosomal subunit (30S-RNAP) and for factor-free and factor-mediated complexes of the transcribing RNAP and the translating ribosome ((Demo, Rasouly et al. 2017; Fan, Conn et al. 2017; Kohler, Mooney et al. 2017; Wang, Molodtsov et al. 2020; Webster, Takacs et al. 2020) and reviewed recently in Webster et al. (Webster and Weixlbaumer 2021)). These models are thought to describe distinct phases of the coupling of transcription and translation: i) The establishing of coupling during which the small ribosomal subunit is recruited to the RNAP to initiate the translation of the nascent RNA (Figure 3.6A). ii) The maintaining of coupling during which transcription and translation of the nascent RNA are coordinated with and without mediating factors (Figure 3.6B). And iii) the presumably rare instances when the polymerase stalls long enough to allow the ribosome to translate all the nascent RNA (Figure 3.6C). These models also suggest that the spatial arrangement between RNAP and ribosome depends on the phase of coupling. The most drastic change in the arrangement between both is seen between the binding of the small ribosomal subunit to the RNAP (=phase i) and complex of translating ribosome and transcribing RNAP with the shortest length of RNA between them (=phase iii). A more than 85 Å repositioning of the RNAP on the ribosome is observed. The only ribosomal protein that contacts the RNAP in both structures is ribosomal protein uS2.

Our results showed that uS2 could form a 1:1 stoichiometric complex with RNAP (Figure 3.5A). However, compared to uS3 and uS4, uS2 had the least effect on transcription, regardless of which Nus factors were present (see Table 3.5). Given the presence of uS2 in the binding interface during two phases of coupling, the least effect on transcription, and the stoichiometric complex formation, uS2 may act as an anchor for RNAP on the ribosome. This would suggest that uS2 binds to RNAP during factor-free and/or factor-mediated coupling without exerting an effect on transcription. In this model, uS2 helps to keep the ribosome and RNAP close to each other, enabling other ribosomal proteins (for example, uS3 and uS4) to exert their intrinsic effect on RNAP.

How do the intrinsic effects of uS3 and uS4 assist transcription-translation coupling?

Our data suggest that the intrinsic effects of uS3 and uS4 are slowing transcription and increasing the time RNAP remains paused. These intrinsic effects may enable lagging ribosomes to catch up with the polymerase. Yet, the effects must subside as the ribosome nears the polymerase for transcription to resume. As the ribosome approaches the polymerase, the length of RNA between RNAP and ribosome shortens. The shortening of the RNA restricts the area the tethered ribosome can contact on the polymerase. The potential contact area between RNAP and the ribosome is even more restricted by NusA and NusG. Thus, the current structures may not capture the RNAP-ribosome arrangements that allow uS3 and uS4 to exert their effects (see Figure 3.6B and 3.6D).

Possible role of the intrinsic effects of uS2, uS3, and uS4 on ribosome assembly

Under equilibrium conditions, ribosomal proteins assemble on the ribosomal RNA in a sequential order (Held, Ballou et al. 1974; Röhl and Nierhaus 1982). First, primary binding proteins, like uS4, bind directly to the RNA; only then can secondary binding proteins bind the RNA. Finally, tertiary binding proteins, such as uS2 and uS3, will be recruited to the maturing ribosome particle. Kinetically, the primary proteins bind fastest to ribosomal RNA, followed by the secondary proteins and then the tertiary proteins. The binding of the proteins occurs in a 5' to 3' direction on the ribosomal RNA (Talkington, Siuzdak et al. 2005; Bunner, Beck et al. 2010). This order in which the ribosomes assemble, matches the direction in which ribosomal RNAs are synthesized, and in vivo the assembly of ribosomes ensues while the RNA is transcribed (Davis and Williamson 2017). For the efficient assembly of ribosomes, ribosomal proteins from all stages of assembly must be present. By transiently binding to the nascent RNA, ribosomal proteins guide the folding of the ribosomal RNA towards the mature state (Duss, Stepanyuk et al. 2019; Rodgers and Woodson 2019).

In vitro, ribosomal protein uS2 is one of the last proteins to join the maturing small ribosomal subunit. Early binding of uS2 will trap the maturing particle in a long-lived assembly intermediate state (Mulder, Yoshioka et al. 2010). The here observed direct binding of uS2 to RNAP may serve to increase uS2’s local concentration during ribosome assembly. Thus, uS2 can assist the folding of the nascent ribosomal RNA without trapping the small ribosomal subunit in an immature state.

The strong intrinsic effects uS3 and uS4 exert on transcription suggests that ribosomal proteins not only guide the folding, but also the transcription of the ribosomal RNA. Transcription of the ribosomal RNA that is too fast or too slow will upset the finetuned assembly of ribosomes (Lewicki, Margus et al. 1993; Schneider, Michel et al. 2007; Duss, Stepanyuk et al. 2019). Therefore, the ribosomal proteins that assemble around the nascent ribosomal RNA as free, transiently, or stably bound to ribosomal RNA or RNAP, all appear to contribute to the efficient and timely assembly of the ribosome (Figure 3.6E).

Implications for ribosome biogenesis beyond ribosome assembly?

In the cell, the free pool of ribosomal proteins is tightly coupled to the transcription of ribosomal RNA. In general, the genes of ribosomal proteins are clustered on long operons. One of the ribosomal proteins in these operons may not only bind to the maturing ribosomal RNA, but also to a regulatory region of the RNA transcript of its operon. An excess of this ribosomal protein will result in its binding to the operon mRNA and to the shutdown of the expression of all genes on the operon (Mikhaylina, Nikonova et al. 2021). This negative feedback ensures that ribosomal proteins are produced ‘just in time’ for ribosome assembly; thus, avoiding the detrimental intrinsic effects ribosomal proteins may exert on transcription in general.

Conclusion:

While we have known about the coupling of transcription with translation and with ribosome assembly for more than half a century, we only now are beginning to

elucidate the molecular bases for the coupling (Huang, Hilal et al. 2020; Rodgers and Woodson 2021; Webster and Weixlbaumer 2021). Here, we gauged the intrinsic effects ribosomal proteins uS2, uS3, and uS4 exert on transcription. These ribosomal proteins are at the RNAP-interface of the ribosome in complexes that capture the ribosome translating an mRNA while it is being transcribed (Kohler, Mooney et al. 2017; Wang, Molodtsov et al. 2020; Webster, Takacs et al. 2020). All three ribosomal proteins reduced ρ-dependent and intrinsic termination independent of the presence of Nus factors. They also increased the time the polymerase required to escape the *his* pause site. Ribosomal protein uS2 was the only one to bind to the polymerase. Yet, it had the least effect on termination and pausing, while uS3 had the most prominent. Based on our results, we suggest that uS2 anchors the transcribing polymerase to the translating ribosome. The effect of uS3 and uS4 on transcription varies with the length of the nascent RNA between the ribosome and polymerase. All three proteins may assist in finetuning the coupling between the transcription of the ribosomal RNA with its assembly into a ribosomal subunit. We further suggest that the intrinsic effects of the ribosomal proteins on transcription may have impelled the tight autoregulation of ribosomal proteins during ribosome biogenesis.

Table 3.1. Sequences of the DNA template for ρ-dependent termination and *his* pause assay

ρ-dependent termination template: +1 is bolded and underlined.

aagggataaatatctaacaccgtgcgtgttgactattttacctctggcggtgataatggttgc**a**tgtagtaagga
ggttgtatggaagaccgcgccgctgagaaaaagcgaagcggcactgctctttaacaatttatcagacaatct
gtgtgggcactcgaagatacggattctagatACCCCGGtcgaacgtcaacttacgtcatttttccgccca
acagtaatataatcaaacaaattaatcccgCAACATAACACCAGTAAATCAATAAT
TTTCTCTAAGTCACTTATTCCTCAGGTAATTGTTAATATATCCAGA
ATGTTAATCAAAATATATTTTCCCTCTATCTTCTCGTTGCGTTAAT
TTGACTAAATTCTCATGGATCCCAAGCTCCAATCCGGACAACCGA
TGAAAGCGGCGACGCGCAGTAACCCACAGCCGCCAGTCCCCTGG
CGGCATTTTAATTTCTTTTGGTccgccgggagcgg

His pause template: +1 is bolded and underlined.

aagggataaatatctaacaccgtgcgtgttgactattttacctctggcggtgataatggttgc**a**tgtagtaagg
aggttgtatggaagacGTTCCTCATCATCACCATCATCCTGACTAGTCTTT
CAGGCGATGTGTGCTGGAAGACATTCAGATCTTCCAGTGGTGCA
TGAACGCATGAGAAAGCCCCCGGAAGATCATCTTCCGGGGGCTT
TT

Table 3.2. Oligonucleotides used for the formation of transcription elongation complex and for the PCR-amplification of template DNA for ρ-dependent termination and *his* pause assays.

Template DNA strand	CCTGTCTGAATCGCTATCGCCGC
Non-template DNA strand	GCGATTCAGACAGG
Nascent RNA strand (Oligoribonucleotide)	rGrArGrUrCrUrGrCrGrGrCrGrArU
Forward primer for template DNA of ρ-dependent termination assay	aagggataaatatctaacaccgtgcgtgttgactattttacctctggcg gtg
Reverse primer for template DNA of ρ-dependent termination assay	ccgctcccggcggaccaaaagaaattaaaatgccgccag
Forward primer for template DNA of *his* pause assay	aagggataaatatctaacaccgtgcgtg
Reverse primer for template DNA of *his* pause assay	aaaagcccccggaagatgatc

Table 3.3. Time points used for data analysis and statistics for RNAP escape from the *his* pause site

Combinations	Time points used to determine slope (seconds)	Half-life (seconds)	R^2 value	Efficiency
RNAP (Chen, Malone et al.)	24, 36, 48, 60, 80	26.3	0.96	0.80
+ NusG	12, 24, 36, 48, 60, 80	18.2	0.95	0.65
+ uS10 (Nus B/E)	36, 48, 60, 80	24.7	0.92	0.90
+ uS2	36, 48, 60, 80, 120	53	0.97	0.85
+ uS4	48, 60, 80, 120, 160	115	0.98	0.60
+ uS3	120, 160, 300, 480	347	>0.99	0.60

Table 3.4. Initial rate of run-off product formation for the *his* pause construct

Component	Time points used	Delay (seconds)	R^2
RNAP (Chen, Malone et al.)	24, 36, 48, 60, 80	17.6	>0.99
+ NusG	12, 24, 36, 48	11.4	0.97
+ uS10 (Nus B/E)	24, 36, 48, 60, 80	21	0.98
+ uS2	36, 48, 60, 80	21.5	>0.99
+ uS4	36, 48	22.1	-
+ uS3	48, 60, 80	27.7	0.99

Table 3.5. Summary table of all measured effects of the ribosomal proteins uS2, uS3, and uS4 on transcription. Green indicates greater read-through while brown indicates less read-through. The darker shade of the green or brown indicates the difference compared to the result without ribosomal protein is being significant. Significance was defined using a two-tailed t-test with a P-value of $\underline{\geq}0.05$.

[a]ρ 'Read-through' is counted as both the read-through of ρ dependent termination sites as well as read out (past the intrinsic terminator to the end of the template).

[b]Termination measured by comparing intrinsic terminator to read-out band intensity.

[c]Efficiency values are difficult to measure accurately, especially with a slow RNAP (see text).

Summary table	W/O rib. protein (compared to ref.)	uS2	uS4	uS3	uS10/ NusB	Data presented in
ρ-dependent termination read-through[a] (RNAP+ρ)	20.7 ± 7.4% (17.9 ± 0.6% in (Said, Hilal et al. 2021))	30.9 ± 0.9%	52.8 ± 11.6%	68.8 ± 5.1%	-	Section 1.2 and Fig. 3.1B
ρ-dependent termination read-through (RNAP+ρ+Nus A/G)	16.7 ± 8.5% (5.7 ± 0.3 in (Said, Hilal et al. 2021))	17.8 ± 1.7%	37 ± 4.4%	41.1 ± 1.3%	-	Section 1.3 and Fig. 3.1B
ρ-dependent termination read-through (RNAP+ρ+Nus A/B/E/G)	15.5 ± 3.6% (11% in (Torres, Condon et al. 2001))	12.8 ± 5.2%	47.9 ± 1.7%	56.1 ± 5.8%	N/A	Section 1.4 and Fig. 3.1B
intrinsic termination[b] (RNAP+ρ)	35.1 ± 3.6% (trend from (Huang, Said et al. 2019))	34.6 ± 2.4%	31 ± 8.1%	25 ± 2.9%	-	Section 2.2 and Fig. 3.2B
intrinsic termination (RNAP+ρ+Nus A/G)	70.5 ± 2.8% (trend from (Huang, Said et al. 2019))	60 ± 2.2%	52.9 ± 11.1%	48.3 ± 4.7%	-	Section 2.2 and Fig. 3.2C
intrinsic termination[b] (RNAP+ρ+Nus A/B/E/G)	61.3 ± 1.1% (trend from (Huang, Said et al. 2019))	71.1 ± 4.8%	55.8 ± 4.7%	44.3 ± 2.7%	N/A	Section 2.2 and Fig. 3.2D

Chapter 4:

Review of Transcription-Translation Coupling

Publication:

Conn, A.B., Diggs, S., Tam, T.K., Blaha, G.M. (2019**)** "Two Old Dogs, One New Trick: A Review of RNA Polymerase and Ribosome Interactions during Transcription-Translation Coupling." *Int. J. Mol. Sci.*, ***20*** 2595.

[PMID: 31137816]

Abstract:

The coupling of transcription and translation is more than mere translation of an mRNA that is still being transcribed. The discovery of physical interactions between RNA polymerase and ribosomes has spurred renewed interest into this long-standing paradigm of bacterial molecular biology. Here we provide a concise presentation of recent insights gained from super-resolution microscopy, biochemical, and structural work, including cryo-EM studies. Based on the presented data, we put forward a dynamic model for the interaction between RNA polymerase and ribosomes in which the interactions are repeatedly formed and broken. Furthermore, we propose that long intervening nascent RNA will loop out and away during the forming the interactions between RNAP and ribosomes. By comparing the effect of the direct interactions between RNA polymerase and ribosomes with those that transcription factors NusG and RfaH mediate, we submit that two distinct modes of coupling exist: factor-free and factor-mediated coupling. Finally, we provide a possible framework for transcription-translation coupling and elude to some open questions in the field.

Introduction:

In bacterial cells, the lack of a physical barrier allows transcription and translation machineries to mingle, thus enabling concurrent translation of an mRNA while it is being transcribed in a process known as transcription-translation coupling (French, Santangelo et al. ; McGary and Nudler 2013). Due to this coupling, ribosomes translating the nascent RNA trail the transcribing RNA polymerase (RNAP) (Das, Goldstein et al. 1967), bringing both physically close to each other (Miller, Hamkalo et al. 1970; Klaholz 2017). This proximity of transcribing RNAP and the first translating ribosome rationalizes long-standing observations, such as transcription polarity and transcription attenuation.

In transcription polarity, a premature stop codon curtails not only the expression of the mutated gene, but also that of all genes on the same polycistronic operon downstream of the mutation. The premature translation termination causes the ribosome to dissociate from the nascent mRNA, allowing transcription termination factor Rho to proceed along the nascent RNA all the way to the RNAP. At the RNAP, the Rho factor induces transcription termination, halting transcription of the downstream genes on the operon (Richardson, Grimley et al. 1975; Adhya and Gottesman 1978) (Figure 4.1A). Premature transcription termination can occur by simply reducing the rate of translation. The slower speed of the first trailing ribosome will increase the length of the intervening nascent RNA between the ribosome and RNAP. This longer RNA gap between RNAP and leading ribosome allows the Rho factor to bind to the nascent RNA ahead of the ribosome in direct line to the RNAP (de Smit, Verlaan et al. 2009). The longer intervening RNA also provides sufficient room for intrinsic terminator signals to fold and

cause the termination of transcription (Elgamal, Artsimovitch et al. 2016). (Figure 4.1B).The intrinsic transcription termination signal consists of a stable hairpin stem loop followed by a uridine-rich sequence (Ray-Soni, Bellecourt et al. 2016).

Programmed decoupling of transcription and translation is also exploited for gene regulation, *i.e.*, transcription attenuation. The most well-known example of transcription attenuation involves the cellular concentration of tryptophan regulating the expression of the *trp* operon. Starvation for tryptophan induces stalling of the first ribosome translating the leader sequence of the operon. The stalled ribosome prevents the formation of a transcription termination signal on the nascent RNA, allowing the RNAP to continue to transcribe downstream genes on the *trp* operon (Yanofsky and Ito 1966; Landick, Carey et al. 1985). In other instances of transcription attenuation, the stalled ribosome leads to transcription termination, thereby halting the expression of downstream genes (Turnbough, Hicks et al. 1983; Yanofsky 2000).

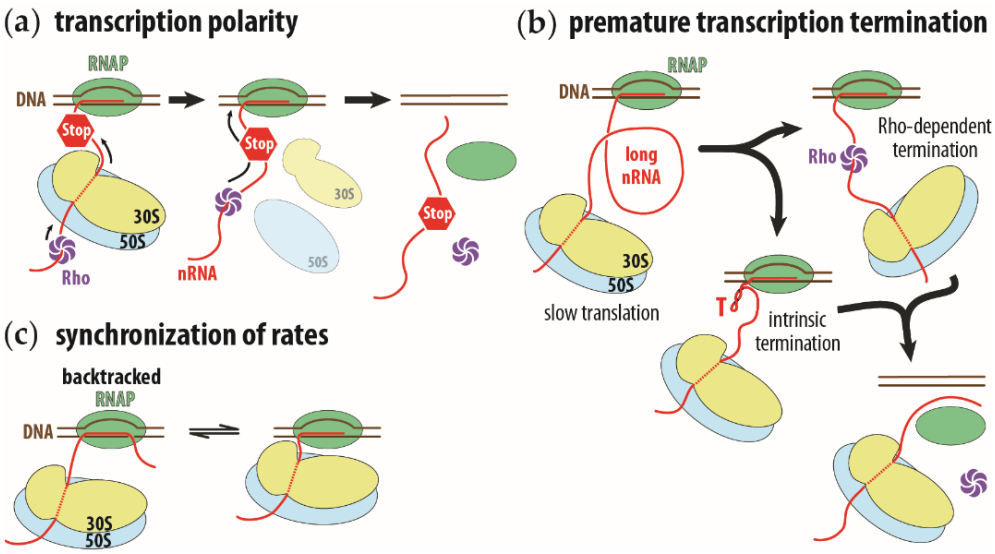

Figure 4.1. Schematic representation of transcription polarity, premature transcription termination on long intervening nascent RNA, and synchronization of transcription and translation rates. (**a**) Transcription polarity is caused by a premature stop codon (STOP sign) on the nascent RNA (nRNA, in red). Translation of the nascent RNA will terminate and the ribosome (in yellow and blue, for small and large ribosomal subunits, respectively) will prematurely dissociate from the nascent RNA. This allows Rho transcription termination factor (in purple) to reach RNAP (in green) and induce premature transcription termination. (**b**) A long intervening nascent RNA allows the Rho factor to bind ahead of the ribosome or allow the intrinsic transcription terminator to fold (hairpin structure indicated with a red capital T). In both instances, transcription terminates. (**c**) Synchronization of transcription rate to translation rate. The running ahead of the RNAP will cause the polymerase to pause and backtrack (complex on the left). The translating ribosome will push the RNAP forward and

reactivate its transcription activity (complex on the right). This running ahead and pausing to wait for the ribosome synchronizes the transcription rate to the translation rate.

The proximity between the transcribing RNAP and its trailing ribosome is maintained under different growth conditions (Vogel and Jensen 1994; Iyer, Le et al. 2018). A slowing of translation induced by either an antibiotic or a mutation results in a corresponding slowing of transcription (Proshkin, Rahmouni et al. 2010). This slowing of translation allows the RNAP to run ahead of the ribosome, where it is more likely to stall and backtrack. While backtracking, the RNAP slides backwards on the nascent RNA and DNA template strand, rezipping the upstream nascent RNA and template DNA while extruding the 3' end out of the NTP entry site. A ribosome trailing closely behind the RNAP will prevent the polymerase from sliding backwards, biasing the polymerase towards the forward direction, extending the nascent RNA (Proshkin, Rahmouni et al. 2010). This interplay between the RNAP running ahead and stalling and being reactivated by a trailing ribosome, results in the matching of RNAP's speed to that of the ribosome, *i.e.*, the rate of transcription is synchronized to the rate of translation (Figure 4.1C). Therefore, inhibiting translation leads to a genome-wide stalling of transcription (Zhang, Mooney et al. 2014). The stalled RNAP acts as a barrier for the DNA replication machinery, jeopardizing the processivity of replication and with it, the integrity of the genome (Mirkin and Mirkin 2007; Dutta, Shatalin et al. 2011).

Increasing the transcription rate by blocking backtracking occurs also on non-protein encoding genes. Rather than a trailing ribosome, a trailing RNAP suppresses stalling and backtracking of the leading RNAP. The trailing polymerase biasing the leading polymerase towards the forward direction explains the higher overall transcription rate of highly transcribed non-coding operons, such as the rRNA operons

(*i.e.*, 85 nts/sec for rRNA vs. 40-55 nts/sec for mRNA) (Epshtein and Nudler 2003; Bremer and Dennis 2008; Klumpp and Hwa 2009).

Do transcription and translation occur in the same cellular compartment?

Although transcription and translation are assumed to occur in the same compartment, this assumption has been recently challenged. In *E. coli*, the genome is segregated from the cytoplasm, forming a dense, compact structure in the center of the cell, known as the nucleoid. The nucleoid sequesters nearly all of the cellular RNAPs (Shepherd, Dennis et al. 2001; Bakshi, Siryaporn et al. 2012) while expelling most of the ribosomes, forcing them to accumulate on the periphery of the nucleoid, particularly at the poles of the cell (Hobot, Villiger et al. 1985; Cabrera and Jin 2003; Bakshi, Siryaporn et al. 2012). This spatial separation of RNAPs and ribosomes suggests that most of transcription and translation occur apart from each other (Bakshi, Choi et al. 2015).

Tracking of individual ribosomal subunits reveals that most of the translating ribosomes are excluded from the nucleoid, while free ribosomal subunits can enter the nucleoid almost as unhindered as tRNAs and translation factors (Sanamrad, Persson et al. 2014; Bakshi, Choi et al. 2015; Stracy, Lesterlin et al. 2015; Plochowietz, Farrell et al. 2017; Mustafi and Weisshaar 2018) . Similarly, tracking of individual RNAP molecules indicates that free RNAPs can move unhindered within the nucleoid at a rate comparable to that of in solution (Stracy, Lesterlin et al. 2015). This unhindered diffusion of the RNAP suggests that RNAP is, in addition to sliding along individual DNA strands, crossing between DNA strands in its search for a transcription start site (von Hippel and Berg 1989). Once a polymerase has found a transcription start site, it initiates and

transcribes approximately 100-150 nucleotides before pausing, *i.e.*, promoter proximal pausing (Mooney, Davis et al. 2009). The polymerase pausing presumably enables one or several ribosomes to initiate translation on the nascent RNA and catch up to the polymerase, thus establishing the coupling of transcription and translation.

Under fast growing conditions, the transcribing RNAPs cluster on the periphery of the nucleoid, while under slow growing conditions they remain distributed throughout the nucleoid (Cabrera and Jin 2003; Stracy, Lesterlin et al. 2015). In a nutrient-rich condition, *E. coli* requires fewer genes to satisfy its metabolic needs, therefore allowing it to redirect its resources towards expressing the genes required for fast growth. This results in the aggregation of RNAPs and ribosomes on these few, highly expressed genes. Possibly driven to increase the nucleoid's conformational flexibility (*i.e.*, entropy) (Mondal, Bratton et al. 2011), these highly expressed genes move to the periphery of the nucleoid where they cluster (Figure 4.2) (Cabrera and Jin 2003; Spahn, Cella-Zannacchi et al. 2015; Stracy, Lesterlin et al. 2015). This suggests that under fast growing conditions all genes are transcribed at the interface between the nucleoid and ribosome-rich cytoplasm, which further implies that all genes that can support coupling, will have transcription and translation coupled.

Under slow growing conditions, RNAP remains evenly distributed in the nucleoid (Cabrera and Jin 2003; Stracy, Lesterlin et al. 2015). Based on the observation that an mRNA undergoes on average 30-60 rounds of translation before it is degraded and only the first round is coupled to transcription (Mitarai, Sneppen et al. 2008), we estimate that no more than 4 % of ribosomes participate in transcription-translation coupling. 10-15 %

of ribosomes are present as free ribosomal subunits, which can enter the nucleoid nearly unhindered (Sanamrad, Persson et al. 2014). As the nucleoid occupies nearly half the volume of the cell, it implies that at least 5 % of ribosomes are available in the nucleoid. This suggests that even under slow growing conditions transcription and translation are coupled. Note that we are implicitly assuming that all protein-encoding genes require or support transcription-translation coupling – an assumption that has not yet been tested.

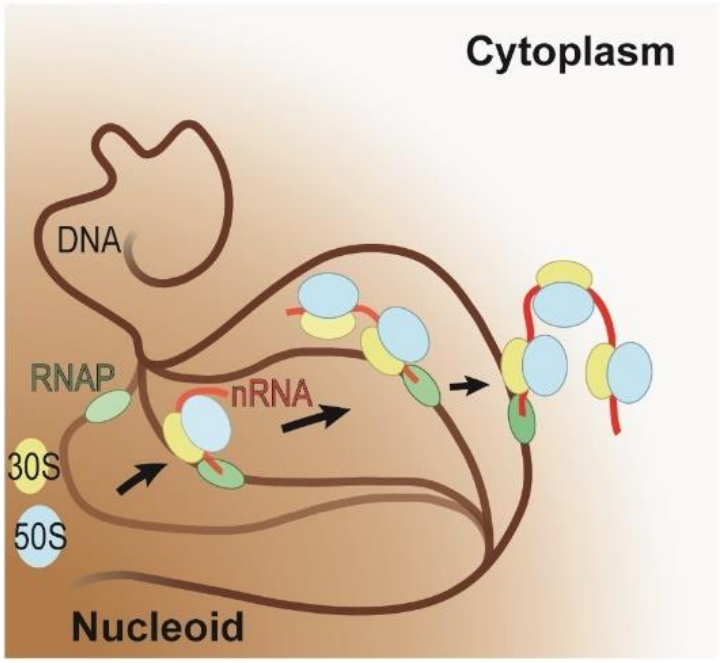

Figure 4.2. Schematic representation of the coupling of transcription and translation on highly expressed genes under fast growing conditions. RNA polymerase (RNAP, in green) initiates transcription on the DNA (in brown) within the nucleoid (brown shaded area). As soon as the polymerase has transcribed a sufficiently long nascent RNA (in red), translation will ensue (large and small ribosomal subunits in blue and yellow, respectively). During coupling the active gene is relocalized to the interface of the nucleoid and cytoplasm. The progression of this relocalization is indicated by arrows and by the progressive increase in opacity of the DNA, RNAP, nascent RNA, and ribosomal subunits.

Does transcription-translation coupling result only from the colocalization of RNAP and ribosomes on nascent RNA?

The above described observations of transcription-translation coupling can be explained by the binding of ribosomes to the nascent RNA of a transcribing RNAP; no physical interactions between the transcribing RNAP and the first trailing ribosome must be evoked. This assumption was first challenged by the NMR structure of the complex of ribosomal protein uS10 bound to transcription factor NusG (Burmann, Schweimer et al. 2010). (Ribosomal protein uS10 is also known as ribosomal protein S10 and as transcription factor NusE. Here we follow the naming convention for ribosomal proteins as set forth in Ban *et al.* (Ban, Beckmann et al. 2014).

NusG stimulates transcription (Burova, Hung et al. 1995; Burns, Richardson et al. 1998) as well as translation (Zellars and Squires 1999). Of the two domains of NusG, the N-terminal domain binds to RNAP, while the C-terminal domain can bind either transcription termination factor Rho (Mooney, Schweimer et al. 2009) or ribosomal protein uS10 (Burmann, Schweimer et al. 2010). The binding of the N-terminal domain of NusG to the RNAP prevents the polymerase from entering long-lived pauses, thereby increasing the overall transcription rate (Herbert, Zhou et al. 2010). On the other hand, the binding of Rho factor to the C-terminal domain places the transcription termination factor near the nascent RNA. This proximity facilitates the loading of Rho factor onto the nascent RNA only a short distance away from the RNAP, thereby promoting Rho-dependent transcription termination. NusG's ability to prevent prolonged transcription pausing and to recruit Rho factor to the RNAP explains the apparently contradictory

effects NusG exerts on transcription, stimulating both transcription elongation and transcription termination (Sullivan and Gottesman 1992; Li, Mason et al. 1993).

The binding interface of NusG on ribosomal protein uS10 within the NusG:uS10 complex is accessible on the ribosome (Burmann, Schweimer et al. 2010) and residues within this interface are critical for binding of NusG to ribosomes both *in vitro* and *in vivo* (Saxena, Myka et al. 2018). NusG appears not only to bind RNAP and ribosome on their own, but also to form a physical link between the transcribing RNAP and the trailing ribosome during transcription-translation coupling (Burmann, Schweimer et al. 2010). Since ribosomal protein uS10 competes with Rho factor for overlapping sites on NusG's C-terminal domain (Burmann, Schweimer et al. 2010; Lawson, Ma et al. 2018), coupling of RNAP and ribosomes via NusG suppresses the recruitment of Rho factor and with it its mediated transcription termination.

Another transcription factor known to physically link RNAP and ribosomes is the NusG-paralog RfaH. While NusG associates with RNAP during expression of almost all genes (Mooney, Davis et al. 2009), RfaH regulates the expression of a handful of operons with a specific signal sequence in the 5' untranslated region (*i.e.*, operon polarity suppressor or *ops* signal) (Bailey, Hughes et al. 1997). The coupling brought about by RfaH enables the expression of exogenous, horizontally transferred genes even if they are not codon-optimized and are missing the translation initiation signals specific for *E. coli* (Burmann, Knauer et al. 2012).

Like NusG, RfaH consists of two domains. Its N-terminal domain is highly similar to NusG's and equally reduces transcription pausing. Both proteins even compete

for binding to overlapping sites on the RNAP, resulting in a mutually exclusive binding of the factors to RNAP *in vivo* (Belogurov, Mooney et al. 2009). The C-terminal domains of both factors, however, are strikingly different. While the C-terminal domain of NusG adopts an all β-sheet structure and is connected via a flexible linker to its N-terminal domain (Steiner, Kaiser et al. 2002), the C-terminal domain of RfaH folds into an all α-helical structure and intimately interacts with its N-terminal domain (Belogurov, Vassylyeva et al. 2007). RNAP will pause upon transcribing the *ops* signal. This allows RfaH to recognize the *ops* sequence on the non-template DNA strand and bind to the polymerase (Artsimovitch and Landick 2000; Kang, Mooney et al. 2018). Upon binding of the N-terminal domain, RfaH's C-terminal domain is released and adopts the all β-sheet structure of NusG (Burmann, Knauer et al. 2012). The transformed C-terminal domain then allows RfaH to recruit ribosomal protein uS10 at the same interface that NusG does (Belogurov, Mooney et al. 2009).

Unlike NusG, RfaH does not bind Rho factor (Burmann, Knauer et al. 2012). Therefore, RfaH hampers Rho-dependent transcription termination in two ways. First, it blocks Rho factor from reaching the RNAP by mediating a tight coupling between RNAP and the first trailing ribosome. Second, it diminishes NusG's stimulatory effect on Rho-dependent termination by competing with NusG for binding to RNAP.

Are RNAP and ribosome only linked together by NusG and RfaH or can they directly interact with each other?

Early genetic studies uncovered an interaction between RNAP and the small ribosomal subunit (Chakrabarti and Gorini 1975; Chakrabarti and Gorini 1977),

indicating that mediating factors such as NusG or RfaH may not be required for the coupling of transcription and translation. Additionally, several ribosomal proteins also serve as transcription factors on their own. For example, ribosomal protein uS4 inhibits premature termination of ribosomal RNA transcription (Torres, Condon et al. 2001), while ribosomal protein uL2 promotes transcription of genes driven from ribosomal RNA promoters (Rippa, Cirulli et al. 2010). Ribosomal protein uS10, which binds the C-terminal domain of NusG as discussed above, is an integral part of a transcription antitermination complex and can bind RNAP on its own (Burmann, Schweimer et al. 2010; Drögemüller, Strauß et al. 2015; Drögemüller, Strauß et al. 2015; Said, Krupp et al. 2017). Finally, ribosomal protein bS1 stimulates the recycling of RNAP during *in vitro* transcription (Sukhodolets, Garges et al. 2006). Although bS1 binds only weakly to ribosomes, it is critical for translation initiation (Boni, Isaeva et al. 1991). By capturing the mRNA in its unfolded form, bS1 provides the ribosome access to the ribosomal binding site (aka Shine-Dalgarno sequence) buried in local secondary structure (Studer and Joseph 2006; Qu, Lancaster et al. 2012). This unfolding of the structured mRNA extends not only downstream towards the Shine-Dalgarno region, but also upstream of the bS1 binding site. In some cases, the upstream unfolding is large enough to accommodate a second ribosome, priming the mRNA for a second round of translation (Andreeva, Belardinelli et al. 2018). Once translation has ensued, it is unable to dissociate from the ribosome (Sørensen, Fricke et al. 1998). This suggests that ribosome-bound bS1 interacts with RNAP during transcription-translation coupling.

Direct interactions between RNAP and ribosomes were also observed in the cryo-EM studies of the small ribosomal subunit bound to RNAP (*i.e.*, the 30S•RNAP complex) and of the ribosome in complex with RNAP, in which the ribosome is translating the nascent RNA being transcribed by the RNAP (*i.e.*, the expressome) (Demo, Rasouly et al. 2017; Kohler, Mooney et al. 2017). In reconstructions of both complexes, the RNAP binds to the ribosome with its nascent RNA exit site while the RNAP binding sites on the ribosome are distinct and non-overlapping (Figure 4.3B-E).

In reconstructions of the 30S•RNAP complex, the RNAP is bound close to the 30S subunit site that recognizes the Shine-Dalgarno sequence of mRNAs. The interface between RNAP and 30S subunit consists of regions of the β' and β subunits close to the nascent RNA exit site on the RNAP and of ribosomal proteins uS2, bS6:bS18 heterodimer, and bS21, and ribosomal RNA helices 26 and 40. Due to the flexibility of ribosomal protein bS1, only parts of the protein were visualized in one of the reconstructed 30S•RNAP particles. In this reconstruction, the C-terminal half of ribosomal protein bS1 interacts with the bound RNAP. In our own studies of the RNAP-30S subunit interface, we found by chemical crosslinking that the β' subunit of RNAP is close to ribosomal proteins bS1, uS2, bS6, uS7, uS9, and uS11; all proteins surrounding the mRNA exit site of the 30S subunit (Figure 4.3B and D) (Fan, Conn et al. 2017).

The 30S subunit of all three reconstructed 30S•RNAP particles adopts the same conformation, in which the diameter of the mRNA exit site is widened. This widening of the 30S subunit's mRNA exit site may allow the nascent RNA to better access the mRNA path on the 30S subunit during translation initiation (Demo, Rasouly et al. 2017). Please

note that in all 30S•RNAP particles the RNAP is neither transcribing a nascent RNA nor bound to DNA (Demo, Rasouly et al. 2017). Therefore, these complexes may not recapitulate a step during translation initiation of the nascent RNA, but simply reflect interactions between 30S subunits and *free* RNAP that may occur in the nucleoid.

In the reconstruction of the expressome, the RNAP docks to the mRNA entry site of the ribosome, allowing the nascent RNA exiting the RNAP to immediately enter the ribosome. The binding interface on the RNAP consists of regions close to the nascent RNA exit site from all subunits and on the ribosome it includes ribosomal proteins uS2, uS3, uS4, uS5, and uS10, and helix 16 of the 30S subunit's ribosomal RNA (Kohler, Mooney et al. 2017) (Figure 4.3C and E). In addition, the C-terminal domain of one of the two α subunits of the bound RNAP is bound to ribosomal protein uS9 and helices 38 and 39 of the 30S subunit's ribosomal RNA. This RNAP binding site is more than 75 Å distant from that seen in the 30S•RNAP particles (Demo, Rasouly et al. 2017; Kohler, Mooney et al. 2017). Please note that the expressome complex was prepared by translating all of the nascent RNA of a preformed, stable RNAP complex. Furthermore, the physical contact between RNAP and the ribosome was favored by the presence of the chemical cross-linker glutaraldehyde during the purification of the complex (Stark 2010; Kohler, Mooney et al. 2017)**.** Therefore, the expressome structure may only reflect a complex with minimal nascent RNA between the RNAP and ribosome (Kohler, Mooney et al. 2017).

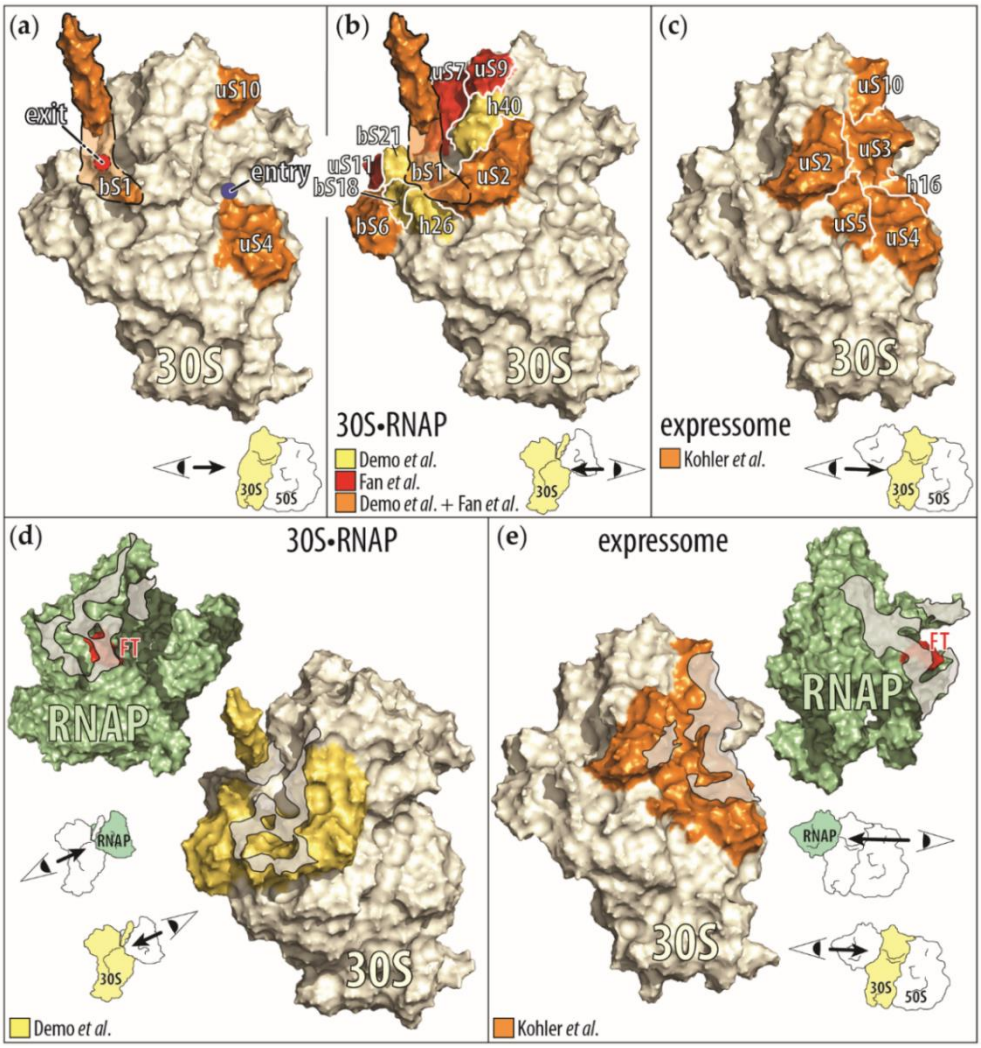
(a)
exit
uS10
bS1
entry
uS4
30S
(b)
uS7
uS9
h40
bS21
uS11
bS18
bS1
uS2
bS6
h26
30S
30S•RNAP
Demo et al.
Fan et al.
Demo et al. + Fan et al.
30S
(c)
uS10
uS2
uS3
h16
uS5
uS4
30S
expressome
Kohler et al.
30S
50S
(d)
30S•RNAP
FT
RNAP
RNAP
30S
30S
Demo et al.
(e)
expressome
FT
RNAP
RNAP
30S
30S
50S
Kohler et al.

Figure 4.3. Display of the RNAP-ribosome interactions and contact points identified by biochemical and cryo-EM studies. (**a**) Ribosomal proteins (in orange) that influence RNAP activity by themselves (bS1 (Sukhodolets, Garges et al. 2006), uS4 (Torres, Condon et al. 2001), and uS10 (Drögemüller, Strauß et al. 2015)) are mapped onto the small ribosomal subunit (30S) derived from the cryo-EM structure of the small ribosomal subunit bound to RNAP (30S•RNAP) (Demo, Rasouly et al. 2017). Because ribosomal protein bS1 is only partially resolved in this structure, we outlined the approximate position of the remaining protein (orange shaded area). In addition, the mRNA entry (blue circle) and exit (red circle with dashed black border indicating its positions behind bS1) sites on the small ribosomal subunit are indicated. In the right corner is a cartoon representation of the direction of the view displayed of the small ribosomal subunit. (**b**) Ribosomal proteins and RNA helices contacting the RNAP upon binding of the small ribosomal subunit to RNAP. Shown are the proteins identified to be close to RNAP in the cryo-EM structure of 30S•RNAP in Demo *et al.* (Demo, Rasouly et al. 2017)and by chemical crosslinking in Fan *et al.* (Fan, Conn et al. 2017). (Proteins observed only in Demo *et al.* are in yellow, those shared by Demo *et al.* and Fan *et al.* are in orange and those observed only in Fan *et al.* are in red). (**c**) Ribosomal proteins (in orange) contacting the RNAP in the cryo-EM structure of a ribosome translating a nascent RNA as it is being synthesized, aka expressome (Kohler, Mooney et al. 2017). Interactions between the C-terminal domain of one of the two α subunits of the RNAP with the ribosome were omitted for clarity. (**d**) and (**e**) Contact interfaces between RNAP and small ribosomal subunit as seen in the cyro-EM structures of the 30S•RNAP complex (d)

and the expressome (e). In both representations the view is onto the contact areas (gray shaded areas) on the RNAP (green) and on the small ribosomal subunit (yellow). Also indicated is the β flap-tip of the RNAP (red, marked with FT), past which the nascent RNA exits the RNAP to enter the small ribosomal subunit.

Although the RNAP positions in both structures are distinct, they may be part of a single, overarching cycle of transcription-translation coupling. We propose that similar to translation initiation of a structured mRNA, during which the 3' end is repositioned on the 30S subunit from the mRNA exit to the mRNA entry site (Marzi, Myasnikov et al. 2007; de Smit, Verlaan et al. 2009), the RNAP is repositioned during translation initiation of the nascent RNA. Therefore, the RNAP-binding site seen in the 30S•RNAP may reflect a state during the beginning phase of the coupling, while the one seen in the expressome may reflect a state during ongoing coupling along a gene or operon.

In both structures, the NusG- and RfaH-binding sites on the RNAP and the ribosome are too far apart to allow NusG or RfaH to bridge both macromolecules. Therefore, another spatial arrangement between RNAP and ribosome must exist that complements already captured and visualized arrangements.

Does the length of intervening RNAs influence the interaction between RNAP and ribosome during coupling?

The structure of the expressome, suggests a continuous, static physical connection between RNAP and the ribosome during coupling. Such a close connection provides a simple explanation for the effects the coupling of translation exerts on transcription. However, the length of intervening nascent RNA between RNAP and ribosome is constantly fluctuating. Because the ribosome steps three nucleotides at a time along the nascent RNA, the ribosome must wait for the RNAP to add three nucleotides, one by one, before taking a step. This causes the length of the intervening RNA to fluctuate between one, two, three, and no extra nucleotides between RNAP and ribosome. Such small

variations in the length of the nascent RNA may be scrunched in between the RNAP and ribosome without breaking the interface.

Larger variations are more difficult to reconcile with a static model of RNAP-ribosome arrangement of the expressome. The transcription and translation rates are dependent on the cellular concentration of different metabolites, *i.e.*, nucleotides and amino acids, respectively. Therefore, these rates will respond differently to concentration fluctuations of these metabolites. These independent responses of transcription and translation will result in varying lengths of intervening nascent RNA. The rate differences are further aggravated by the apparent independent distribution of transcription and translation regulatory elements along genes. (For more specific information on the different regulatory elements for translation, see review by Rodnina (Rodnina 2016) and for those for transcription, see review by Artsimovitch (Artsimovitch 2018). These larger fluctuations in the length of the intervening RNA can be accommodated by a repeated breaking and forming of the expressome depending on the length of the intervening RNA.

Because the interactions between RNAP and ribosomes can be repeatedly formed and broken, it suggests that the interactions between both are dynamic. Such a dynamic view of the interactions is supported by the moderate strength of the RNAP affinity for ribosomes (*i.e.*, a low micromolar dissociation constant of the RNAP•ribosome complex (Fan, Conn et al. 2017)). We suggest that the interactions between the RNAP and ribosomes are not only more dynamic but are possibly independent of the length of the intervening nascent RNA. Due to the tethering via the nascent RNA, the local

concentration of the first trailing ribosome close to the RNAP will exceed the dissociation constant of the RNAP•ribosome complex even with thousands of nucleotides of intervening nascent RNA (Figure 4.4A) (Conant, Goodarzi et al. 2008). To accommodate such long intervening RNA, the RNA has to loop out and away from the RNAP-ribosome complex (Figure 4.4B). Similar looping of the nascent RNA has been attributed to the antitermination observed during transcription of ribosomal RNA (Condon, Squires et al. 1995; Krupp, Said et al. 2019) and during transcription of lambda bacteriophage genome (Conant, Goodarzi et al. 2008; Said, Krupp et al. 2017). Such dynamic binding and dissociation of the RNAP-ribosome complex could explain the stochastic behavior of transcription-translation coupling observed *in vivo* (Li, Zhang et al. 2016; Chen and Fredrick 2018). These lines of argument should also apply to the RNAP-ribosome complex formation mediated by NusG and RfaH.

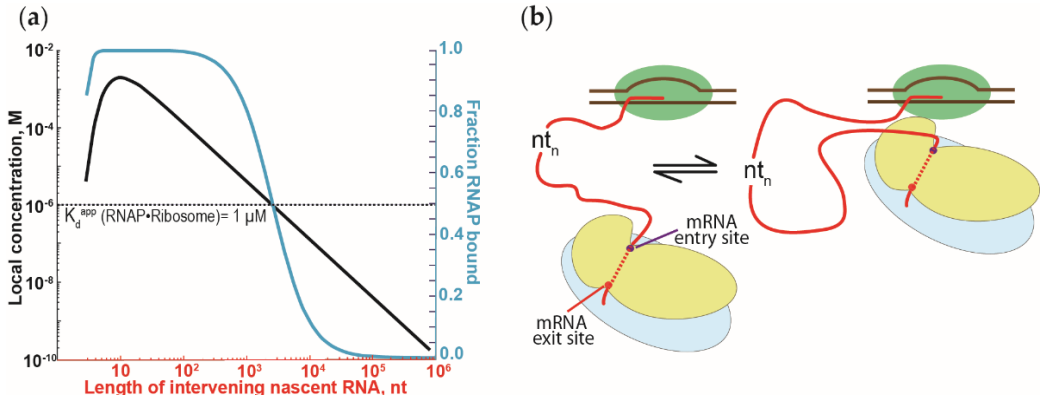

Figure 4.4. The effect of tethering of RNAP and ribosomes by nascent RNA on the RNAP•ribosome complex formation. (**a**) Dependence of RNAP•ribosome complex formation on length of intervening nascent RNA. The intervening nascent RNA was modeled as a freely jointed chain. The local concentration of the first trailing ribosome around the RNAP that it is tethered to (left y-axis) and the fraction of RNAP-ribosome complex formation (in blue, right y-axis) are plotted against the length of the intervening nascent RNA. Local concentration and fraction of complex formation were calculated following Conant *et al.* (Conant, Goodarzi et al. 2008) and Rippe (Rippe 2001). (**b**) Schematic representation of the binding equilibrium dynamics between the first trailing ribosome (in blue and yellow for large and small ribosomal subunits, respectively) and the RNAP (in green), tethered via the nascent RNA (red). Binding of the RNAP and ribosome will cause the intervening nascent RNA to loop out and away from the RNAP-ribosome complex.

What is the current framework for transcription-translation coupling?

We can discern two possible modes of transcription-translation coupling, factor-free and factor-mediated coupling; a distinction also eluded to by others, *e.g.* (Artsimovitch 2018).

In factor-free coupling, the RNAP is initially recruited to the mRNA exit site of the 30S subunit (Demo, Rasouly et al. 2017). During translation initiation, the RNAP relocalizes from the mRNA exit to the mRNA entry site of the 30S subunit (Kohler, Mooney et al. 2017). Due to tethering by the nascent RNA and a moderate affinity of the ribosome for RNAP, the complex between the first trailing ribosome and RNAP will repeatedly form and dissociate. These frequent encounters between RNAP and ribosome enable the coupling to accommodate a fluctuating length of intervening nascent RNA.

Factor-mediated coupling is most apparent for coupling mediated by RfaH. Here, the coupling also affects translation of the nascent RNA, in particular its initiation (Burmann, Knauer et al. 2012). This therefore points to RfaH already being bound to the RNAP during the first step of translation initiation when the 30S subunit recruits the nascent RNA. Due to RfaH linkage of RNAP and the trailing ribosome, the spatial arrangement of RNAP and the ribosome differs from those captured for factor-free coupling.

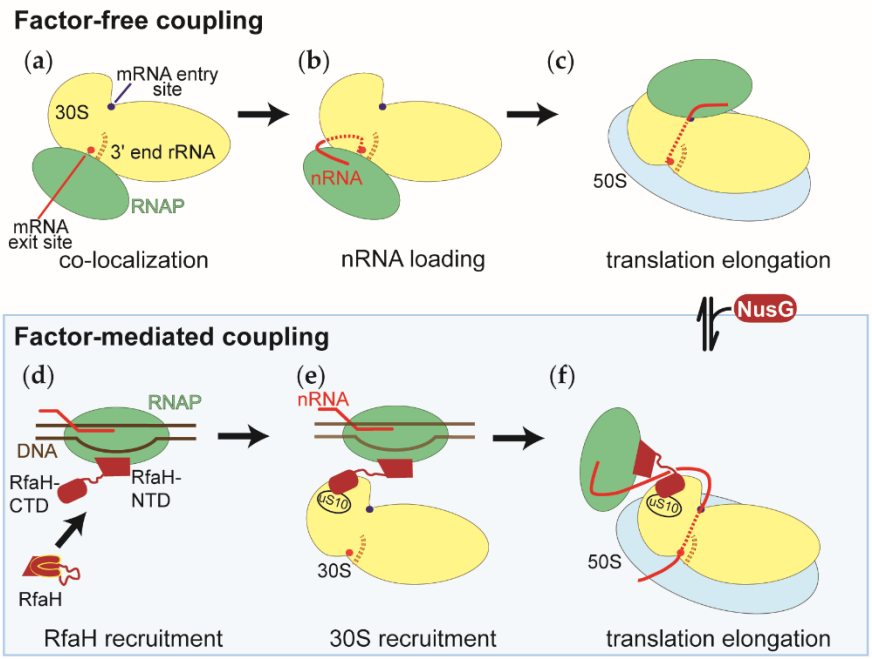

Figure 4.5. Model of RNAP-ribosome arrangements during factor-free and factor-mediated coupling of transcription and translation. The representation of the small ribosomal subunit (30S in yellow) is the same in all panels, with both RNAP binding sites facing the reader. RNAP, the large ribosomal subunit (50S), DNA, and nascent RNA are shown in green, blue, brown, and red, respectively. NusG and RfaH, the factors that physically link RNAP and ribosomes during factor-mediated coupling are shown in dark red. (**a**) Co-localization of RNAP and small ribosomal subunits within the nucleoid. (**b**) Recruitment of nascent RNA to the small ribosomal subunit during the first step of translation initiation. Also shown is the positioning of the 5' end of the nascent RNA relative to the 3' end of the ribosomal RNA of the small ribosomal subunit (3' end rRNA). In many cases, both ends engage in base pairing interactions. (**c**) During translation initiation, RNAP relocalizes on the 30S subunit from the mRNA exit site shown in (a) and (b) to the mRNA entry site. Shown is the RNAP-ribosome complex with the shortest

intervening nascent RNA. (**d**) Recruitment of transcription factor RfaH to the RNAP which has transcribed and paused at the *ops* signal sequence. RfaH's C-terminal domain undergoes a conformational change from an all α helical to an all β sheet structure. (**e**) Recruitment of the small ribosomal subunit (30S) to RNAP-RfaH complex before initiation of translation. (**f**) During factor-mediated coupling, the RNAP and ribosome are held close to each other by either transcription factor RfaH or NusG. The NuG-mediated coupling is established by binding of NusG to the factor-free coupled RNAP and ribosome.

NusG-mediated coupling appears to be a hybrid of factor-mediated and factor-free coupling. Unlike RfaH, NusG is not recruited at a defined point during transcription of a gene, but is recruited after the RNAP has cleared a promoter proximal pausing site (Mooney, Davis et al. 2009). This implies that NusG is recruited to RNAP after translation of the nascent RNA has assisted the polymerase in clearing the pause site. Therefore, NusG can reorganize the RNAP-ribosome arrangement from factor-free to factor-mediated coupling (Figure 4.5).

Which questions remain?

The discovery of direct physical interactions between RNAP and ribosomes hints that individual transcription events can immediately be relayed to the ribosome, affecting its translational activity. Conversely, individual translation events can be relayed to the RNAP, thus affecting its transcriptional activity. The mutual influence of transcription and translation on coupling raises the tantalizing prospective of a novel mechanism of regulation. Any mechanism of the mutual regulation will have to specify: 1) the phases of transcription and translation that are coupled, 2) the functional states of the RNAP and ribosome that interact, and 3) the effect this regulation exerts on the coupled processes.

Most of our current understanding of transcription-translation coupling was gained from work with a narrow set of model genes and operons under a few conditions. A comprehensive list of genes that support or require coupling for expression remains elusive. Modern genome-wide approaches may overcome this shortcoming in the foreseeable future. It will be interesting to see how this list of genes depends on the presence of NusG or varies with environmental and growth conditions.

Although we focused in this review on transcription-translation coupling alone, it is important to realize transcription and translation couples with other critical cellular processes. For example, transcription couples to DNA repair (Spivak 2016; Pani and Nudler 2017) and translation couples to protein folding (Seligmann and Warthi 2017; Thommen, Holtkamp et al. 2017) and protein translocation (Woldringh 2002; Elvekrog and Walter 2015). The integration of all these coupled processes into a comprehensive view will be required to gain a full appreciation of the effects that transcription-translation coupling exert on the physiology of the bacterial cell. With the resurgence of interest in transcription-translation coupling, we look forward to new exciting insights into all aspects of coupling and the ramifications for regulation of gene expression in bacteria.

Acknowledgments: We would like to apologize sincerely for failing to cite the work of many colleagues whose contributions have shaped our current understanding and made the recent advances possible. We also would like to thank Tim Rowsell and Dr. Sean O'Leary for critical discussions.

Appendix:

This section of the thesis aims to document all the painfully gained rules on how to preform transcription assays successfully and avoid common problems in the process. The following data were at the date of completion of the thesis unpublished. For additional information, I would highly recommend reading (Artsimovitch and Henkin 2009) as it provides a rational for most of the transcription assays presented here.

Based on my experience, the critical elements for a successful transcription assay are: i) strict avoidance of RNase in the components used in the transcription assay, ii) optimized assay conditions and iii) flawless execution of the denaturing polyacrylamide gel electrophoresis and following analysis of the gel. Many of these elements entail several salient points which are not obvious to the novice. Therefore, I have decided to provide detailed protocols for each of the above-mentioned elements.

General rules to avoid RNases into components of a transcription assay:

Use certified RNase free disposable plasticware and chemical whenever possible. Otherwise consider all plasticware was soak in 1/10 dilute muriatic acid (HCl) for at least one hour and rinsed thoroughly with DEPC-treated water or water straight from distill. Chromatography system (Akta or EconoPump) and chromatography columns are RNase-freed with 0.2-0.5 M NaOH over at least a column volume before thoroughly rinsing with DEPC treated water and buffer. All glassware is RNase-freed by baking for at least two hours at 180 C. Stock solutions of salts that are not chemically modified by DEPC were

stirred with 1 mL of DEPC per liter for at least one hour before eliminating the remaining DEPC by autoclaving for three hours.

Preparation of DNA template for in vitro transcription assays

DNA templates for transcription assays were prepared by standard PCR amplification in a 500 µL PCR reaction mixture using a Taq 2X master mix according to New England Biolabs (see NEB # M0270L). The 500 µL reaction mixture was then aliquoted into 50 µL aliquots into 200 µL PCR tubes. For amplification of the DNA template cycle parameters were used which were specific for each template. For the *his* pause template the denaturing step was completed at 94C for 15 seconds, the annealing step was done at 55C for 15 seconds, and the extending step was completed at 68C for 15 seconds. Thirty cycles of amplification were performed. For the ρ termination template the denaturing step was completed at 94C for 10 seconds, the annealing step was done at 60C for 15 seconds, and the annealing step was done at 68C for 30 seconds. Thirty cycles of amplification were completed. After PCR amplification, a small amount of sample is run on a 1% agarose gels for quality control of the reaction. If the PCR was successful, the product was combined and purified using QIAquick PCR Purification kit. It is important to use this kit as opposed to other kits. The QIAquick kit does not use RNases for the purification of DNA. The resulting templates is ethanol precipitated using sodium acetate (pH 5.2), resuspended in a small volume (10-20 uL) of water or 5 mM Tris-HCl. The DNA concentration of the solution is determined with the help of the nanodrop. The expected yield of the double-stranded DNA is between 1-5 µM.

Designing the DNA template:

Special considerations are required when designing DNA templates, in particular: (1) The sequence of the +1 and +2 nucleotides, which are critical for efficient transcription, and (2) the mode the transcription is performed, i.e., a single round or multi rounds of transcription.

To address the difficulties of RNA polymerase to efficiently initiate transcription, one may opt to increase the concentration of nucleotides in the assay. However, increasing the concentration of triphosphate nucleotides in the transcription assay would dilute the relative concentration of radioactive labeled nucleotide, and with it the strength of the signal produced by the produced transcripts because less radioactive nucleotides would be incorporated. Additionally, Cytosine is liable to be deaminated into Uracil, which can cause RNAP to incorporate Uracil when Uracil may be purposely left out of a reaction mixture, to halt RNAP. Furthermore, the yield of transcripts may be increased with the use of dinucleotides that can act as primers for the RNA polymerase, thus allowing the concentration of all mononucleotides to remain low producing a strong signal for all transcription products.

Single-round transcription assays are required whenever termination or time-based measurements are performed. Single-round transcription assays allow RNA polymerase to complete only one round of transcription. This can be accomplished because the first ~12-20 nts after the +1 site are a combination of only three of the four nucleotides. By omitting one of the nucleotides RNA polymerase will halt and stay in this

initially transcribed sequence (ITS). If other factors are also going to be added (like transcription factors) they can be added after the formation of the halted complex. To begin the time-dependent portion of the experiment, a mixture of all four nucleotides is added to the solution (called the chase). The addition of the last nucleotide allows for the release of the halted RNA polymerase. Additionally, the chase solution will contain either Rifampicin or Heparin, both of which inhibit reinitiation of RNA polymerase. This ensures the data obtained beyond the ITS represents a single-round of transcription.

Buffer selection for transcription assays:

The 10X Initiating NTPs are stored in DEPC-treated water. The 5X chase solution is stored in 10X TGA [$T_{200}Na_{200}M_{20}DTT_{10}E_{1}Gol_{50\%}$]). To dissolve the Rifampicin in the 5X chase solution it is dissolved to 20 mg/mL in DMSO. The 10X TGA follows (Artsimovitch and Henkin 2009) and the 10X ρ TGA follows [$T_{400}K_{500}MC_{50}DTT_{1}Gol_{30\%}$] (Said, Hilal et al. 2021) to be as reproducible across different groups as possible. Steve uses a less popular running buffer, 20X TTE (composed of 215 g of Tris-base, 71.3 g of Taurine, and 20 mL of 0.5 M EDTA per 1L). TTE has the advantage of eliminating squiggles in the bands which tend to form when using TBE. To stop reactions a 2X STOP buffer is used, containing 24 g Urea, 4 mL 10X TBE, and 1 mL 0.5 M EDTA, and fill with DEPC-treated water to 50 mL. One may have to heat to 65C to get the powders into solution. Lastly, add the dyes into solution,100 mg Xylene cyanol and 100 mg Bromophenol blue.

Formation of halted transcription complexes

Halted RNA polymerase complexes were formed by mixing nuclease-free water, 10X buffer (either TGA or ρ TGC), 10x initiating NTPs (lacking one nucleotide), template DNA, a radioactively labelled nucleotide (typically A- or GTP, α carbon is radioactive), and RNA polymerase holoenzyme. The order of addition of components is important, avoid adding radioactive nucleotide last since RNA polymerase will begin transcribing once all nucleotides, unlabeled or radioactively labelled, are present. For convenience, all the components are mixed except the RNA polymerase and the radioactive nucleotide. This can be done in the general lab, however all the work with radioactive material must be performed in a designated space (Blaha lab designated hot room – Boyce 5457). RNA polymerase is added last to the assay (following one of '10 golden rules of in vitro assays' as laid out in Blaha laboratory manual). The mixture is incubated at 37C for 15 minutes. A small portion of the sample was taken for a time point of zero. This time point is also a good way to access the purity of the nucleotides present in the assay. If read-through is seen in this sample on the gel, it means that the nucleotides used were of insufficient purity. Next, 5x chase solution containing rifampicin (inhibiting re-initiation by RNA polymerase) and all four nucleotides is added. The samples are incubated at 37°C for varying amounts of time. Each reaction is stopped by the addition of an equal volume of 2x STOP buffer and immediately heat denatured at 95°C for at least two minutes before storing at -20°C until further use.

Specific considerations for different transcription assays

For my thesis I perform two main types of measurements of *E. coli* RNA polymerase transcription activity: rate of secondary structure read-through and antitermination.

Rate of secondary structure read-through:

For secondary structure read-though the well-studied HisPause sequence was used (Chan and Landick 1993). The HisPause is a stem-loop that forms in the RNA exit tunnel of RNA polymerase (Kang, Mishanina et al. 2018). To help accentuate this pause the chase NTP concentrations are different than that of a standard transcription assay. The rGTP concentration in the 5X chase solution is 15 times less than that of the other ribonucleotides. The buffer Steve used for this assay is 10X TGA. The full length of the construct is ~150 nucleotides long, which resolves nicely on a 10% denaturing polyacrylamide gel (Torres, Condon et al. 2001; Artsimovitch and Henkin 2009; Said, Hilal et al. 2021). For the HisPause assays, time points of 12, 24, 36, 48, 60, 80, 120, 160, and 300 seconds were used on the first attempt. If the assay were with a lower rGTP chase concentration or with lower temperature, a shift toward later time points (1200 seconds) were included. For six samples, mix 120 µL of DEPC-treated water with 18.6 µL 10X TGA buffer, 18.6 µL 10X initiating NTPs, and 2.8 µL of DNA template 7 (at 222.7 ng/µL or 2.4 µM AKA pIA226 HisPause template). After taking these samples to the hot room and mixing, 2.5 µL of radioactive GTP and then 3 µL of a 1:50 dilution RNA polymerase holoenzyme (stock 65 mg/mL or 138 µM) were added. The protein

stocks are made as an eight-fold concentrated (8X) solutions. Each trial receives 23.6 µL of the 1.14X halted complex and 3.4 µL of the 8X protein factors. This is incubated for 3 minutes at 37°C before adding 6.75 µL of the 5X chase solution. It is important to already have the 2X STOP buffer added to the time point tubes before adding the 5X chase solution.

Antitermination

To study termination a template with differing characteristics downstream from the ITS was used. The downstream features are the BoxBAC, which is also known as the antitermination sequence (AT) which bind to N-utilizing (or Nus) factors (Berg, Squires et al. 1989; Quan, Zhang et al. 2005) as well as several *rut* sites which bind Rho factor. This is followed by several Rho release sites, which allow for Rho-dependent termination (Platt 1981). The first termination site occurs at +267 nucleotides with several others occurring downstream. There is also an intrinsic terminator stem loop as well as a run-off at the end of the PCR product. Unlike the secondary-structure read-through, the NTP concentration are the same at 200 µM each (in the chase at 1X). The buffer used in this assay is 10X ρ TGC [$T_{400}K_{500}M_{50}DTT_{1}Gol_{30\%}$ at 10X] with all counterions being consistent. The full length of the construct is 426 nts, which can be resolved well on a 4% denaturing polyacrylamide gel. For the antitermination assays a single time point at 360 seconds is taken. The halted complex is formed at 1.14X, with the proteins being formed in an 8X solution of their final concentration. For each sample, 3.5 µL of the open complex is added to 0.5 µL of a given protein mixture is being tested. This mixture is

incubated at 37C for 3 minutes, followed by the addition of 1 µL of 5X chase solution. Since the exact timing is not as critical as for other assays multiple trials can easily be run in parallel.

Flawless execution of the denaturing polyacrylamide gel electrophoresis (PAGE) and following analysis of gel.

The protocol is broken into multiple sections: Preparing the gel cassette, pouring the gel, pre-running, loading, and running the gel, disassembly and exposing of get to phosphor imager screen, and finally quantification of the imaged gels. The protocols apply for both, larger sequencing gels (35 x 43 cm) and smaller analytical gels (approximately about half the dimensions of the sequencing gel). Preparation of the gel cassette, i.e., cleaning the gel glass plates, spacers, and comb. Estimated time 45 minutes to one hour.

Wear gloves throughout the cleaning, two gloves on your dominant hand and one on the nondominant hand. Gather the following RNase free materials: one 100 mL beaker, a 1 mL micropipette (P1000) with a box tips, a 200 uL micropipette (P200) with a box tips, a defunct pipette that will be used as a small hammer (P1000 from the radioactive room), razor blade, thick 1½ inch wide electrical tape, extra-large Kimwipes (cat#: 34256), GE or other chromatography paper, and a 60 mL syringe, 5 and 25 mL serological pipettes, and an electronic pipette aid (Easypet 3 (Eppendorf)). Furthermore, gather the following chemicals: 120 mg APS dissolved in 1 mL of DEPC treated water, an Acrylamide/Bisacrylamide casting solution of choice, TEMED, SigmaCote

(trademark), 20X TTE, 10 N NaOH, 100% ethanol, and distilled water in a spray bottle, (See Figure A.1 for materials).

Figure A.1: Materials that are needed to pour a gel, not including glass plates or spacers.

Grab a small and large glass gel plates from the radioactive room, label one side of each plate to keep track of the cleaned side. Pour ~20-50 mL of 10N NaOH onto the large plate. With the dominant hand covered with two gloves rub the 10N NaOH onto the large glass plate. Let the NaOH incubate on glass plate for 30 second to a minute. Place the plate into the sink and rinse off the NaOH thoroughly with deionized water. While this is happening remove the first glove from dominate with which you rubbed the NaOH onto the glass plate and dispose of it. Once the NaOH has been rinsed off the large plate, spray a dilute soap solution (10% Liquinox) onto a sponge (3M sponge). Use both the rough and smooth sides of the sponge to clean both sided of the large glass plate, rinse again (see figure A.2A for sponge and figure A.2B amount of soap). Although small/shorter glass plate is not NaOH treated, it needs to be thoroughly sponged down with soap. The plates are considered clean when no particles are on the glass plate that would obstruct the free flow of running water over the plate. Otherwise, the plate must be sponged down with soap and rinsed again. This is repeated until all particles on the large and short plate are removed. Once the plates are clean set up the glass plates titled on paper towels to air dry, at the location the gel is being poured (figure A.2C). Spray both glass plates with 100% ethanol and wipe them down with two sheets of extra-large kimwipes (37 x 43 cm). Pick up each glass plate and inspect for any dust. From experience it is best to look straight down the glass surface, horizontal to the field of sight (figure A.2D for visual). Grab the spacers with sponges attached and the comb that will be used for the experiment. Spray each component with 100% ethanol, hold them at one end, and gently dry them with an extra-large Kimwipe.

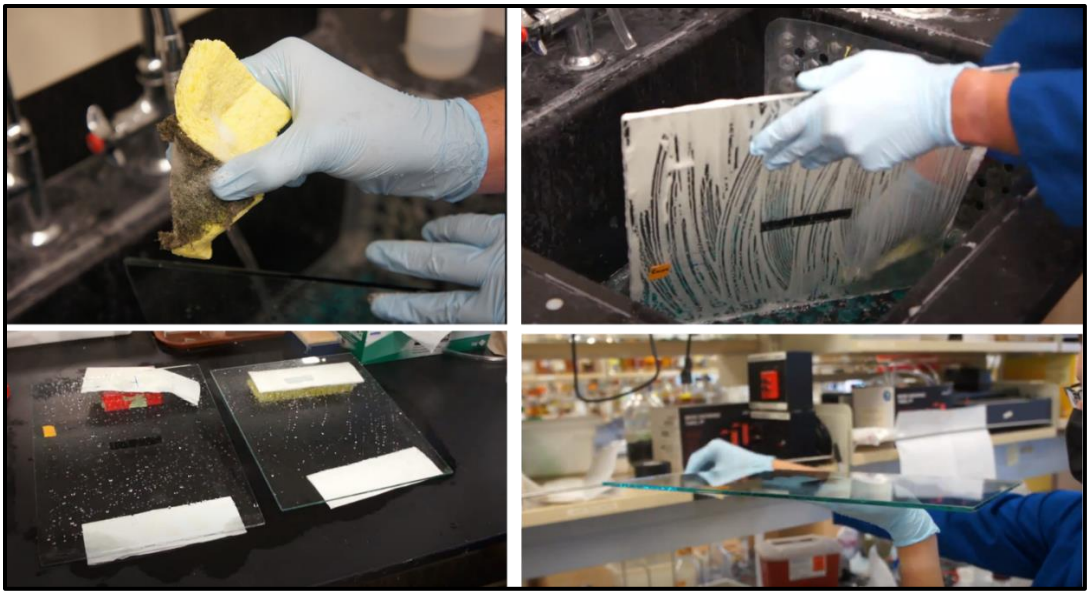

Figure A.2: Steps for cleaning gel glass plates. Top left panel: sponge used for cleaning gel glass plates, with a soft and course side. Top right panel: Glass plate covered in soap during thorough sponging down of plate. Bottom left panel: Setup of sponged down and rinsed gel glass plates during air drying. Bottom right panel: Inspection of gel glass plates for dust or other debris. Steve, visible on the right, has the glass plate lifted to allow him to look across the plate horizontally.

Next, pipette 250-400 uL of Sigmacote onto the short glass plate. Use a small piece of Kimwipe (roughly 10 x 10 cms) to spread the Sigmacote quickly and firmly across one side of the plate. At this point the plate surface should feel smooth from the Sigmacote. If any spots do not feel completely smooth, add an additional small amount of Sigmacoat onto the spot and continue spreading it. Let the coated plate sit for 30 seconds to one minute on the bench. Spray the coated surface over the sink with distilled water to remove the excess of Sigmacoat. Hold the small plate with your nondominant hand and spray it with distilled water. If you are unable to balance the glass plate in one hand, place the plate on something while spraying the coated surface down with distilled water. Spray the coated short gel glass plate liberally with distilled water to ensure all the excess Sigmacote has been removed. Dry short plate with Kimwipes. At this point do not spray or treat the short glass plate with any other chemicals as it will damage the Sigmacoat coating of the plate.

Grab the large plate and balance it on a pipette tip box or something of similar size and sturdiness. Place the spacers to the outside of the plate along the long side of the plate. Make sure the spacers are on the edge of long side and reach the top of the plate. No spacer is required at the bottom of the plate as it will be covered by filter paper. The filter paper will stretch across the length of the plate on the bottom and will close the gap between the end of the spacer and bottom of the gel plate (see figure A.3A at this point). To cut the filter paper into shape, Steve places the filter under the long glass plate with the spacer plates and marks on the paper with a sharpie the sides of the glass plate on it as a template for how large the paper will need to be. Using the paper guillotine, the filter

paper is cut into shape and fills the gap between end of spacer and bottom edge of glass plate. Place the cut filter paper onto the large plate directly where the spacers end. Next, place the short plate directly over the large plate, ensuring that there is not any space between the small plate and the sponge on each spacer. Clamp the gel cassette together with one large binder clip to each side (see figure A.3B at this point).

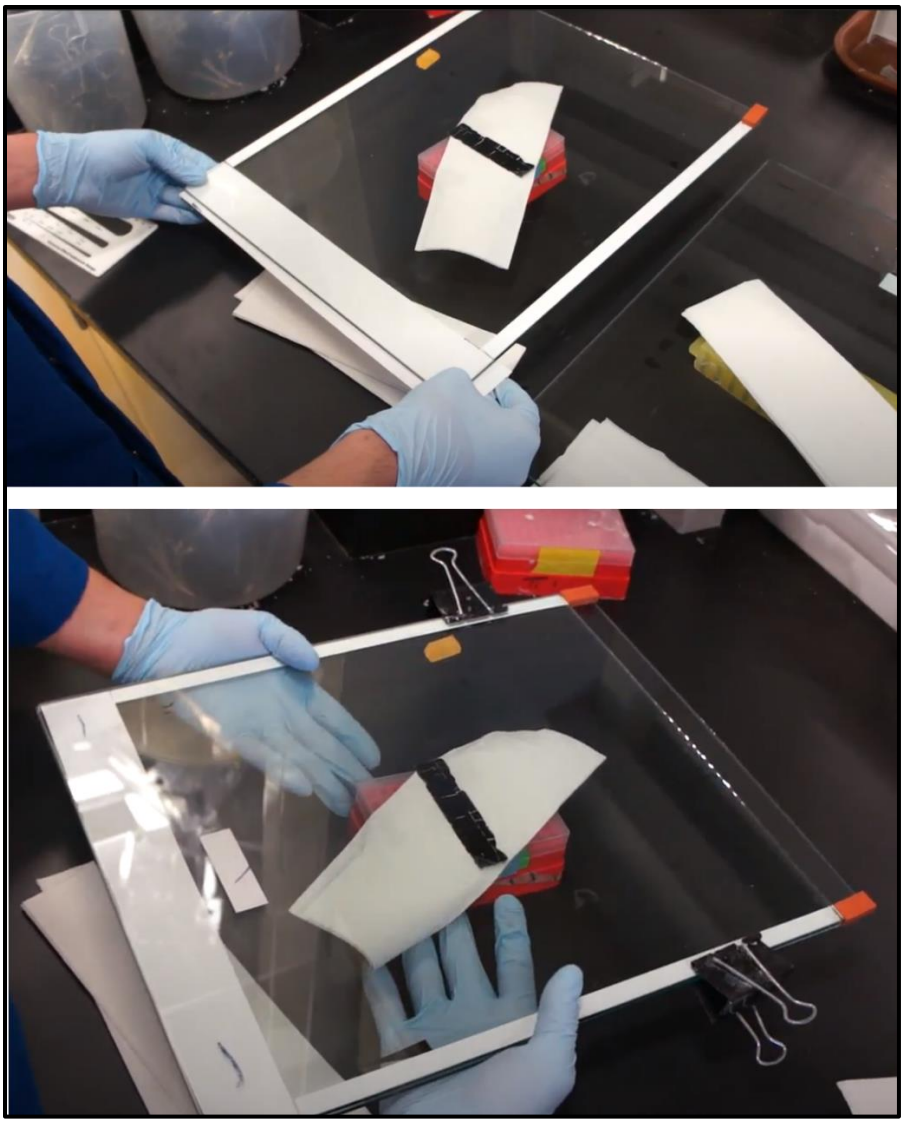

Figure A.3: Glass plate cassette prior to pouring of gel. Top panel: The large plate is beneath the short plate on the tip box, while the filter paper is being marked for cutting into size. Bottom panel: Binder clips are clamping the short plate (on top) and large plate (beneath short plate) together. Care should be taken that the orange sponges on the spacers are snuggly fit against the edge of the shorter plate. This is critical to prevent leaking of running buffer during electrophoresis. The filter paper has to fit snuggly below the spacers and not stick out of the glass plates, otherwise the sealing of the gel cassette will fail.

At this point seal the cassette with 1½ inch wide electrical tape. Start with one long piece of tape that will extend whole bottom edge of the gel and extend a quarter of the way up each side of the long edge (see figure A.8A). Getting a tight seal is crucial to ensure no gel solution will escape from the cassette preventing air bubbles or other deformations from forming during the pouring of the gel. With a razor blade cut a slit in the tape at each corner of the glass plate (see figure A8B). Starting from the cut corner, pull the tape up and push onto the glass plate. This is done with each hand, moving approximately 3 cm along the tape each time a piece of the tape is pulled up and pushed down, onto the glass plate (see figure A.8C). This process is repeated along the tape at the bottom of the gel. At this point the folded tape should be free of creases and folds, and thus airtight. Repeat the folding process starting from the slit in the tape for the remaining five stretches of tape. To complete the sealing of the gel cassette, a strip of electrical tape is applied to each long side, reaching all the way to the sponges of the spacers. These side pieces of tape do not need to reach the slit to the corner of the site, but they must overlap with the applied tape to ensure a complete seal. Apply the tape using the same pull and push technique as for applying the first piece of tape. This will ensure the tape is applied straight, without wrinkles. Add large binder clips starting from the top of the gel, right below the sponges of the spacers all the way to the bottom of the gel, just below the top of the inserted filter paper (see figure A.8D).

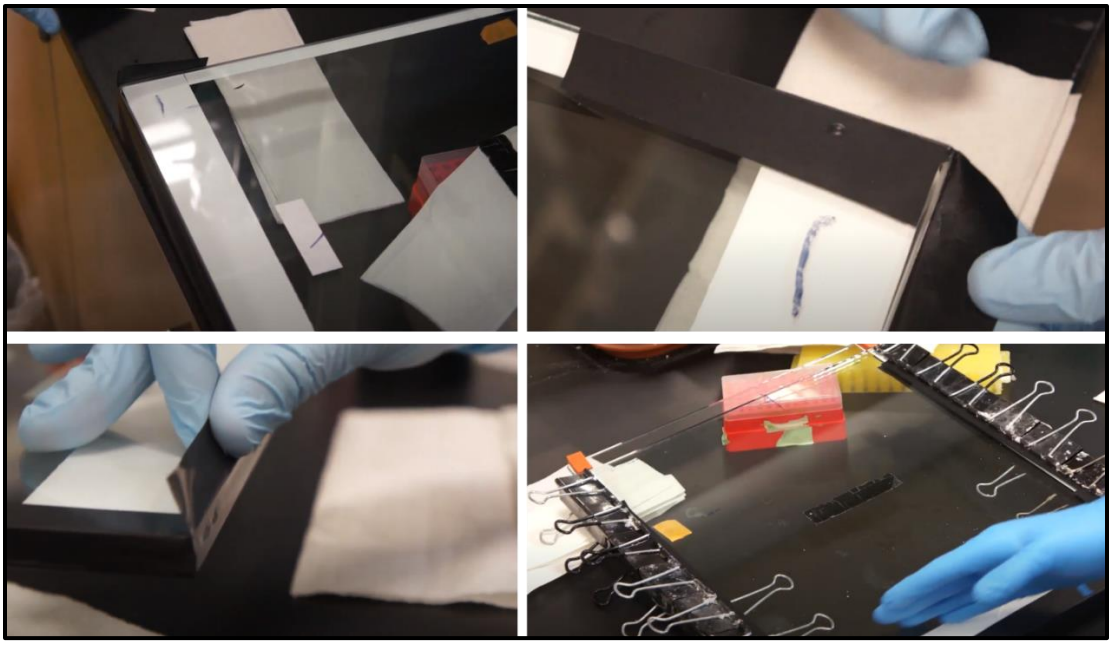

Figure A.4: Taping off the glass plates prior to casting the gel. Top left panel: The tape attached to the side at the bottom edge of the glass plates cassette, with the tape wrapping around the corner glass cassette, ending above the edge of the filter paper-spacer interface. Top right panel: The cut needed to make a tight seal at the corner of the glass plates. Bottom left panel: The right hand of Steve is seen as he is pulling the electrical tape up and pushing it away from him to create a strong seal. Not seen is the left hand which is following the right hand performing the same motion as Steve is moving along the tape. Bottom right panel: The taped and clamped gel glass cassette prior to pouring the gel.

Pouring the gel

Pour 97 mL of casting solution into a RNase-free 150 mL beaker. Add 2.5 mL of 20X TTE. Attach the 25 mL serological pipette to an electronic pipette aid (e.g.: Eppendorf Easypipet), set the volumes on the 1 mL and 200 uL micro pipettes to 266 uL (for 10% APS) and 40 uL (for TEMED), respectively. The gel plate cassette should be tilted upwards and slightly to the side so that the bottom left corner of the cassette is the lowest point, and the top right corner of the cassette is the highest point (the syringe without a needle attached will be placed on the upper left edge of the cassette). Add 40 uL of TEMED and then quickly add 266 uL of 10% APS. Mix the casting solution by pipetting up and down 25-30 mLs, being careful to avoid introducing air bubbles into the solution. Fill 60 mL of the solution into a syringe by placing syringe into solution and slowly pulling the plunger of syringe up. Place the filled syringe on the top left corner of the long glass plate that is above the upper edge on the short plate. Add the gel solution into the gel cassette by slowly pushing the plunger. While pouring the gel tap the cassette with the defunct P1000 micro pipette with your dominant hand (see figure A.5A). The tapping will minimize the formation of air bubbles during the pouring process. From experience, we know that at least one bubble will form half of the time when tapping is omitted during pouring, while only one out of five times when plates are tapped during pouring. Once most of the gel solution has been added remove whatever is making the right side slightly higher (Steve typically uses a PCR rack). Lastly, place the comb in position and continue adding casting solution (see figure A.5B). For the gels used for analyzing the effect factors exert on transcription, Steve used a shark tooth comb. For this

the comb is inserted up-side down (teeth pointing away from gel) into the poured gel cassette. Before electrophoresis the comb is removed and reinserted into the gel slot left behind right-side up (with teeth pointing to gel even slightly pricking the gel.) The sample is pipetted between the teeth of the comb.

If the casting solution is poured too quickly and the filter paper has not had enough time to soak up the casting solution, it will not be saturated with it by the end of pouring the gel and will continue to soak up casting solution during polymerization. This will cause the gel solution to be pulled from the pour area leading to the formation of air pockets within the gel. Therefore, wait for a minute or two (or once the filter paper is 75% soaked) before laying the gel cassette flat on top of a level, sturdy pipette tip box, inserting comb, and let the gel polymerize for at least an hour.

Preparing stock casting solution

Making the stock casting solution correctly is critical for producing sharp gel bands in gel electrophoresis. Because of this, we give a concert example how Steve would make a 500 mL stock of a 10% casting solution for denaturing Urea polyacrylamide gel electrophoresis. Pour 125 mL of 40% AA:BAA (19:1) into the 1L beaker. The 40% AA:BAA (19:1) can be stored for extended amounts of time (more than a year) when stored at 4°C and wrapped in aluminum foil (which keeps the solution in the dark). Next, place the solution on a heated stir plate and add an RNase-free stirring bar. Add 210 grams of urea to the solution, stir at 300-600 rpm while heating the solution. Adjust the volume to 500 mL with DEPC treated water. Urea will not go into

solution until the volume of the solution reaches approximately 500 mL. It will take 5-10 minutes for the urea to go into solution. During this time ensure that the stir plate does start cooking the solution (watch for steam). Once the urea is in solution add 4-5 g of MBD-ULTRA beads (catalog: RTM-8798 from ResinTech Inc.) and turn off the heat. Let the solution stir for at least 30 minutes after the beads are added.

At this point Steve would start cleaning the vacuum filtration flask by soaking in 1/10 diluted muriatic acid. Seal the vacuum intake line of the flask with parafilm and fill the flask to the brim with acid. In a separate beaker submerge the rubber stopper for the vacuum flask in 1:10 diluted muriatic acid. Soak the flask and the stopper for at least 30 minutes, before rinsing both repeatedly with either RNase-free water or double-distilled H_2O straight from the distiller. To remove all the ion exchange beads from the casting solution, filter the solution through a 500 mL vacuum filter (pore size 0.22 µm) into an RNase-free bottle. Transfer the solution into the muriatic acid treated vacuum filtration flask with a RNase-free magnetic stirring bar. Attach a vacuum line to the flask and close the top of the flask with the rubber stopper. Turn on the vacuum and stir the solution at 150-300 rpm for at least 30 minutes. After 30 minutes carefully transfer the solution to an RNase-free bottle with the appropriate cap. The casting solution can be stored for several months at 4°C as long as there is no buffer, TEMED, or APS added to the solution.

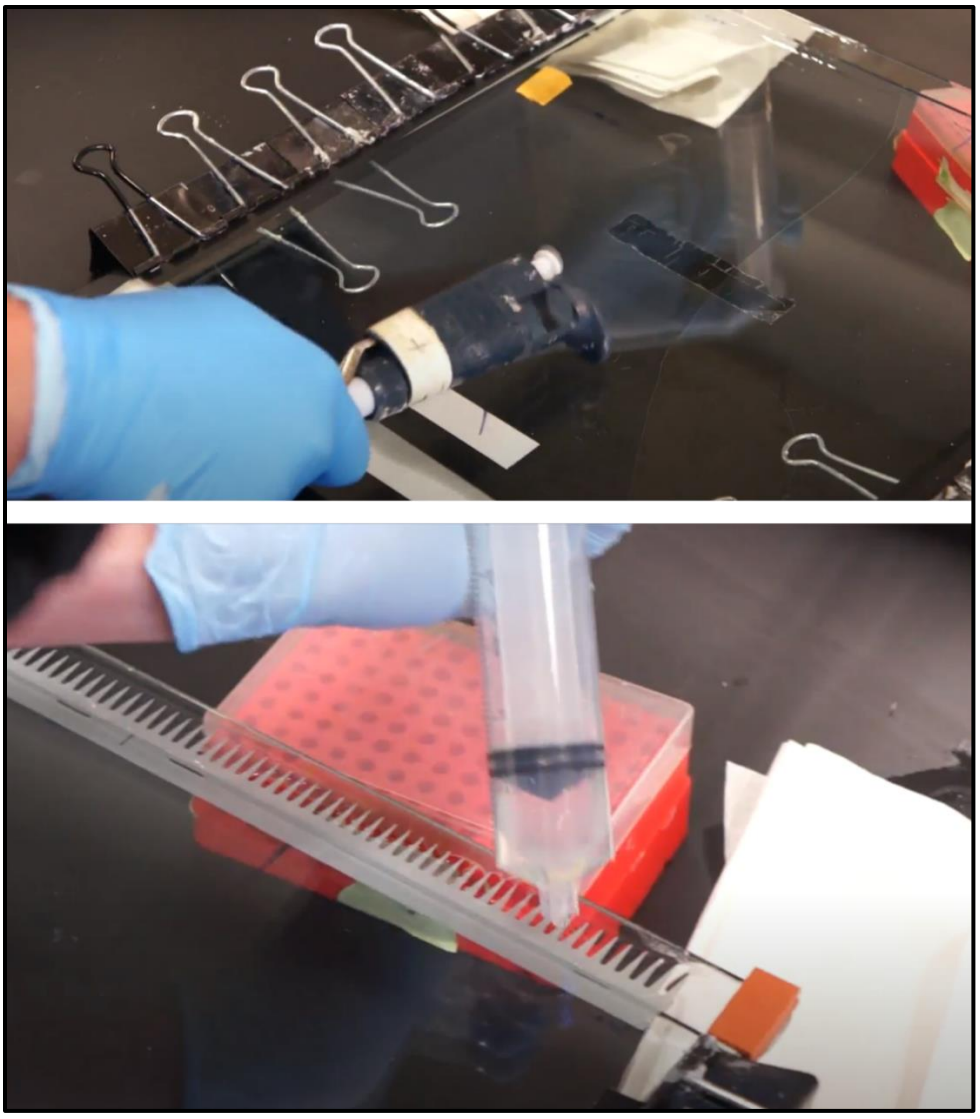

Figure A.5: Pouring the gel. Top panel: Gel casting/polymerization solution as it is being poured via syringe into the glass plates. A defunct P1000 micropipette used to tap the glass plate to prevent the formation of any air bubbles. The solution is flowing down and across the cassette. Bottom panel: Inserting of a shark tooth comb gel. Once the casting/polymerization solution has been completely poured the shark tooth comb is inserted into the top of the gel with its teeth pointing outwards all the way to the height of the small ~1 cm long, narrow slotted holes in the comb (two slotted holes of the comb are visible in the left upper corner of the picture).

Prerunning and running of the gel:

Once the gel has polymerized, it is ready to be pre-run. Clamp the polymerized gel to the rig and close any buffer drainage ports (Figure A.6A). Add a total 1L of running buffer (0.5X TTE) into the top and bottom tank of the rig. Steve usually fills the top tank with buffer until the meniscus of the buffer reaches the sponges, and then adds an additional 100 mL. The bottom tank gets the rest of the buffer. The filter paper should be touching the buffer in the lower tank. If not, additional buffer is added to the bottom tank. Mark with a sharpie where the bottom of the shark teeth comb is on the gel, and then remove the comb. Rinse the gel slot left behind by the removed comb with buffer from the top tank by pipetting up down into to slot with a 1 mL micropipette with a filter tip (Figure A.6B). Connect the gel to the power supply and prerun the gel at constant 115-130 Watts. Check the temperature of the gel with an infrared thermometer. The temperature should reach a constant 55°C across the gel. Note: prerunning is not necessary for native PAGE ((Petrov, Tsa et al. 2013) for details).

Figure A.6: Prerunning setup. Top panel: Placing the polymerized gel into the gel rig. The port for draining the top buffer tank is seen of the right side of the rig close to the bottom clamp for the gel. Bottom panel: The blue sharpie lines drawn at the height of where the inverted shark tooth comb penetrated the gel.

Once the prerun is complete, use a 1 mL micropipette (= P1000) with a filter tip to expel any remaining urea from the gel slot left behind by the shark teeth comb. Insert the shark tooth comb with the teeth facing downwards to the gel, using the blue sharpie lines a guide for the depth of insertion of the teeth (Figure A.6B). The teeth should only barely puncture the gel. Samples for denaturing PAGE should be heated for approximately two minutes at 95-100°C and then spun down at max speed before loading on the gel. Steve has found that heat denaturing all the samples before loading is the most convenient way of preparing the samples for loading, allowing for a more streamline and rapid loading. When planning to load a gel keep in mind the volume of radioactive sample (in microliters) that will be added. Add an equal sample volume of only 2X loading dye in the lanes directly to the left and right of a sample. For example, lane 1 is loading buffer/dye, lane 2 is sample, lane 3 is 2X loading buffer/dye, lane 4 is sample, lane 5 2x loading buffer/dye, and so on. Once all the samples are loading run the gel at 100-120 Watts while using the bromophenol blue dye line as an indicator for the run process (reference bromophenol blue position on a given percent gel (Sambrook, Fritsch et al. 1989)). Monitor the temperature, watts, and voltage. The temperature should hover around 50-55°C after the first 10 minutes of electrophoresis after the loading process.

Imaging the gel with a phosphorimager screen

Once the gel run is complete, drain the buffer from the top tank into the bottom tank. While the running buffer is draining prepare the film cassette, wrapping the cassette with cling plastic wrap (i.e., Saran Wrap). Steve wraps the white checkered side of the

film cassette and tapes the corners on the back of the cassette, so that the cling wrap is fixed in place. Next, take the gel out of the rig and place it in the sink. Run cool water over the gel cassette to cool the glass plates down. Removing the short, siliconized plate while the gel is still warm will cause the gel to form waves on the edges and distort the bands. If the steps for cleaning the gel have been done as described above, removing the short plate is surprisingly easy. Place two of the smaller radiation shields on the counter next to the sink. Behind the shield place the plastic wrapped film cassette. Open the plastic wrapped cassette. Turn off the water that is cooling down the gel. Dry the gel cassette with paper towels and dispose of them as solid, radioactive waste. Place the dried gel into the cassette with short glass plate facing up towards the ceiling (Figure A.7). Use a small metal spatula as well as a gel separator (green wedge from BioRad) to apply pressure between the two glass plates. The short, siliconized glass plate will separate from the gel and the long glass plate, while the spacers can easily be removed without ripping the gel. Apply a layer of plastic wrap on top of the gel, making sure it is stretched out to avoid any large wrinkles in the wrap. Steve uses the shields to hold the plastic wrap for him in place while he is stretching and tightening the foil over the exposed gel since the plastic cling wrap will lightly hold onto the plastic shield. Once the exposed gel is covered with plastic wrap, a freshly erased (within 30 minutes to 8 hours) phosphor imager screen is place on top of the wrapped gel and the film the cassette closed and held tight using several large binder clips. Be sure the order is, cassette → plastic wrap fixed cassette → Glass plate → gel → plastic wrap → screen → cassette. Please note the white side of phosphor imager screen is the side that records the radioactivity. The black side is

only a plastic backing. Therefore, whenever you are exposing the screen to light or radioactivity, have the white side face the source of the radiation (i.e., the light during erasing and the gel during exposing).

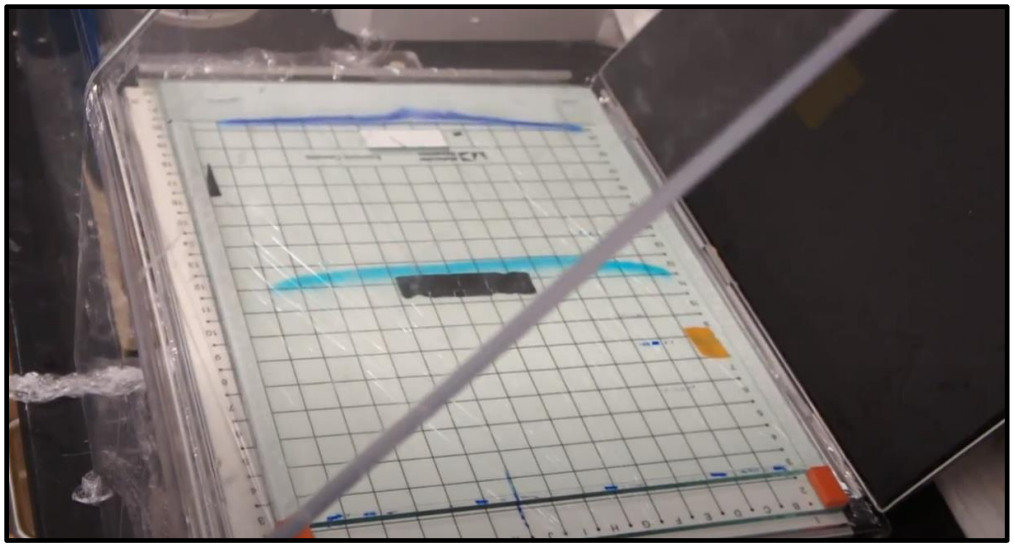

Figure A.7: Wrapping the exposed gel with plastic cling wrap. Using two small self-standing L-shaped plexiglass radiation shields Steve has covered the exposed gel with plastic wrap. On top of the base of the L-shaped shields sits the plastic wrapped cassette, in which the gel cassette was placed. After removing the short glass gel plate and spacers, the gel is exposed (shown). The exposed gel is covered with one layer of cling wrap before a phosphoimager screen is placed onto it.

Scanning of exposed phosphorimager screens

While reading this section keep in mind that the software for image quant is very costly and that GE doesn't give out floating licenses. There is a manual for the software, which is over 150 pages. However, there isn't a user-friendly step-by-step guide on how to do the basics for quantifying the products of transcription assays or other similar assays. Here, Steve provides an introduction on how to do "the basics" in a step-by-step fashion with a brief introduction to the user interface. These steps are based on the software that is currently (Oct. 2021) installed inside Keen Hall on the UCR campus. Before heading over to Keen Hall be sure to transfer the phosphor imager screen to a new cassette. Bringing over radioactive material to Keen Hall is strictly prohibited and dangerous.

Before scanning in the phosphorimager screen the Typhoon must be warmer up. To access the Typhoon on the desktop, click on the Typhoon program on the taskbar at the bottom of the desktop screen (it literally looks like the typhoon – bottom of Figure A.9, the third button to the right of the window start key). Keep in mind the screen that has been exposed has NOT been put into the Typhoon at this time. Once the Typhoon program is open, mark the position on the Typhoon that will be scanned. Do this by left clicking and dragging from A1 to R22, since the gel is the size of the entire screen (Figure A.8, blue box). If the gel and screen is smaller it is acceptable to do a smaller range, but playing it safe and doing the entire screen can be done without determinant. The instrument status (above the blue box) will either be "Warming up…" or "ready". If the system is ready, you can begin scanning. First, physically put the phosphorimager

screen into the Typhoon by lifting up the handle and placing the blank/all white side that was exposed to the radioactivity on the glass side of the Typhoon. Next, enter in the Pixel size (Figure A.8, green box). For transcription assays, especially those you wish to quantify you should use no more than 100 microns pixel size. Figure A.8, purple box shows where to find what Total Scan Time which will depend on the area (A1 to R22) and pixel size selected (smaller pixels will mean longer scans). Start the scanning of the screen by clicking the 'S C A N…' button (Figure A.8, red box). At this point the file is saved on the computer and the scan will take ~20 minutes. Once the scan is completed the quantification of bands of the scanned in gel can started using ImageQuant TL (Wang, Wu et al.).

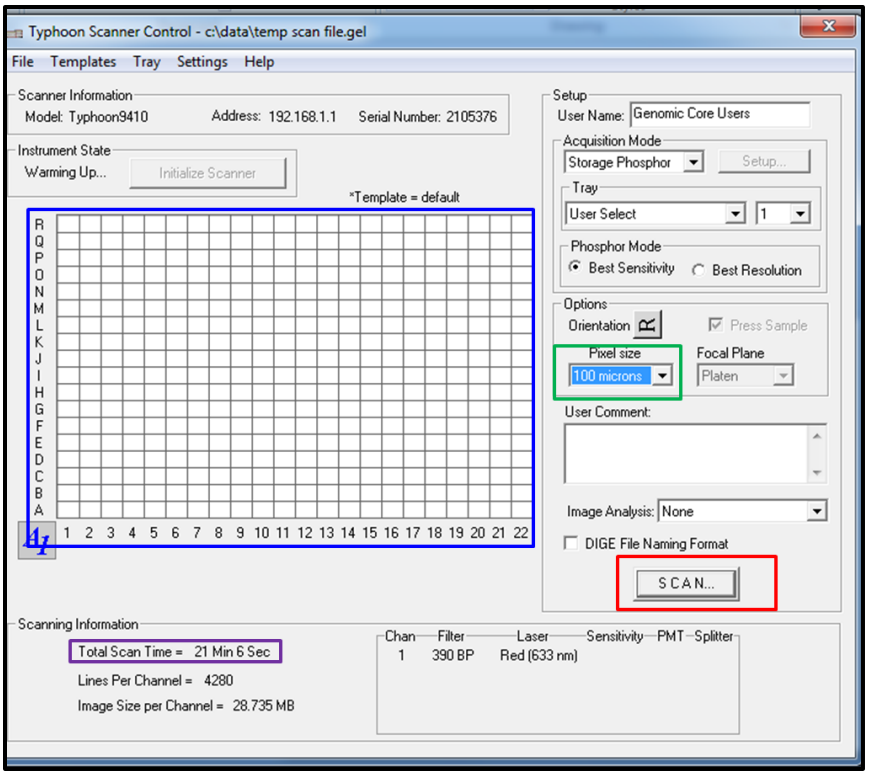

Figure A.8: Typhoon Scanner control software interface. Boxed are important elements of the interface. Blue box: the area that will be used during scanning in. Green box: the pixel size drop-down menu. Red box: ‘S C A N…’ button used to execute the scan on the Typhoon.

Quantification of gels using ImageQuant®

a) Orienting the image and adjusting contrast within image.

To open ImageQuant TL (Wang, Wu et al.) click on the blue IQ icon on the desktop taskbar. This will open the Control Centre of IQ, click on the 1D gel analysis button, and open the image file of the scanned gel. This will open a set of windows that look like that of Figure A.9. To start, click the "Edit Image" option, green box in Figure A.9. This will open a window with the image in it. Click on the image button and rotate the gel into correct orientation, with the gel loading wells on top. Left click the image drop-down menu again and select 'Contrast…'. A small box will appear allowing the adjustment of the contrast. To save the properly oriented and contrast adjusted image, save the image file, by clicking on 'File' in the menu bar of the program and selecting "Save as". It is recommended to save the file under a name that consists of the date of the experiment in the format of year, month, and day (i.e., yyyymmdd), a brief description of experiment followed by "_orient_constrast" as a ".gel" file and as a ".tif" file. The ".tif" file format is a format that can be read by many third-party applications and is therefore ideal for documentation purposes. Close out of the ImageQuant TL program and reopen it with the newly saved .gel file. A large drawback to the ImageQuant software is that only one tab can be opened at a time because of licensing restrictions.


File Edit View Analysis Window Help
Open
Export
Print
Preview
Annotate
Contrast
Colour
Options
Edit Image
Single
Overlay
Channel1
Channel2
Channel3
Channel4
Automatic
Stepwise
Automatic analysis steps:
Lane Creation
Background Subtraction
Band Detection
Manual only analysis steps:
Molecular Size Calibration
Quantity Calibration
Normalisation
1D Analysis
If required, select an area of interest in the Image window
Press the Automatic button to run through the selected steps
Press the Stepwise button to run through the steps one by one
Click for help
Image Window [1:4]
Lane
There are no lanes to show.
Measurements Window
No lanes have been created.
Selected Lane
All Lanes
Comparison
X Pos: 2796 Y Pos: 1780 Value: 14.02
2:33 PM
5/5/2021

Figure A.9: The 1D analysis control interface of ImageQuant (Wang, Wu et al.) with important interface areas boxed. Blue box: Menu bar for main functions of the program, i.e., "File", "Edit", "View", and "Analysis". The "File" function is used to open, save, and export files. The "Analysis" dropdown menu is used to easily navigate the functions like background subtraction or edit lanes. "Edit" and "View" functions are not required for the here described protocol of quantifying the gel image. Green box: "Edit Image" function which opens a new window with the current image allowing the user to flip the image and change the contrast of the image. Purple box: "Stepwise" function which is used to manually go through the steps of quantification. Black box: "Image Window (1.4)" used for defining lanes and bands in the image. Orange box: "Lane" window used to visualize the profiles of integrated lanes. Yellow box: "Measurement Window" displays the numerical values derived from the integrated bands displayed in the "Image Window (1.4)", i.e., black box described above. Red box: "All Lanes" tab to view the values of all the lanes. Light blue box: "Control panel" allowing the user to reopen any closed windows.

b) Defining lanes within the gel image.

To begin analyzing and quantifying the gel image, click on the “Stepwise” option (purple box in figure A.9). Select within the “Select edit mode:” drop-down window (black box in figure A.10) “Create Lanes” and then “manual instead of automatic”. If it is not already selected, select the “Parameters” tab (green box in figure A.10). Next, select the number of lanes to be quantified. (In figure A10, 9 lanes were selected as all of the lanes were part of a time series.) The settings for the other parameters are: (yellow box in figure A.10) the default value of one for the “Number of Tiers” (option not used in this guide) and 90% for “Lane % width”. A “Lane % width” of 90% is recommend, to avoid neighboring lanes from overlapping with each other. Avoiding overlap between lanes is the key reason why only every other lane of the gel was loaded with sample. If every lane were loaded, the lanes would bleed into each other, substantially increasing the challenge for setting correct boundaries between each lane. To set the boundaries of a lane, left click at a corner of the area that contains the “Number of Lanes” (i.e., 9 in figure A.10) and drag the courser across the area of lanes to be quantified (see red box in figure A.10 for selected area). Once the area is selected, the area is divided into “Number of Lanes” strips (Figure A.10). To adjust the strips to fit better the lanes of the gel image, click on the “Edit Multiple Lanes” options in the “Select edit mode:” drop-down window (black box in figure A.10), follow by either “Bend / Resize Lane Box” or “Move Lane Box Edges” option. Both options are useful depending on the adjustment that is required. To fine-tune the alignment of the image strips with the lanes of the gel image, select “Edit Single Lane” in the “Select edit mode:” drop-down window followed by the “Move”

option to tweak individual lanes. Once the lane creation step is finished move on to the band detection steps.

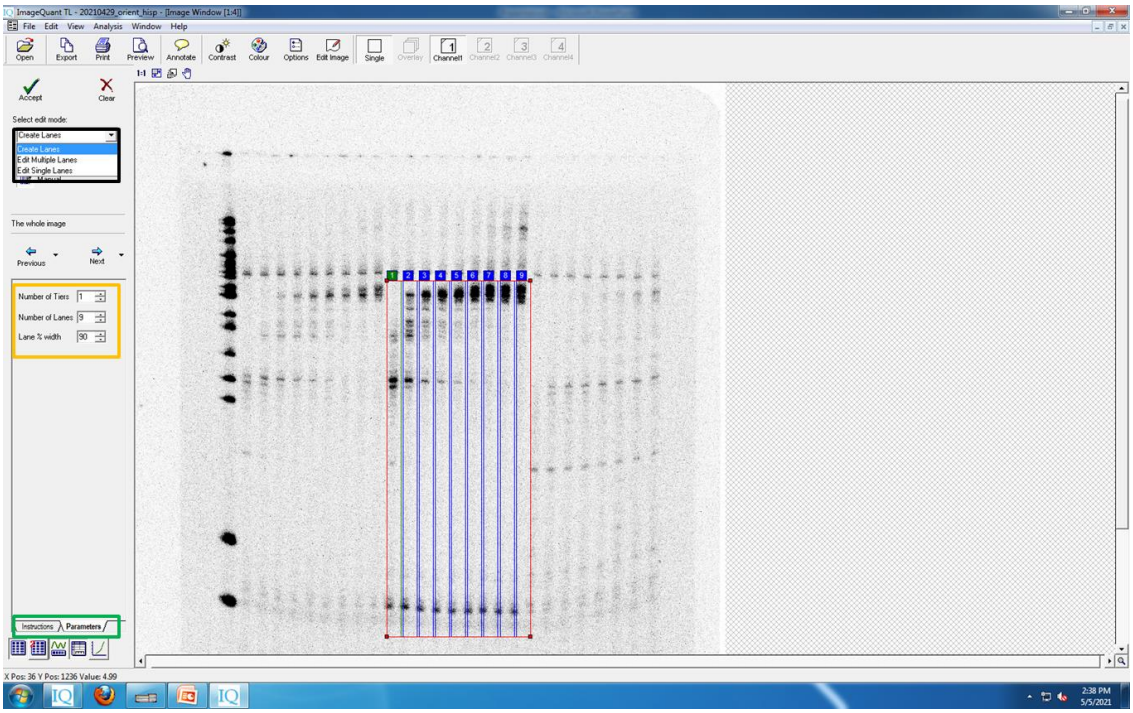
ImageQuant TL - 20210429_orient_hisp - [Image Window [14]]
File Edit View Analysis Window Help
Open Export Print Preview Annotate Contrast Colour Options Edit Image Single Overlay Channel1 Channel2 Channel3 Channel4
Accept
Clear
Select edit mode:
Create Lanes
Create Lanes
Edit Multiple Lanes
Edit Single Lanes
The whole image
Previous
Next
Number of Tiers 1
Number of Lanes 9
Lane % width 90
Instructions
Parameters
1 2 3 4 5 6 7 8 9
X Pos: 36 Y Pos: 1236 Value: 4.99
2:38 PM
5/5/2021

Figure A.10: “Creating Lanes” function within IQ. Important areas within the interface are boxed. Black box: “Select edit mode:” drop-down window for selecting one of the different edit modes: “Creating Lanes”, “Editing Multiple Lanes”, and “Editing Single Lanes”. Green box: “Instructions” and “Parameters” tabs. Orange box: Selection of “Number of Tiers”, “Number of Lanes”, and “Lane % width”.

c) Detection of bands within each lane:

Click on the analysis tab dropdown (blue box in figure A.9) and then the “Band Detection” option. A left mouse click will add a band which looks like a black square rotated 45 degrees with two redlined above and below the square (Figure A.11). To delete a band right mouse click on the black square. The area of a band after left clicking is standard but can be adjusted to accommodate larger or smaller bands. To adjust the band, left click and holding over the red boundary and adjust to the required size. For measurement to be more accurate, a background subtraction should be performed.

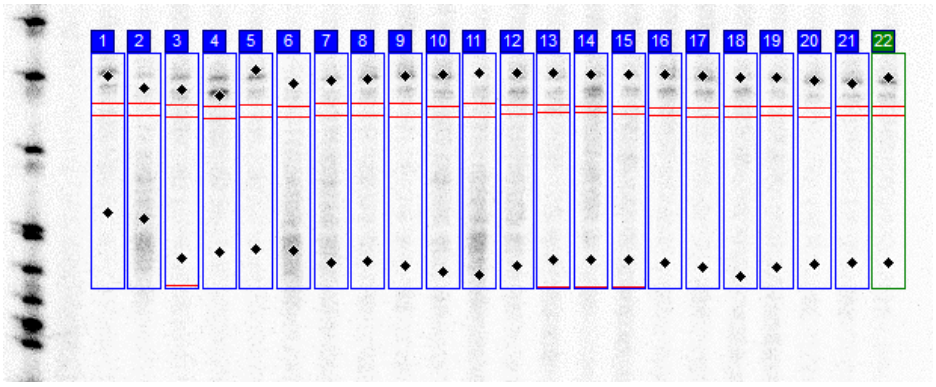

Figure A.11: Exported image of what bands look like in ImageQuant.

d) Background subtraction of integrated bands.

Once all the bands have been selected, click on the “Analysis” dropdown followed by the “Background Subtraction” option. The program provides several distinct methods for background subtraction and choosing the “right” subtraction method can be challenging, if not outright controversial. We recommend using the same background subtraction method across the board (i.e., for a series of experiments) so that the results can be compared without bias. Steve prefers to apply the “Rolling Ball” background subtraction method. The “Rolling Ball” subtraction allows the user to select a ball size. The ball size defines the diameter of the ball that is rolled over the inverted lane profile. (If you select the ball size too small more of the signal/peak is considered background. In the extreme with very small ball size all of the area under the signal/peak is subtracted. Steve uses a ball size of 500.) A lane profile that contains a series of intense sharp peaks and small, tiny peaks a ball of user-set size is rolled over the inverted (upside down profile). The path of the ball rolling over the inverted profile set the background value under the peak. The ball will not enter the gorges formed by the sharp peaks in the profile. According to the “Image Quant” user manual the other background subtraction methods are not as useful for comparing integrated and subtracted intensities from multiple scans (such as the “Minimum Profile” method of background subtraction). The automatic method is called rubber band, which is described as stretching a rubber band over the lane profile. This method does not offer any changing of parameters, which can leave experimenters with worries about reproducibility between different sets of analysis

or gels. Interestingly, after having run the quantification using both the rubber band and rolling ball subtraction methods the numbers varied only very slightly. Once you have selected the background method of choice the lane profile and measurement window will populate with data.

e) Verifying the lane and band selection and exporting the integrated data.

Export your completely processed file as a “bitmap” file and inspect the map to verify the lane cutoffs and band selections. Once the lane and band selection are verified, export the data as an “Excel” file, by clicking on the “Measurement Window” (yellow box in figure A.9) followed by “Edit” (figure A.9, blue box) and then “Export to Excel”. This will open an “Excel” spreadsheet in the same format as in “Measurement Window”. When calculating data look at the raw values minus the background. Use the ‘band %’ column for most of the resulting excel analysis. The band percent tab looks at the integrated intensity minus the background of each band in a selected lane.

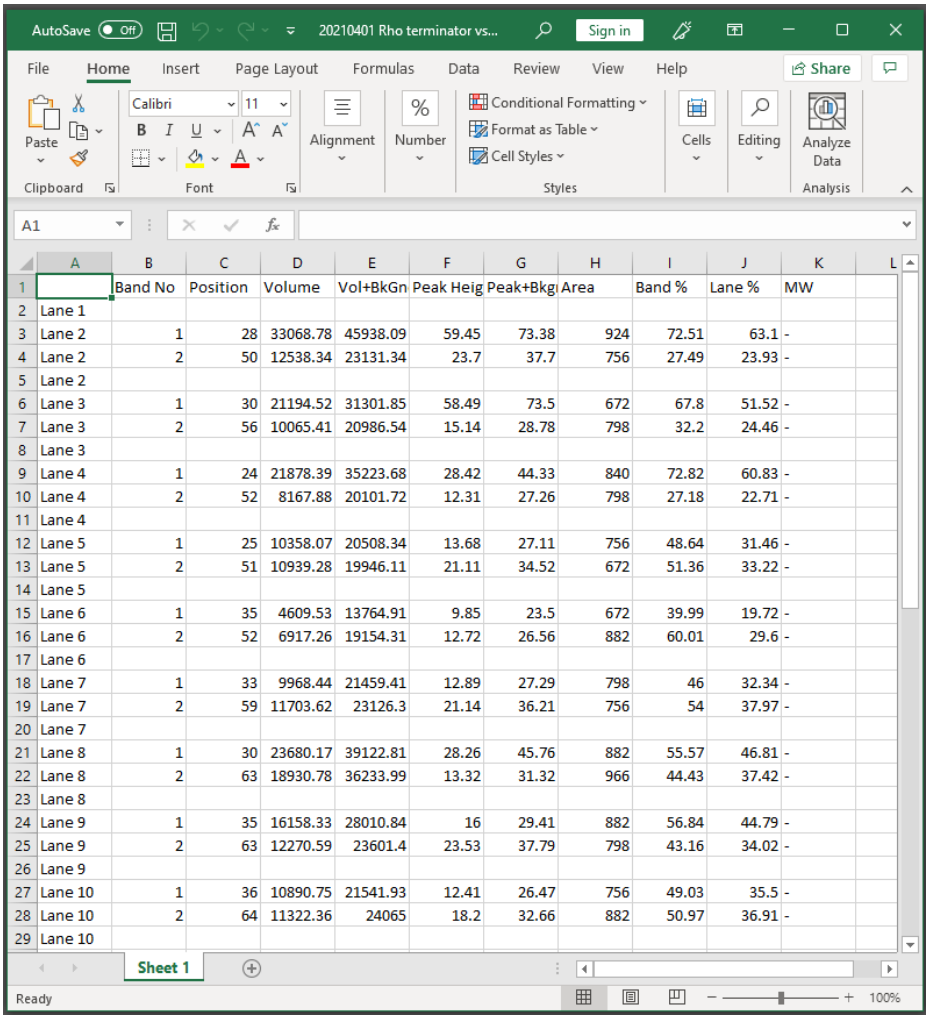

	A	B	C	D	E	F	G	H	I	J	K	L
1		Band No	Position	Volume	Vol+BkGn	Peak Heig	Peak+Bkg	Area	Band %	Lane %	MW	
2	Lane 1											
3	Lane 2	1	28	33068.78	45938.09	59.45	73.38	924	72.51	63.1	-	
4	Lane 2	2	50	12538.34	23131.34	23.7	37.7	756	27.49	23.93	-	
5	Lane 2											
6	Lane 3	1	30	21194.52	31301.85	58.49	73.5	672	67.8	51.52	-	
7	Lane 3	2	56	10065.41	20986.54	15.14	28.78	798	32.2	24.46	-	
8	Lane 3											
9	Lane 4	1	24	21878.39	35223.68	28.42	44.33	840	72.82	60.83	-	
10	Lane 4	2	52	8167.88	20101.72	12.31	27.26	798	27.18	22.71	-	
11	Lane 4											
12	Lane 5	1	25	10358.07	20508.34	13.68	27.11	756	48.64	31.46	-	
13	Lane 5	2	51	10939.28	19946.11	21.11	34.52	672	51.36	33.22	-	
14	Lane 5											
15	Lane 6	1	35	4609.53	13764.91	9.85	23.5	672	39.99	19.72	-	
16	Lane 6	2	52	6917.26	19154.31	12.72	26.56	882	60.01	29.6	-	
17	Lane 6											
18	Lane 7	1	33	9968.44	21459.41	12.89	27.29	798	46	32.34	-	
19	Lane 7	2	59	11703.62	23126.3	21.14	36.21	756	54	37.97	-	
20	Lane 7											
21	Lane 8	1	30	23680.17	39122.81	28.26	45.76	882	55.57	46.81	-	
22	Lane 8	2	63	18930.78	36233.99	13.32	31.32	966	44.43	37.42	-	
23	Lane 8											
24	Lane 9	1	35	16158.33	28010.84	16	29.41	882	56.84	44.79	-	
25	Lane 9	2	63	12270.59	23601.4	23.53	37.79	798	43.16	34.02	-	
26	Lane 9											
27	Lane 10	1	36	10890.75	21541.93	12.41	26.47	756	49.03	35.5	-	
28	Lane 10	2	64	11322.36	24065	18.2	32.66	882	50.97	36.91	-	
29	Lane 10											

Figure A.12: Excel file example after image analysis on a Typhoon imager.

References:

Adhya, S. and M. Gottesman (1978). "Control of transcription termination." Annu Rev Biochem **47**: 967-996.

Agirrezabala, X., H. Y. Liao, et al. (2012). "Structural characterization of mRNA-tRNA translocation intermediates." Proc Natl Acad Sci U S A **109**(16): 6094-6099.

Aitken, C. E., P. Beznosková, et al. (2016). "Eukaryotic translation initiation factor 3 plays distinct roles at the mRNA entry and exit channels of the ribosomal preinitiation complex." Elife **26**(5): 20934.

Alpi, E., J. Griss, et al. (2015). "Analysis of the tryptic search space in UniProt databases." Proteomics **15**(1): 48-57.

Amiri, H. and H. F. Noller (2019). "Structural evidence for product stabilization by the ribosomal mRNA helicase." Rna **25**(3): 364-375.

Andreeva, I., R. Belardinelli, et al. (2018). "Translation initiation in bacterial polysomes through ribosome loading on a standby site on a highly translated mRNA." Proc Natl Acad Sci U S A **115**(17): 4411-4416.

Arora, S., S. P. Bhamidimarri, et al. (2013). "Role of the ribosomal P-site elements of m^2G966, m^5C967, and the S9 C-terminal tail in maintenance of the reading frame during translational elongation in Escherichia coli." J Bacteriol **195**(16): 3524-3530.

Artsimovitch, I. (2018). "Rebuilding the bridge between transcription and translation." Mol Microbiol **108**(5): 467-472.

Artsimovitch, I. and T. M. Henkin (2009). "In vitro approaches to analysis of transcription termination." Methods **47**(1): 37-43.

Artsimovitch, I. and R. Landick (2000). "Pausing by bacterial RNA polymerase is mediated by mechanistically distinct classes of signals." Proc Natl Acad Sci U S A **97**(13): 7090-7095.

Artsimovitch, I., V. Svetlov, et al. (2003). "Co-overexpression of Escherichia coli RNA polymerase subunits allows isolation and analysis of mutant enzymes lacking lineage-specific sequence insertions." J Biol Chem **278**(14): 12344-12355.

Aylett, C. H., D. Boehringer, et al. (2015). "Structure of a yeast 40S-eIF1-eIF1A-eIF3-eIF3j initiation complex." Nat Struct Mol Biol **22**(3): 269-271.

Baggett, N. E., Y. Zhang, et al. (2017). "Global analysis of translation termination in E. coli." PLoS Genet **13**(3).

Bailey, M. J., C. Hughes, et al. (1997). "RfaH and the ops element, components of a novel system controlling bacterial transcription elongation." Mol Microbiol **26**(5): 845-851.

Bakshi, S., H. Choi, et al. (2015). "The spatial biology of transcription and translation in rapidly growing Escherichia coli." Front Microbiol **6**(636).

Bakshi, S., A. Siryaporn, et al. (2012). "Superresolution imaging of ribosomes and RNA polymerase in live *Escherichia coli* cells." Mol Microbiol **85**(1): 21-38.

Bakshi, S., A. Siryaporn, et al. (2012). "Superresolution imaging of ribosomes and RNA polymerase in live Escherichia coli cells." Mol Microbiol **85**(1): 21-38.

Ban, N., R. Beckmann, et al. (2014). "A new system for naming ribosomal proteins." Curr Opin Struct Biol **24**: 165-169.

Belogurov, G. A. and I. Artsimovitch (2015). "Regulation of Transcript Elongation." Annual Review of Microbiology **69**(1): 49-69.

Belogurov, G. A. and I. Artsimovitch (2019). "The Mechanisms of Substrate Selection, Catalysis, and Translocation by the Elongating RNA Polymerase." J Mol Biol **431**(20): 3975-4006.

Belogurov, G. A., R. A. Mooney, et al. (2009). "Functional specialization of transcription elongation factors." Embo J **28**(2): 112-122.

Belogurov, G. A., A. Sevostyanova, et al. (2010). "Functional regions of the N-terminal domain of the antiterminator RfaH." Mol Microbiol **76**(2): 286-301.

Belogurov, G. A., M. N. Vassylyeva, et al. (2007). "Structural basis for converting a general transcription factor into an operon-specific virulence regulator." Mol Cell **26**(1): 117-129.

Berg, D. and M. Chamberlin (1970). "Physical studies on ribonucleic acid polymerase from Escherichia coli B." Biochemistry **9**(26): 5055-5064.

Berg, K. L., C. Squires, et al. (1989). "Ribosomal RNA operon anti-termination. Function of leader and spacer region box B-box A sequences and their conservation in diverse micro-organisms." J Mol Biol **209**(3): 345-358.

Blaha, G., U. Stelzl, et al. (2000). "Preparation of functional ribosomal complexes and effect of buffer conditions on tRNA positions observed by cryoelectron microscopy." Methods Enzymol **317**: 292-309.

Bocharov, E. V., A. G. Sobol, et al. (2004). "From structure and dynamics of protein L7/L12 to molecular switching in ribosome." J Biol Chem **279**(17): 17697-17706.

Boni, I. V., D. M. Isaeva, et al. (1991). "Ribosome-messenger recognition: mRNA target sites for ribosomal protein S1." Nucleic Acids Res **19**(1): 155-162.

Borin, B. N., W. Tang, et al. (2014). "Helicobacter pylori RNA polymerase α-subunit C-terminal domain shows features unique to ε-proteobacteria and binds NikR/DNA complexes." Protein Sci **23**(4): 454-463.

Box, G. E. P., J. S. Hunter, et al. (2005). Statistics for experimenters : design, innovation, and discovery. Hoboken, N.J., Wiley-Interscience.

Bratton, B. P., R. A. Mooney, et al. (2011). "Spatial distribution and diffusive motion of RNA polymerase in live Escherichia coli." J Bacteriol **193**(19): 5138-5146.

Bremer, H. and P. P. Dennis (2008). "Modulation of Chemical Composition and Other Parameters of the Cell at Different Exponential Growth Rates." EcoSal Plus **3**(1): 3.

Brodersen, D. E., W. M. Clemons, Jr., et al. (2002). "Crystal structure of the 30 S ribosomal subunit from Thermus thermophilus: structure of the proteins and their interactions with 16 S RNA." J Mol Biol **316**(3): 725-768.

Buckingham, R. H., G. Grentzmann, et al. (1997). "Polypeptide chain release factors." Mol Microbiol **24**(3): 449-456.

Bunner, A. E., A. H. Beck, et al. (2010). "Kinetic cooperativity in Escherichia coli 30S ribosomal subunit reconstitution reveals additional complexity in the assembly landscape." Proc Natl Acad Sci U S A **107**(12): 5417-5422.

Burmann, B. M., S. H. Knauer, et al. (2012). "An α helix to β barrel domain switch transforms the transcription factor RfaH into a translation factor." Cell **150**(2): 291-303.

Burmann, B. M., K. Schweimer, et al. (2010). "A NusE:NusG complex links transcription and translation." Science **328**(5977): 501-504.

Burns, C. M., L. V. Richardson, et al. (1998). "Combinatorial effects of NusA and NusG on transcription elongation and Rho-dependent termination in Escherichia coli." J Mol Biol **278**(2): 307-316.

Burova, E., S. C. Hung, et al. (1995). "Escherichia coli NusG protein stimulates transcription elongation rates in vivo and in vitro." J Bacteriol **177**(5): 1388-1392.

Byrgazov, K., S. Manoharadas, et al. (2012). "Direct interaction of the N-terminal domain of ribosomal protein S1 with protein S2 in Escherichia coli." PLoS One **7**(3): 7.

Cabrera, J. E. and D. J. Jin (2003). "The distribution of RNA polymerase in Escherichia coli is dynamic and sensitive to environmental cues." Mol Microbiol **50**(5): 1493-1505.

Cabrera, J. E. and D. J. Jin (2003). "The distribution of RNA polymerase in *Escherichia coli* is dynamic and sensitive to environmental cues." Mol. Microbiol. **50**(5): 1493-1505.

Caliskan, N., V. I. Katunin, et al. (2014). "Programmed -1 frameshifting by kinetic partitioning during impeded translocation." Cell **157**(7): 1619-1631.

Camarero, J. A., A. Shekhtman, et al. (2002). "Autoregulation of a bacterial sigma factor explored by using segmental isotopic labeling and NMR." Proc Natl Acad Sci U S A **99**(13): 8536-8541.

Carafa, Y. d. A., E. Brody, et al. (1990). "Prediction of rho-independent Escherichia coli transcription terminators: a statistical analysis of their RNA stem-loop structures." Journal of molecular biology **216**(4): 835-858.

Carter, A. P., W. M. Clemons, Jr., et al. (2001). "Crystal structure of an initiation factor bound to the 30S ribosomal subunit." Science **291**(5503): 498-501.

Chakrabarti, S. L. and L. Gorini (1975). "A link between streptomycin and rifampicin mutation." Proc Natl Acad Sci U S A **72**(6): 2084-2087.

Chakrabarti, S. L. and L. Gorini (1977). "Interaction between mutations of ribosomes and RNA polymerase: a pair of strA and rif mutants individually temperature-insensitive but temperature-sensitive in combination." Proc Natl Acad Sci U S A **74**(3): 1157-1161.

Chakraborty, A., D. Wang, et al. (2012). "Opening and closing of the bacterial RNA polymerase clamp." Science **337**(6094): 591-595.

Chan, C. L. and R. Landick (1993). "Dissection of the his leader pause site by base substitution reveals a multipartite signal that includes a pause RNA hairpin." J Mol Biol **233**(1): 25-42.

Chan, C. L. and R. Landick (1997). "Effects of neutral salts on RNA chain elongation and pausing by Escherichia coli RNA polymerase." J Mol Biol **268**(1): 37-53.

Chatterjee, S., A. Chauvier, et al. (2021). "A translational riboswitch coordinates nascent transcription-translation coupling." Proc Natl Acad Sci U S A **118**(16): 2023426118.

Chen, J., B. Malone, et al. (2020). "Structural basis for helicase-polymerase coupling in the SARS-CoV-2 replication-transcription complex." Cell **182**(6): 1560-1573. e1513.

Chen, J., A. Petrov, et al. (2014). "Dynamic pathways of -1 translational frameshifting." Nature **512**(7514): 328-332.

Chen, M. and K. Fredrick (2018). "Measures of single- versus multiple-round translation argue against a mechanism to ensure coupling of transcription and translation." Proc Natl Acad Sci U S A **115**(42): 10774-10779.

Christian, T., C. Evilia, et al. (2004). "Distinct origins of tRNA(m1G37) methyltransferase." J Mol Biol **339**(4): 707-719.

Conant, C. R., J. P. Goodarzi, et al. (2008). "The antitermination activity of bacteriophage lambda N protein is controlled by the kinetics of an RNA-looping-facilitated interaction with the transcription complex." J Mol Biol **384**(1): 87-108.

Condon, C., C. Squires, et al. (1995). "Control of rRNA transcription in Escherichia coli." Microbiol Rev **59**(4): 623-645.

Conn, A. B., S. Diggs, et al. (2019). "Two Old Dogs, One New Trick: A Review of RNA Polymerase and Ribosome Interactions during Transcription-Translation Coupling." Int J Mol Sci **20**(10).

Cox, J. and M. Mann (2008). "MaxQuant enables high peptide identification rates, individualized p.p.b.-range mass accuracies and proteome-wide protein quantification." Nat Biotechnol **26**(12): 1367-1372.

Culver, G. M. and H. F. Noller (1999). "Efficient reconstitution of functional Escherichia coli 30S ribosomal subunits from a complete set of recombinant small subunit ribosomal proteins." Rna **5**(6): 832-843.

Darst, S. A., N. Opalka, et al. (2002). "Conformational flexibility of bacterial RNA polymerase." Proc Natl Acad Sci U S A **99**(7): 4296-4301.

Das, H. K., A. Goldstein, et al. (1967). "Attachment of ribosomes to nascent messenger RNA in Escherichia coli." J Mol Biol **24**(2): 231-245.

Davis, J. H. and J. R. Williamson (2017). "Structure and dynamics of bacterial ribosome biogenesis." Philos Trans R Soc Lond B Biol Sci **372**(1716).

de Smit, M. H., P. W. Verlaan, et al. (2008). "Intracistronic transcriptional polarity enhances translational repression: a new role for Rho." Mol Microbiol **69**(5): 1278-1289.

de Smit, M. H., P. W. Verlaan, et al. (2009). "In vivo dynamics of intracistronic transcriptional polarity." J Mol Biol **385**(3): 733-747.

Decker, K. B. and D. M. Hinton (2013). "Transcription regulation at the core: similarities among bacterial, archaeal, and eukaryotic RNA polymerases." Annu Rev Microbiol **67**: 113-139.

Demo, G., A. Rasouly, et al. (2017). "Structure of RNA polymerase bound to ribosomal 30S subunit." Elife **13**(6): 28560.

DeVito, J. and A. Das (1994). "Control of transcription processivity in phage lambda: Nus factors strengthen the termination-resistant state of RNA polymerase induced by N antiterminator." Proc Natl Acad Sci U S A **91**(18): 8660-8664.

Diaconu, M., U. Kothe, et al. (2005). "Structural basis for the function of the ribosomal L7/12 stalk in factor binding and GTPase activation." Cell **121**(7): 991-1004.

Dodd, J. and W. E. Hill (1987). "Physical characteristics of ribosomal protein S4 from Escherichia coli." J Biol Chem **262**(6): 2478-2484.

Dombroski, A. J., W. A. Walter, et al. (1992). "Polypeptides containing highly conserved regions of transcription initiation factor sigma 70 exhibit specificity of binding to promoter DNA." Cell **70**(3): 501-512.

Drögemüller, J., M. Strauß, et al. (2015). "Determination of RNA polymerase binding surfaces of transcription factors by NMR spectroscopy." Sci Rep **5**(16428).

Drögemüller, J., M. Strauß, et al. (2015). "Exploring RNA polymerase regulation by NMR spectroscopy." Sci Rep **5**(10825).

Dudenhoeffer, B. R., H. Schneider, et al. (2019). "SuhB is an integral part of the ribosomal antitermination complex and interacts with NusA." Nucleic Acids Res **47**(12): 6504-6518.

Duss, O., G. A. Stepanyuk, et al. (2019). "Transient Protein-RNA Interactions Guide Nascent Ribosomal RNA Folding." Cell **179**(6): 1357-1369.

Dutta, D., K. Shatalin, et al. (2011). "Linking RNA polymerase backtracking to genome instability in E. coli." Cell **146**(4): 533-543.

Ederth, J., R. A. Mooney, et al. (2006). "Functional interplay between the jaw domain of bacterial RNA polymerase and allele-specific residues in the product RNA-binding pocket." J Mol Biol **356**(5): 1163-1179.

Elgamal, S., I. Artsimovitch, et al. (2016). "Maintenance of Transcription-Translation Coupling by Elongation Factor P." mBio **7**(5): 01373-01316.

Elvekrog, M. M. and P. Walter (2015). "Dynamics of co-translational protein targeting." Curr Opin Chem Biol **29**: 79-86.

Endesfelder, U., K. Finan, et al. (2013). "Multiscale spatial organization of RNA polymerase in Escherichia coli." Biophys J **105**(1): 172-181.

Epshtein, V. and E. Nudler (2003). "Cooperation between RNA polymerase molecules in transcription elongation." Science **300**(5620): 801-805.

Fan, H., A. B. Conn, et al. (2017). "Transcription-translation coupling: direct interactions of RNA polymerase with ribosomes and ribosomal subunits." Nucleic Acids Res **45**(19): 11043-11055.

Farnham, P. J., J. Greenblatt, et al. (1982). "Effects of NusA protein on transcription termination in the tryptophan operon of Escherichia coli." Cell **29**(3): 945-951.

Fong, B. A., A. R. Gillies, et al. (2010). "Purification of Escherichia coli RNA polymerase using a self-cleaving elastin-like polypeptide tag." Protein Sci **19**(6): 1243-1252.

Franklin, N. C. and S. E. Luria (1961). "Transduction by bacteriophage P-1 and the properties of the lac genetic region in E. coli and S. dysenteriae." Virology **15**: 299-311.

French, S. L., T. J. Santangelo, et al. Transcription and translation are coupled in Archaea, Mol Biol Evol. 2007 Apr;24(4):893-5. doi: 10.1093/molbev/msm007. Epub 2007 Jan 20.

Gibbs, M. R., K. M. Moon, et al. (2017). "Conserved GTPase LepA (Elongation Factor 4) functions in biogenesis of the 30S subunit of the 70S ribosome." Proc Natl Acad Sci U S A **114**(5): 980-985.

Gill, S. C., S. E. Weitzel, et al. (1991). "Escherichia coli sigma 70 and NusA proteins. I. Binding interactions with core RNA polymerase in solution and within the transcription complex." J Mol Biol **220**(2): 307-324.

Gordiyenko, Y., S. Deroo, et al. (2008). "Acetylation of L12 increases interactions in the Escherichia coli ribosomal stalk complex." J Mol Biol **380**(2): 404-414.

Griffin, N. M., J. Yu, et al. (2010). "Label-free, normalized quantification of complex mass spectrometry data for proteomic analysis." Nat Biotechnol **28**(1): 83-89.

Grigoriadou, C., S. Marzi, et al. (2007). "The translational fidelity function of IF3 during transition from the 30 S initiation complex to the 70 S initiation complex." J Mol Biol **373**(3): 551-561.

Grunberg-Manago, M., P. Dessen, et al. (1975). "Light-scattering studies showing the effect of initiation factors on the reversible dissociation of Escherichia coli ribosomes." J Mol Biol **94**(3): 461-478.

Guajardo, R. and R. Sousa (1997). "A model for the mechanism of polymerase translocation." J Mol Biol **265**(1): 8-19.

Gualerzi, C. O. and C. L. Pon (2015). "Initiation of mRNA translation in bacteria: structural and dynamic aspects." Cell Mol Life Sci **72**(22): 4341-4367.

Gusarov, I. and E. Nudler (1999). "The mechanism of intrinsic transcription termination." Mol Cell **3**(4): 495-504.

Gusarov, I. and E. Nudler (2001). "Control of intrinsic transcription termination by N and NusA: the basic mechanisms." Cell **107**(4): 437-449.

Hao, Z., V. Epshtein, et al. (2021). "Pre-termination Transcription Complex: Structure and Function." Mol Cell **81**(2): 281-292.

Harris, S. J., R. C. Williams, Jr., et al. (1995). "Self-association of Escherichia coli DNA-dependent RNA polymerase core enzyme." Biochemistry **34**(27): 8752-8762.

Hawley, D. K. and W. R. McClure (1983). "Compilation and analysis of Escherichia coli promoter DNA sequences." Nucleic Acids Res **11**(8): 2237-2255.

Held, W. A., B. Ballou, et al. (1974). "Assembly mapping of 30 S ribosomal proteins from Escherichia coli. Further studies." J Biol Chem **249**(10): 3103-3111.

Herbert, K. M., A. La Porta, et al. (2006). "Sequence-resolved detection of pausing by single RNA polymerase molecules." Cell **125**(6): 1083-1094.

Herbert, K. M., J. Zhou, et al. (2010). "E. coli NusG inhibits backtracking and accelerates pause-free transcription by promoting forward translocation of RNA polymerase." J Mol Biol **399**(1): 17-30.

Hobot, J. A., W. Villiger, et al. (1985). "Shape and fine structure of nucleoids observed on sections of ultrarapidly frozen and cryosubstituted bacteria." J. Bacteriol. **162**(3): 960-971.

Holschuh, K. and H. G. Gassen (1982). "Mechanism of translocation. Binding equilibria between the ribosome, mRNA analogues, and cognate tRNAs." J Biol Chem **257**(4): 1987-1992.

Huang, Y.-H., N. Said, et al. (2019). "Structural basis for the function of SuhB as a transcription factor in ribosomal RNA synthesis." Nucleic acids research **47**(12): 6488-6503.

Huang, Y. H., T. Hilal, et al. (2020). "Structure-Based Mechanisms of a Molecular RNA Polymerase/Chaperone Machine Required for Ribosome Biosynthesis." Mol Cell **79**(6): 1024-1036.

Imbert, I., J. C. Guillemot, et al. (2006). "A second, non-canonical RNA-dependent RNA polymerase in SARS coronavirus." Embo J **25**(20): 4933-4942.

Irastortza-Olaziregi, M. and O. Amster-Choder (2021). "Coupled Transcription-Translation in Prokaryotes: An Old Couple With New Surprises." Front Microbiol **11**(624830).

Iyer, S., D. Le, et al. (2018). "Distinct mechanisms coordinate transcription and translation under carbon and nitrogen starvation in Escherichia coli." Nat Microbiol **3**(6): 741-748.

Jacob, F., J. Monod, et al. (1961). Cellular Regulatory Mechanisms. Cold Spring Harbor Symp. Quant. Biol.

Jain, C. (2008). "The E. coli RhlE RNA helicase regulates the function of related RNA helicases during ribosome assembly." Rna **14**(2): 381-389.

Kaempfer, R. (1970). "Dissociation of ribosomes on polypeptide chain termination and origin of single ribosomes." Nature **228**(5271): 534-537.

Kang, J. Y., T. V. Mishanina, et al. (2018). "RNA Polymerase Accommodates a Pause RNA Hairpin by Global Conformational Rearrangements that Prolong Pausing." Mol Cell **69**(5): 802-815.

Kang, J. Y., T. V. Mishanina, et al. (2019). "Mechanisms of Transcriptional Pausing in Bacteria." J Mol Biol **431**(20): 4007-4029.

Kang, J. Y., R. A. Mooney, et al. (2018). "Structural Basis for Transcript Elongation Control by NusG Family Universal Regulators." Cell **173**(7): 1650-1662.

Kang, J. Y., P. D. Olinares, et al. (2017). "Structural basis of transcription arrest by coliphage HK022 Nun in an Escherichia coli RNA polymerase elongation complex." Elife **20**(6): 25478.

Kansara, S. G. and M. V. Sukhodolets (2011). "Oligomerization of the E. coli core RNA polymerase: formation of (α2ββ'ω)2-DNA complexes and regulation of the oligomerization by auxiliary subunits." PLoS One **6**(4): 0018990.

Kaplan, C. D., K. M. Larsson, et al. (2008). "The RNA polymerase II trigger loop functions in substrate selection and is directly targeted by alpha-amanitin." Mol Cell **30**(5): 547-556.

Karimi, R., M. Y. Pavlov, et al. (1999). "Novel roles for classical factors at the interface between translation termination and initiation." Mol Cell **3**(5): 601-609.

Kashkina, E., M. Anikin, et al. (2006). "Elongation complexes of Thermus thermophilus RNA polymerase that possess distinct translocation conformations." Nucleic Acids Res **34**(14): 4036-4045.

Kato, T., H. Yoshida, et al. (2010). "Structure of the 100S ribosome in the hibernation stage revealed by electron cryomicroscopy." Structure **18**(6): 719-724.

Katunin, V. I., A. Savelsbergh, et al. (2002). "Coupling of GTP hydrolysis by elongation factor G to translocation and factor recycling on the ribosome." Biochemistry **41**(42): 12806-12812.

Kim, H. K., F. Liu, et al. (2014). "A frameshifting stimulatory stem loop destabilizes the hybrid state and impedes ribosomal translocation." Proc Natl Acad Sci U S A **111**(15): 5538-5543.

Kireeva, M., M. Kashlev, et al. (2010). "Translocation by multi-subunit RNA polymerases." Biochim Biophys Acta: 25.

Klaholz, B. P. (2017). "The Ribosome Holds the RNA Polymerase on Track in Bacteria." Trends Biochem Sci **42**(9): 686-689.

Klumpp, S. and T. Hwa (2009). "Traffic patrol in the transcription of ribosomal RNA." RNA Biol **6**(4): 392-394.

Kohler, R., R. A. Mooney, et al. (2017). "Architecture of a transcribing-translating expressome." Science **356**(6334): 194-197.

Komissarova, N., J. Becker, et al. (2002). "Shortening of RNA:DNA hybrid in the elongation complex of RNA polymerase is a prerequisite for transcription termination." Mol Cell **10**(5): 1151-1162.

Komissarova, N. and M. Kashlev (1997). "Transcriptional arrest: Escherichia coli RNA polymerase translocates backward, leaving the 3' end of the RNA intact and extruded." Proc Natl Acad Sci U S A **94**(5): 1755-1760.

Krupp, F., N. Said, et al. (2019). "Structural Basis for the Action of an All-Purpose Transcription Anti-termination Factor." Mol Cell **74**(1): 143-157.

Landick, R., J. Carey, et al. (1985). "Translation activates the paused transcription complex and restores transcription of the trp operon leader region." Proc Natl Acad Sci U S A **82**(14): 4663-4667.

Landick, R., D. Wang, et al. (1996). "Quantitative analysis of transcriptional pausing by Escherichia coli RNA polymerase: his leader pause site as paradigm." Methods Enzymol **274**: 334-353.

Larson, M. H., R. A. Mooney, et al. (2014). "A pause sequence enriched at translation start sites drives transcription dynamics in vivo." Science **344**(6187): 1042-1047.

Lau, L. F., J. W. Roberts, et al. (1982). "Transcription terminates at lambda tR1 in three clusters." Proceedings of the National Academy of Sciences **79**(20): 6171-6175.

Laursen, B. S., H. P. Sørensen, et al. (2005). "Initiation of protein synthesis in bacteria." Microbiol Mol Biol Rev **69**(1): 101-123.

Lawson, M. R., W. Ma, et al. (2018). "Mechanism for the Regulated Control of Bacterial Transcription Termination by a Universal Adaptor Protein." Mol Cell **71**(6): 911-922.

Lee, S. J. and J. D. Gralla (2004). "Osmo-regulation of bacterial transcription via poised RNA polymerase." Mol Cell **14**(2): 153-162.

Lesnik, E. A., R. Sampath, et al. (2001). "Prediction of rho-independent transcriptional terminators in Escherichia coli." Nucleic Acids Res **29**(17): 3583-3594.

Lewicki, B. T., T. Margus, et al. (1993). "Coupling of rRNA transcription and ribosomal assembly in vivo. Formation of active ribosomal subunits in Escherichia coli requires transcription of rRNA genes by host RNA polymerase which cannot be replaced by bacteriophage T7 RNA polymerase." J Mol Biol **231**(3): 581-593.

Li, G. W., E. Oh, et al. (2012). "The anti-Shine-Dalgarno sequence drives translational pausing and codon choice in bacteria." Nature **484**(7395): 538-541.

Li, J., S. W. Mason, et al. (1993). "Elongation factor NusG interacts with termination factor rho to regulate termination and antitermination of transcription." Genes Dev **7**(1): 161-172.

Li, R., Q. Zhang, et al. (2016). "Effects of cooperation between translating ribosome and RNA polymerase on termination efficiency of the Rho-independent terminator." Nucleic Acids Res **44**(6): 2554-2563.

Linn, T. and J. Greenblatt (1992). "The NusA and NusG proteins of Escherichia coli increase the in vitro readthrough frequency of a transcriptional attenuator preceding the gene for the beta subunit of RNA polymerase." Journal of Biological Chemistry **267**(3): 1449-1454.

Liu, B., Y. Zuo, et al. (2015). "Structural basis for transcription reactivation by RapA." Proc Natl Acad Sci U S A **112**(7): 2006-2010.

Mandell, Z. F., R. T. Oshiro, et al. (2021). "NusG is an intrinsic transcription termination factor that stimulates motility and coordinates gene expression with NusA." Elife **9**(10): 61880.

Maracci, C., F. Peske, et al. (2014). "Ribosome-induced tuning of GTP hydrolysis by a translational GTPase." Proc Natl Acad Sci U S A **111**(40): 14418-14423.

Markus, M. A., R. B. Gerstner, et al. (1998). "The solution structure of ribosomal protein S4 delta41 reveals two subdomains and a positively charged surface that may interact with RNA." Embo J **17**(16): 4559-4571.

Martin, R. G., W. K. Gillette, et al. (2002). "Complex formation between activator and RNA polymerase as the basis for transcriptional activation by MarA and SoxS in Escherichia coli." Mol Microbiol **43**(2): 355-370.

Marzi, S., A. G. Myasnikov, et al. (2007). "Structured mRNAs regulate translation initiation by binding to the platform of the ribosome." Cell **130**(6): 1019-1031.

Mason, S. W. and J. Greenblatt (1991). "Assembly of transcription elongation complexes containing the N protein of phage lambda and the Escherichia coli elongation factors NusA, NusB, NusG, and S10." Genes Dev **5**(8): 1504-1512.

McGary, K. and E. Nudler (2013). "RNA polymerase and the ribosome: the close relationship." Curr Opin Microbiol **16**(2): 112-117.

Mikhaylina, A. O., E. Y. Nikonova, et al. (2021). "[Regulation of Ribosomal Protein Synthesis in Prokaryotes]." Mol Biol **55**(1): 20-41.

Miller, O. L., Jr., B. A. Hamkalo, et al. (1970). "Visualization of bacterial genes in action." Science **169**(3943): 392-395.

Mirkin, E. V. and S. M. Mirkin (2007). "Replication fork stalling at natural impediments." Microbiol Mol Biol Rev **71**(1): 13-35.

Miskin, R., A. Zamir, et al. (1970). "Inactivation and reactivation of ribosomal subunits: The peptidyl transferase activity of the 50 s subunit of Escherichia coli." Journal of molecular biology **54**(2): 355-378.

Mitarai, N., K. Sneppen, et al. (2008). "Ribosome collisions and translation efficiency: optimization by codon usage and mRNA destabilization." J Mol Biol **382**(1): 236-245.

Mitra, P., G. Ghosh, et al. (2017). "Rho Protein: Roles and Mechanisms." Annual Review of Microbiology **71**(1): 687-709.

Moazed, D. and H. F. Noller (1989). "Intermediate states in the movement of transfer RNA in the ribosome." Nature **342**(6246): 142-148.

Mohammad, F., C. J. Woolstenhulme, et al. (2016). "Clarifying the Translational Pausing Landscape in Bacteria by Ribosome Profiling." Cell Rep **14**(4): 686-694.

Mondal, J., B. P. Bratton, et al. (2011). "Entropy-based mechanism of ribosome-nucleoid segregation in E. coli cells." Biophys J **100**(11): 2605-2613.

Mooney, R. A., S. E. Davis, et al. (2009). "Regulator trafficking on bacterial transcription units in vivo." Mol Cell **33**(1): 97-108.

Mooney, R. A., K. Schweimer, et al. (2009). "Two structurally independent domains of E. coli NusG create regulatory plasticity via distinct interactions with RNA polymerase and regulators." J Mol Biol **391**(2): 341-358.

Morrison, C. A., G. Tischendorf, et al. (1977). "Accessibility of proteins in 50S ribosomal subunits of Escherichia coli to antibodies: an ultracentrifugation study." Mol Gen Genet **151**(3): 245-252.

Mulder, A. M., C. Yoshioka, et al. (2010). "Visualizing ribosome biogenesis: parallel assembly pathways for the 30S subunit." Science **330**(6004): 673-677.

Murakami, K. S. (2013). "X-ray crystal structure of Escherichia coli RNA polymerase σ70 holoenzyme." J Biol Chem **288**(13): 9126-9134.

Murakami, K. S. and S. A. Darst (2003). "Bacterial RNA polymerases: the wholo story." Curr Opin Struct Biol **13**(1): 31-39.

Murakami, K. S., S. Masuda, et al. (2002). "Structural Basis of Transcription Initiation: An RNA Polymerase Holoenzyme-DNA Complex." Science **296**(5571): 1285-1290.

Mustafi, M. and J. C. Weisshaar (2018). "Simultaneous Binding of Multiple EF-Tu Copies to Translating Ribosomes in Live Escherichia coli." mBio **9**(1): 02143-02117.

Nedialkov, Y. A., K. Opron, et al. (2013). "The RNA polymerase bridge helix YFI motif in catalysis, fidelity and translocation." Biochim Biophys Acta **2**: 187-198.

Nevskaya, N., S. Tishchenko, et al. (2005). "Ribosomal protein L1 recognizes the same specific structural motif in its target sites on the autoregulatory mRNA and 23S rRNA." Nucleic Acids Res **33**(2): 478-485.

Nudler, E. and M. E. Gottesman (2002). "Transcription termination and anti-termination in E. coli." Genes Cells **7**(8): 755-768.

O'Reilly, F. J., L. Xue, et al. (2020). "In-cell architecture of an actively transcribing-translating expressome." Science **369**(6503): 554-557.

Pani, B. and E. Nudler (2017). "Mechanistic insights into transcription coupled DNA repair." DNA Repair **56**: 42-50.

Peters, J. M., A. D. Vangeloff, et al. (2011). "Bacterial transcription terminators: the RNA 3'-end chronicles." J Mol Biol **412**(5): 793-813.

Petrov, A., A. Tsa, et al. (2013). "Analysis of RNA by analytical polyacrylamide gel electrophoresis." Methods Enzymol **530**: 301-313.

Platt, T. (1981). "Termination of transcription and its regulation in the tryptophan operon of E. coli." Cell **24**(1): 10-23.

Plochowietz, A., I. Farrell, et al. (2017). "In vivo single-RNA tracking shows that most tRNA diffuses freely in live bacteria." Nucleic Acids Res **45**(2): 926-937.

Proshkin, S., A. R. Rahmouni, et al. (2010). "Cooperation between translating ribosomes and RNA polymerase in transcription elongation." Science **328**(5977): 504-508.

Qin, Y., N. Polacek, et al. (2006). "The highly conserved LepA is a ribosomal elongation factor that back-translocates the ribosome." Cell **127**(4): 721-733.

Qu, X., L. Lancaster, et al. (2012). "Ribosomal protein S1 unwinds double-stranded RNA in multiple steps." Proc Natl Acad Sci U S A **109**(36): 14458-14463.

Quan, S., N. Zhang, et al. (2005). "Transcriptional polarity in rRNA operons of Escherichia coli nusA and nusB mutant strains." J Bacteriol **187**(5): 1632-1638.

Raguin, O., A. Gruaz-Guyon, et al. (2002). "Equilibrium expert: an add-in to Microsoft Excel for multiple binding equilibrium simulations and parameter estimations." Anal Biochem **310**(1): 1-14.

Ramakrishnan, V. (2002). "Ribosome structure and the mechanism of translation." Cell **108**(4): 557-572.

Ratje, A. H., J. Loerke, et al. (2010). "Head swivel on the ribosome facilitates translocation by means of intra-subunit tRNA hybrid sites." Nature **468**(7324): 713-716.

Ray-Soni, A., M. J. Bellecourt, et al. (2016). "Mechanisms of Bacterial Transcription Termination: All Good Things Must End." Annu Rev Biochem **85**: 319-347.

Richardson, J. P., C. Grimley, et al. (1975). "Transcription termination factor rho activity is altered in Escherichia coli with suA gene mutations." Proc Natl Acad Sci U S A **72**(5): 1725-1728.

Rippa, V., C. Cirulli, et al. (2010). "The ribosomal protein L2 interacts with the RNA polymerase alpha subunit and acts as a transcription modulator in Escherichia coli." J Bacteriol **192**(7): 1882-1889.

Rippe, K. (2001). "Making contacts on a nucleic acid polymer." Trends Biochem Sci **26**(12): 733-740.

Roberts, J. W. (2019). "Mechanisms of Bacterial Transcription Termination." J Mol Biol **431**(20): 4030-4039.

Robertson, J. M., H. Paulsen, et al. (1988). "Pre-steady-state kinetic studies on ribosomal translocation." Methods Enzymol **164**: 581-597.

Rodgers, M. L. and S. A. Woodson (2019). "Transcription Increases the Cooperativity of Ribonucleoprotein Assembly." Cell **179**(6): 1370-1381.

Rodgers, M. L. and S. A. Woodson (2021). "A roadmap for rRNA folding and assembly during transcription." Trends in biochemical sciences.

Rodnina, M. V. (2016). "The ribosome in action: Tuning of translational efficiency and protein folding." Protein Sci **25**(8): 1390-1406.

Röhl, R. and K. H. Nierhaus (1982). "Assembly map of the large subunit (50S) of Escherichia coli ribosomes." Proc Natl Acad Sci U S A **79**(3): 729-733.

Ruff, E. F., A. C. Drennan, et al. (2015). "E. coli RNA Polymerase Determinants of Open Complex Lifetime and Structure." J Mol Biol **427**(15): 2435-2450.

Ruff, E. F., W. S. Kontur, et al. (2015). "Using solutes and kinetics to probe large conformational changes in the steps of transcription initiation." Methods Mol Biol: 2392-2392_2314.

Ruff, E. F., M. T. Record, Jr., et al. (2015). "Initial events in bacterial transcription initiation." Biomolecules **5**(2): 1035-1062.

Saecker, R. M., M. T. Record, Jr., et al. (2011). "Mechanism of bacterial transcription initiation: RNA polymerase - promoter binding, isomerization to initiation-competent open complexes, and initiation of RNA synthesis." J Mol Biol **412**(5): 754-771.

Said, N., T. Hilal, et al. (2021). "Steps toward translocation-independent RNA polymerase inactivation by terminator ATPase ρ." Science **371**(6524): eabd1673.

Said, N., F. Krupp, et al. (2017). "Structural basis for λN-dependent processive transcription antitermination." Nat Microbiol **2**(17062): 62.

Salah, P., M. Bisaglia, et al. (2009). "Probing the relationship between Gram-negative and Gram-positive S1 proteins by sequence analysis." Nucleic Acids Res **37**(16): 5578-5588.

Sambrook, J., E. F. Fritsch, et al. (1989). Molecular cloning: a laboratory manual, Cold spring harbor laboratory press.

Sanamrad, A., F. Persson, et al. (2014). "Single-particle tracking reveals that free ribosomal subunits are not excluded from the Escherichia coli nucleoid." Proc Natl Acad Sci U S A **111**(31): 11413-11418.

Saxena, S., K. K. Myka, et al. (2018). "Escherichia coli transcription factor NusG binds to 70S ribosomes." Mol Microbiol **108**(5): 495-504.

Schilling-Bartetzko, S., F. Franceschi, et al. (1992). "Apparent association constants of tRNAs for the ribosomal A, P, and E sites." J Biol Chem **267**(7): 4693-4702.

Schmeing, T. M., K. S. Huang, et al. (2005). "Structural insights into the roles of water and the 2' hydroxyl of the P site tRNA in the peptidyl transferase reaction." Mol Cell **20**(3): 437-448.

Schmeing, T. M., R. M. Voorhees, et al. (2009). "The crystal structure of the ribosome bound to EF-Tu and aminoacyl-tRNA." Science **326**(5953): 688-694.

Schmidt, M. C. and M. J. Chamberlin (1987). "nusA protein of Escherichia coli is an efficient transcription termination factor for certain terminator sites." Journal of molecular biology **195**(4): 809-818.

Schmidt, M. C. and M. J. Chamberlin (1987). "nusA protein of Escherichia coli is an efficient transcription termination factor for certain terminator sites." J Mol Biol **195**(4): 809-818.

Schneider, C. A., W. S. Rasband, et al. (2012). "NIH Image to ImageJ: 25 years of image analysis." Nat Methods **9**(7): 671-675.

Schneider, D. A., A. Michel, et al. (2007). "Transcription elongation by RNA polymerase I is linked to efficient rRNA processing and ribosome assembly." Mol Cell **26**(2): 217-229.

Schwartz, A., E. Margeat, et al. (2007). "Transcription termination factor rho can displace streptavidin from biotinylated RNA." J Biol Chem **282**(43): 31469-31476.

Seligmann, H. and G. Warthi (2017). "Genetic Code Optimization for Cotranslational Protein Folding: Codon Directional Asymmetry Correlates with Antiparallel Betasheets, tRNA Synthetase Classes." Comput Struct Biotechnol J **15**: 412-424.

Selmer, M., C. M. Dunham, et al. (2006). "Structure of the 70S ribosome complexed with mRNA and tRNA." Science **313**(5795): 1935-1942.

Sevostyanova, A., G. A. Belogurov, et al. (2011). "The β subunit gate loop is required for RNA polymerase modification by RfaH and NusG." Mol Cell **43**(2): 253-262.

Shaner, S. L., D. M. Piatt, et al. (1982). "Aggregation equilibria of Escherichia coli RNA polymerase: evidence for anion-linked conformational transitions in the protomers of core and holoenzyme." Biochemistry **21**(22): 5539-5551.

Sharma, M. R., C. Barat, et al. (2005). "Interaction of Era with the 30S ribosomal subunit implications for 30S subunit assembly." Mol Cell **18**(3): 319-329.

Shepherd, N., P. Dennis, et al. (2001). "Cytoplasmic RNA Polymerase in Escherichia coli." J Bacteriol **183**(8): 2527-2534.

Shine, J. and L. Dalgarno (1975). "Determinant of cistron specificity in bacterial ribosomes." Nature **254**(5495): 34-38.

Shoji, S., S. E. Walker, et al. (2009). "Ribosomal translocation: one step closer to the molecular mechanism." ACS Chem Biol **4**(2): 93-107.

Skordalakes, E. and J. M. Berger (2003). "Structure of the Rho transcription terminator: mechanism of mRNA recognition and helicase loading." Cell **114**(1): 135-146.

So, A., E. Davie, et al. (1967). "Effects of cations on DNA-dependent RNA polymerase." Proceedings of the National Academy of Sciences of the United States of America **58**(4): 1739.

Sørensen, M. A., J. Fricke, et al. (1998). "Ribosomal protein S1 is required for translation of most, if not all, natural mRNAs in Escherichia coli in vivo." J Mol Biol **280**(4): 561-569.

Spahn, C., F. Cella-Zannacchi, et al. (2015). "Correlative super-resolution imaging of RNA polymerase distribution and dynamics, bacterial membrane and chromosomal structure in Escherichia coli." Methods Appl Fluoresc **3**(1): 2050-6120.

Spivak, G. (2016). "Transcription-coupled repair: an update." Arch Toxicol **90**(11): 2583-2594.

Squires, C. L., J. Greenblatt, et al. (1993). "Ribosomal RNA antitermination in vitro: requirement for Nus factors and one or more unidentified cellular components." Proc Natl Acad Sci U S A **90**(3): 970-974.

Stark, H. (2010). "GraFix: stabilization of fragile macromolecular complexes for single particle cryo-EM." Methods Enzymol **481**: 109-126.

Steiner, T., J. T. Kaiser, et al. (2002). "Crystal structures of transcription factor NusG in light of its nucleic acid- and protein-binding activities." Embo J **21**(17): 4641-4653.

Steitz, J. A. and K. Jakes (1975). "How ribosomes select initiator regions in mRNA: base pair formation between the 3' terminus of 16S rRNA and the mRNA during initiation of protein synthesis in Escherichia coli." Proc Natl Acad Sci U S A **72**(12): 4734-4738.

Steitz, T. A. A mechanism for all polymerases, Nature. 1998 Jan 15;391(6664):231-2. doi: 10.1038/34542.

Stevens, A., A. J. Emery, Jr., et al. (1966). "Sedimentation properties of E. coli RNA polymerase and its complexes with polyuridylic acid." Biochem Biophys Res Commun **24**(6): 929-936.

Stevenson-Jones, F., J. Woodgate, et al. (2020). "Ribosome reactivates transcription by physically pushing RNA polymerase out of transcription arrest." Proceedings of the National Academy of Sciences **117**(15): 8462-8467.

Stöffler, G., R. Hasenbank, et al. (1973). "The accessibility of proteins of the Escherichia coli 30S ribosomal subunit to antibody binding." Mol Gen Genet **127**(2): 89-110.

Stracy, M., C. Lesterlin, et al. (2015). "Live-cell superresolution microscopy reveals the organization of RNA polymerase in the bacterial nucleoid." Proc Natl Acad Sci U S A **112**(32): 29.

Studer, S. M. and S. Joseph (2006). "Unfolding of mRNA secondary structure by the bacterial translation initiation complex." Mol Cell **22**(1): 105-115.

Suh, W. C., S. Leirmo, et al. (1992). "Roles of magnesium in the mechanism of formation and dissociation of open complexes between Escherichia coli RNA polymerase and the. lambda. PR promoter: kinetic evidence for a second open complex requiring magnesium." Biochemistry **31**(34): 7815-7825.

Sukhodolets, M. V. and S. Garges (2003). "Interaction of Escherichia coli RNA polymerase with the ribosomal protein S1 and the Sm-like ATPase Hfq." Biochemistry **42**(26): 8022-8034.

Sukhodolets, M. V., S. Garges, et al. (2006). "Ribosomal protein S1 promotes transcriptional cycling." Rna **12**(8): 1505-1513.

Sullivan, S. L. and M. E. Gottesman (1992). "Requirement for E. coli NusG protein in factor-dependent transcription termination." Cell **68**(5): 989-994.

Sussman, J. K., E. L. Simons, et al. (1996). "Escherichia coli translation initiation factor 3 discriminates the initiation codon in vivo." Mol Microbiol **21**(2): 347-360.

Sutherland, C. and K. S. Murakami (2018). "An Introduction to the Structure and Function of the Catalytic Core Enzyme of Escherichia coli RNA Polymerase." EcoSal Plus **8**(1): 0004-2018.

Svetlov, V. and I. Artsimovitch (2015). "Purification of bacterial RNA polymerase: tools and protocols." Methods Mol Biol: 2392-2392_2392.

Svetlov, V., G. A. Belogurov, et al. (2007). "Allosteric control of the RNA polymerase by the elongation factor RfaH." Nucleic Acids Res **35**(17): 5694-5705.

Takyar, S., R. P. Hickerson, et al. (2005). "mRNA helicase activity of the ribosome." Cell **120**(1): 49-58.

Talkington, M. W., G. Siuzdak, et al. (2005). "An assembly landscape for the 30S ribosomal subunit." Nature **438**(7068): 628-632.

Thommen, M., W. Holtkamp, et al. (2017). "Co-translational protein folding: progress and methods." Curr Opin Struct Biol **42**: 83-89.

Thomsen, N. D. and J. M. Berger (2009). "Running in reverse: the structural basis for translocation polarity in hexameric helicases." Cell **139**(3): 523-534.

Tomšic, J., L. A. Vitali, et al. (2000). "Late events of translation initiation in bacteria: a kinetic analysis." The EMBO journal **19**(9): 2127-2136.

Torres, M., C. Condon, et al. (2001). "Ribosomal protein S4 is a transcription factor with properties remarkably similar to NusA, a protein involved in both non-ribosomal and ribosomal RNA antitermination." Embo J **20**(14): 3811-3820.

Turnbough, C. L., Jr., K. L. Hicks, et al. (1983). "Attenuation control of pyrBI operon expression in Escherichia coli K-12." Proc Natl Acad Sci U S A **80**(2): 368-372.

Turtola, M. and G. A. Belogurov (2016). "NusG inhibits RNA polymerase backtracking by stabilizing the minimal transcription bubble." Elife **4**(5): 18096.

Vassylyev, D. G., S. Sekine, et al. (2002). "Crystal structure of a bacterial RNA polymerase holoenzyme at 2.6 A resolution." Nature **417**(6890): 712-719.

Vizcaíno, J. A., A. Csordas, et al. (2016). "2016 update of the PRIDE database and its related tools." Nucleic Acids Res **44**(22): 28.

Vogel, U. and K. F. Jensen (1994). "The RNA chain elongation rate in Escherichia coli depends on the growth rate." J Bacteriol **176**(10): 2807-2813.

von Hippel, P. H. and O. G. Berg (1989). "Facilitated target location in biological systems." J Biol Chem **264**(2): 675-678.

Wang, C., V. Molodtsov, et al. (2020). "Structural basis of transcription-translation coupling." Science **369**(6509): 1359-1365.

Wang, D., D. A. Bushnell, et al. (2009). "Structural basis of transcription: backtracked RNA polymerase II at 3.4 angstrom resolution." Science **324**(5931): 1203-1206.

Wang, Q., J. Wu, et al. (2020). "Structural basis for RNA replication by the SARS-CoV-2 polymerase." Cell **182**(2): 417-428. e413.

Washburn, R. S., P. K. Zuber, et al. (2020). "Escherichia coli NusG Links the Lead Ribosome with the Transcription Elongation Complex." iScience **23**(8): 9.

Webster, M. W., M. Takacs, et al. (2020). "Structural basis of transcription-translation coupling and collision in bacteria." Science **369**(6509): 1355-1359.

Webster, M. W. and A. Weixlbaumer (2021). "Macromolecular assemblies supporting transcription-translation coupling." Transcription: 1-23.

Westermeier, R. (2006). "Sensitive, quantitative, and fast modifications for Coomassie Blue staining of polyacrylamide gels." Proteomics **2**: 61-64.

Woldringh, C. L. (2002). "The role of co-transcriptional translation and protein translocation (transertion) in bacterial chromosome segregation." Mol Microbiol **45**(1): 17-29.

Wu, A., Y. Peng, et al. (2020). "Genome composition and divergence of the novel coronavirus (2019-nCoV) originating in China." Cell host & microbe **27**(3): 325-328.

Yamamoto, H., D. Wittek, et al. (2016). "70S-scanning initiation is a novel and frequent initiation mode of ribosomal translation in bacteria." Proceedings of the National Academy of Sciences **113**(9): E1180-E1189.

Yan, S., J. D. Wen, et al. (2015). "Ribosome excursions during mRNA translocation mediate broad branching of frameshift pathways." Cell **160**(5): 870-881.

Yanofsky, C. (2000). "Transcription attenuation: once viewed as a novel regulatory strategy." J Bacteriol **182**(1): 1-8.

Yanofsky, C. and J. Ito (1966). "Nonsense codons and polarity in the tryptophan operon." J Mol Biol **21**(2): 313-334.

Yarnell, W. S. and J. W. Roberts (1999). "Mechanism of intrinsic transcription termination and antitermination." Science **284**(5414): 611-615.

Yusupova, G., L. Jenner, et al. (2006). "Structural basis for messenger RNA movement on the ribosome." Nature **444**(7117): 391-394.

Yuzenkova, Y. and N. Zenkin (2010). "Central role of the RNA polymerase trigger loop in intrinsic RNA hydrolysis." Proc Natl Acad Sci U S A **107**(24): 10878-10883.

Zamir, A., R. Miskin, et al. (1971). "Inactivation and reactivation of ribosomal subunits: amino acyl-transfer RNA binding activity of the 30 s subunit of Escherichia coli." Journal of molecular biology **60**(2): 347-364.

Zamir, A., R. Miskin, et al. (1974). [40] The inactivation and reactivation of Escherichia coli ribosomes. Methods in enzymology, Elsevier. **30:** 406-426.

Zavialov, A. V., L. Mora, et al. (2002). "Release of peptide promoted by the GGQ motif of class 1 release factors regulates the GTPase activity of RF3." Mol Cell **10**(4): 789-798.

Zellars, M. and C. L. Squires (1999). "Antiterminator-dependent modulation of transcription elongation rates by NusB and NusG." Mol Microbiol **32**(6): 1296-1304.

Zengel, J. M., D. Mueckl, et al. (1980). "Protein L4 of the E. coli ribosome regulates an eleven gene r protein operon." Cell **21**(2): 523-535.

Zhang, J., M. Palangat, et al. (2010). "Role of the RNA polymerase trigger loop in catalysis and pausing." Nat Struct Mol Biol **17**(1): 99-104.

Zhang, W., J. A. Dunkle, et al. (2009). "Structures of the Ribosome in Intermediate States of Ratcheting." Science **325**(5943): 1014-1017.

Zhang, Y., S. Hong, et al. (2018). "Alternative Mode of E-Site tRNA Binding in the Presence of a Downstream mRNA Stem Loop at the Entrance Channel." Structure **26**(3): 437-445.

Zhang, Y., R. A. Mooney, et al. (2014). "DksA guards elongating RNA polymerase against ribosome-stalling-induced arrest." Mol Cell **53**(5): 766-778.